

The Conceptual Design of a 3000 lb Class Parasite Unmanned Combat Aerial Vehicle

a project presented to
The Faculty of the Department of Aerospace Engineering
San Jose State University

in partial fulfillment of the requirement of the degree
Master of Science in Aerospace Engineering

by

Chris Lam

Fall 2023

approved by

Prof. Sean Montgomery

Faculty Advisor

© 2023

Chris Lam

ALL RIGHTS RESERVED

ABSTRACT

The Conceptual Design of a 3000 lb Class Parasite Unmanned Combat Aerial Vehicle

By Chris Lam

Parasite fighter is a concept of deploying smaller aircraft from the larger mothership, extending the range of the smaller aircraft. The objective of this project is to resurrect this idea, combine it with modern UAV design and create a miniature UCAV that can aid fighter pilots in their mission, similar to the loyal wingman drones that countries around the world have been pursuing. The resulting design is a small aircraft with a wingspan of only 3.2 m [10.6 ft] and a gross weight of 1,272 kg [1,808 lb]. A pair of pylons on the fuselage allows the aircraft to carry a pair of AIM-9 or AIM-120 missiles. One manned fighter can carry a pair of drones on the wingtips and deploy them near the battlefield. However, perhaps due to the unique role and the abnormally low weight of the aircraft, the traditional preliminary design method has generated dubious results at times, questioning the validity of the design.

ACKNOWLEDGEMENTS

I would like to thank Professor Sean Montgomery for his instruction. He has given insightful comments and feedback. Although the project has become more complex and drawn out than expected, he remained patient and encouraging throughout, yet rigorous, ensuring adequate attention and thought were given to each part of the design.

I would also like to thank my parents. Only with their support can I tackle this project without worry and distraction. Only with their encouragement can I carry on and complete my work.

TABLE OF CONTENTS

ABSTRACT	iii
ACKNOWLEDGEMENTS	iv
TABLE OF CONTENTS	v
LIST OF FIGURES	xi
LIST OF TABLES	xiii
List of Symbols	xiv
1. Mission Specification	1
1.1 Introduction and Motivation.....	1
1.2 Literature Review	1
1.2.1 Parasite Fighter	1
1.2.2 Unmanned Combat Aerial Vehicle (UCAV).....	3
1.2.3 Comparative Study	4
1.3 Mission Specification.....	5
1.3.1 Project Proposal	5
1.3.2 Mission Requirement.....	5
1.3.3 Project Profile.....	6
1.4 Methodology	6
2. Weight Estimate	7
2.1 Introduction	7
2.2 Detailed Explanation	7
2.2.1 Assumptions	7
2.2.2 Hand Calculation	8
2.2.3 RDS	9
2.3 Results	9
2.4 Discussion	10
2.5 Conclusion.....	10
3. Wing and Propulsion Sizing	11
3.1 Introduction	11
3.2 Detailed Explanation	11
3.2.1 Stall Speed	11
3.2.2 Cruise Speed.....	11

3.2.3 Landing	12
3.2.4 Climbing	12
3.2.5 Maneuvering	12
3.3 Discussion	13
3.4 Conclusion.....	13
4. Configuration Selection.....	14
4.1 Overall Selection	14
4.2 Wing Configuration.....	14
4.3 Empennage Configuration.....	15
4.4 Propulsion Configuration	15
4.5 Landing Gear Configuration	15
4.6 Payload Configuration.....	16
5. Fuselage Design.....	17
5.1 Fuselage Layout	17
5.2 Discussion	18
5.3 Conclusion.....	18
6. Wing Design	19
6.1 Wing Platform Design.....	19
6.1.1 Wing Platform Design Criteria.....	19
6.1.2 Wing Platform Design	19
6.2 Airfoil Selection	20
6.3 High Lift Devices	21
6.4 Wing Controls	21
6.5 Wing Design Analysis.....	22
6.6 Discussion	23
6.7 Conclusion.....	24
7. Empennage Design	25
7.1 Canard Design.....	25
7.1.1 Canard Airfoil Selection.....	25
7.1.2 Canard Platform Design	25
7.2 Vertical Stabilizer Design	27
7.2.1 Vertical Stabilizer Airfoil Selection	27

7.2.2 Vertical Stabilizer Platform Design.....	27
7.3 Discussion	30
7.4 Conclusion.....	30
8. Landing Gear Design.....	31
8.1 Landing Gear Layout Design	31
8.2 Landing Gear Layout Discussion.....	32
8.3 Tire Sizing and Discussion.....	33
8.4 Landing Gear Stability	34
8.4.1 Tip-back Angle	34
8.4.2 Overturn Angle.....	36
8.4.3 Wingtip Angle	36
9. Class I Weight and Balance Analysis.....	37
9.1 Introduction	37
9.2 Component Weight Breakdown.....	37
9.3 Discussion	39
10. Class II Weight and Balance Analysis	40
10.1 Introduction	40
10.2 Component Weight Breakdown	40
10.3 Center of Gravity Location of Various Loading Scenarios.....	42
10.4 Discussion	43
10.5 Conclusion.....	43
11. Drag Polar.....	44
11.1 Introduction	44
11.2 Breakdown and Calculation	44
11.2.1 Coefficient of Drag of Wing.....	44
11.2.2 Coefficient of Drag for Empennage	46
11.2.3 Coefficient of Drag for Fuselage	46
11.2.5 Coefficient of Drag for Payload	47
11.3 Results.....	47
11.4 Discussion	49
12. Subsystem Arrangement	51
12.1 Introduction.....	51

12.2 Flight Control Subsystem.....	51
12.2 Avionics Subsystem	51
12.3 Electrical Subsystem	52
12.4 Hydraulic Subsystem	52
12.5 Fuel Subsystem	54
12.6 Docking system.....	55
13. Structure.....	56
13.1 Fuselage Structure.....	56
13.1.1 Fuselage Structure Design.....	56
13.1.2 Fuselage Structure Discussion.....	57
13.2 Wing Structure	57
13.2.1 Wing Structure Design	57
13.2.2 Wing Structure Discussion.....	58
13.3 Canard Structure.....	59
13.1.1 Canard Structure Design.....	59
13.1.2 Canard Structure Discussion	60
13.4 Vertical Stabilizer Structure.....	60
13.1.1 Vertical stabilizer structure Design	60
13.1.2 Vertical stabilizer Structure Discussion	60
14. V-n Diagram.....	62
14.1 Introduction.....	62
14.2 Results.....	62
14.3 Detailed Explanation.....	62
14.4 Discussion	63
15. Stability and Control Analysis.....	64
15.1 Longitudinal Stability.....	64
15.2 Longitudinal Stability Discussion.....	64
15.3 Directional Stability	66
15.4 Directional Stability Discussion.....	66
15.5 Trim Diagram.....	67
15.6 Trim Diagram Discussion	68
16. Installed Power and Thrust Characteristics.....	69

16.1 Inlet Sizing	69
16.2 Inlet Sizing Discussion.....	69
16.3 Inlet Design	69
16.4 Inlet Design Discussion.....	71
16.5 Prediction of Installed Power and Thrust.....	71
16.6 Prediction of Installed Power and Thrust Discussion	72
17. Critical Performance Requirements	74
17.1 Introduction	74
17.2 Stall Performance	74
17.2.1 Stall Performance Equations	74
17.2.2 Stall Performance Result	74
17.3 Cruise and Range Performance	75
17.3.1 Cruise and Range Performance Equations	75
17.3.2 Cruise and Range Performance Result	76
17.4 Maneuvering Performance	77
17.4.1 Maneuvering Performance Equations	77
17.4.2 Maneuvering Performance Result	77
17.5 Climbing Performance	79
17.5.1 Climbing Performance Equations.....	79
17.5.2 Climbing Performance Result	79
17.6 Landing Performance	81
17.6.1 Landing Performance Equations	81
17.6.2 Landing Performance Result	81
18. Final 3 View and Subsystem Drawings.....	82
19. Cost Analysis	87
19.1 Introduction	87
19.2 Research, Development, Test, and Evaluation Cost for Prototype Estimation.....	87
19.3 Manufacturing and Acquisition Cost Estimation	87
19.4 Operating Cost Estimation	88
19.5 Life Cycle Cost Estimation	88
19.6 Cost Estimation Result	88
19.6 Cost Estimation Discussion.....	90

20. Reference	91
Appendix A. RDS Weight Estimate 500 lb Payload	93
Appendix B. RDS Weight Estimate 850 lb Payload 1000 km Range	98
Appendix C. Matlab Matching Graph.....	103
Appendix D. Matlab Excel Canard Area Measurement	106
Appendix E. Excel Class I Weight and Balance.....	108
Appendix F. Matlab Class II Weight and Balance	114
Appendix G. RDS Weight and Balance – Fighters	119
Appendix H. RDS Weight and Balance – General Aviation.....	122
Appendix I. Matlab Drag Polar.....	125
Appendix J. Matlab V-n Diagram.....	134
Appendix K. Matlab Stability X-Plot.....	137
Appendix L. Matlab Installed Thrust and Inlet.....	143
Appendix M. Matlab Critical Performance	146
Appendix N. Matlab Cost Analysis	155

LIST OF FIGURES

Figure 2.1 - Raymer’s lift-to-drag ratio estimation.....	7
Figure 4.1 - Isometric and three-view drawing of the aircraft.....	14
Figure 5.1 - Fuselage dimensions.	17
Figure 5.2 - Fuselage cross-section.....	17
Figure 6.1 - Wing drawing.....	20
Figure 6.2 - MH 60 airfoil.....	20
Figure 6.3 - Aileron drawing.	21
Figure 6.4 - Leading edge of the MH 60 airfoil.....	22
Figure 6.5 - Graphs to determine $CL_{maxbase}$ and ΔCL_{max}	23
Figure 6.6 - Calculation of CL_{max} using XFLR5.....	24
Figure 7.1 - MH 64 Airfoil.	25
Figure 7.2 - Canard drawing.	26
Figure 7.3 - Canard moment arm.....	26
Figure 7.4 - NACA 0010 airfoil.....	27
Figure 7.5 - Vertical stabilizer drawing.	28
Figure 7.6 - Vertical Stabilizer Moment Arm.....	29
Figure 7.7 - Rudder dimensions.....	29
Figure 8.1 - Isometric and three views of the aircraft with extended landing gear.	31
Figure 8.2 - Side view of landing gear deployment.....	32
Figure 8.3 - Side view of landing gear deployment.....	32
Figure 8.4 - Tip-back angle and C.G. - main gear angle.	35
Figure 8.5 - Overturn angle.....	35
Figure 8.6 - Wingtip angle.	36
Figure 11.1 - Wave divergence diagram.....	45
Figure 11.2 - Drag polar of the aircraft.....	47
Figure 11.3 - Lift-to-drag ratio of the aircraft at different Mach numbers	48
Figure 11.4 - Drag polar of the aircraft without transonic lift-induced drag.	48
Figure 11.5 - Lift-to-drag ratio of the aircraft at different Mach numbers	49
Figure 12.1 - Electrical system components.....	53
Figure 12.2 - Hydraulic system components.	53
Figure 12.3 - Fuel System.....	54
Figure 12.4 - Wingtip clearance when docked.	55
Figure 13.1 - Top view of fuselage structure layout.....	56
Figure 13.2 - Side and section view of fuselage structure layout.	57
Figure 13.3 - Wing structure.....	58
Figure 13.4 - Canard structure.	59
Figure 13.5 - Vertical stabilizer structure.	61
Figure 14.1 - V-n diagram for sea level conditions.	62
Figure 15.1 - Directional x-plot.	65
Figure 15.2 - Directional x-plot.	67
Figure 15.3 - Trim diagram.....	68
Figure 16.1 - Engine inlet dimension.....	70

Figure 16.2 - Engine air duct.	70
Figure 16.3 - Available installed and uninstalled thrust at altitude.	72
Figure 17.1 - Stall speed at altitude.	75
Figure 17.2 - Range of the aircraft traveling at different Mach numbers.	76
Figure 17.3 - Required and available thrust in a 5-G sustained turn.	78
Figure 17.4 - Coefficient of lift in a 5-G sustained turn.	78
Figure 17.5 - Rate of climb at altitude.	80
Figure 17.6 - Climb angle at altitude.	80
Figure 18.1 - Drawing of the aircraft with landing gear up.	82
Figure 18.2 - Drawing of the aircraft with landing gear down.	83
Figure 18.3 - Drawing of the aircraft structure.	83
Figure 18.4 - Drawing of subsystems and structure.	84
Figure 18.5 - Drawing of the electrical system.	84
Figure 18.6 - Drawing of the hydraulic system.	85
Figure 18.7 - Drawing of the fuel system.	85
Figure 18.8 - Drawing of theUCAV docked to the right wing of F-16.	86

LIST OF TABLES

Table 2.1 - Variables and values used in weight fraction calculation.	9
Table 2.2 - Calculated weight fraction.....	9
Table 3.1 - Matching graph.....	13
Table 6.1 - Wing parameter.	19
Table 7.1 - Canard parameter.....	27
Table 7.2 - Vertical stabilizer parameter.....	28
Table 9.1 - Component Weight Fractions of different aircraft.	38
Table 9.2 - Component weight and location using class I method.	39
Table 10.1 - Roskam's fighter equation result.....	40
Table 10.2 - RDS fighter equation result.	41
Table 10.3 - RDS general aviation equation result.	42
Table 10.4 - Center of gravity location variation for different estimations.	42
Table 17.1 - Range of the aircraft traveling at Mach 0.85.....	76
Table 17.2 - Landing distances of the aircraft.	81
Table 19.1 - Life Cycle Cost Breakdown	89

List of Symbols

Symbol	Definition	Unit (SI)	Unit (Imperial)
A or AR	Aspect ratio	-	
A_c	Engine inlet area	m^2	ft^2
AEP	Airplane estimated price	USD	
b	Wingspan	m	ft
C	Cost	USD	
C_{ACQ}	Total cost of acquisition	USD	
C_{aed}	Airframe engineering and design cost	USD	
C_{apc}	Airplane production cost	USD	
C_C	Cruise specific fuel consumption	$mg/(Ns)$	$hr^{(-1)}$
C_{CONMAT}	Program cost of consumable materials	-	
C_f	Turbulent mean skin-friction coefficient	-	
C_L	Loiter specific fuel consumption	$mg/(Ns)$	$hr^{(-1)}$
C_D	Coefficient of drag	-	
C_{D_L}	Coefficient of lift-induced drag	-	
C_{D_0}	Zero-lift coefficient of drag	-	
C_{DEPOT}	Program cost associated with depots	USD	
C_{dst}	Development support and test cost	USD	
$C_{(e+a)}$	Engine and avionics cost	USD	
C_{fta}	Flight test airplanes cost	USD	
C_{fto}	Flight test operations cost	USD	
C_{fin}	Financing cost	USD	
C_{int}	Cost of interiors	USD	
C_L	Coefficient of lift	-	
C_{L_0}	Zero-lift coefficient of lift	-	
C_{L_α}	Lift-curve slope	deg^{-1} or rad^{-1}	
C_{MAN}	Total manufacturing phase cost	USD	
C_{MISC}	Program miscellaneous cost	USD	
C_m	Coefficient of moment	-	
C_{man}	Manufacturing labor cost	USD	
C_{n_β}	Yawing-moment-due-to-sideslip derivative	deg^{-1} or rad^{-1}	
$C_{n_{\delta r}}$	Yawing-moment-due-to-rudder derivative	deg^{-1} or rad^{-1}	
C_{OPS}	Total operations phase cost	USD	
$C_{PERSDIR}$	Program direct personnel cost	USD	
$C_{PERSIND}$	Program indirect personnel cost	USD	

C_{POL}	Program cost of fuel, oil and lubricants	USD	
C_{PRO}	Manufacturing phase profit	USD	
C_{pro}	Profit (cost)	USD	
C_{RDTE}	Total RDTE phase cost	USD	
C_{SPARES}	Program cost of spares	USD	
C_{tool}	Tooling cost	USD	
C_{qc}	Quality control cost	USD	
CGR	Climb gradient	rad	
E	Endurance	hr	
e	Span efficiency factor	-	
GW	Gross weight	kg	lbs
i	Angle of incidence	deg or rad	
k_{β}	Sideslip to rudder feedback gain	-	
LCC	Life cycle cost	USD	
$(L/D)_c$	Cruise lift-to-drag ratio	-	
$(L/D)_L$	Loiter lift-to-drag ratio	-	
M	Mach number	-	
M_{DD}	Drag divergence Mach number	-	
\dot{m}_a	Engine mass flow rate	kg/s	slugs/s
\dot{m}_{comb}	Combustion mass flow rate	kg/s	slugs/s
\dot{m}_{cool}	Cooling mass flow rate	kg/s	slugs/s
N_m	Number of production airplanes built	USD	
P_{extr}	Extracted power	kW	hp
p	Pressure	Pa	psi
n	Load factor	-	
R	Range	km	nmi
R_{LS}	Lifting surface correction factor	-	
R_{wf}	Wing/fuselage interference factor	-	
RC	Rate of climb	m/s	fpm
S	Lifting surface area	m ²	ft ²
S_{wet}	Wetted area	m ²	ft ²
s_{air}	Air distance in landing	m	ft
s_L	Landing distance	m	ft
s_{LG}	Landing ground distance	m	ft
T	Temperature	°C	°F
T	Thrust	N	lbs
T_{av}	Available thrust	N	lbs
$T_{tst/av}$	Available uninstalled thrust	N	lbs
T/W	Thrust-to-weight ratio	-	
t/c	Thickness ratio	-	
W	Weight	kg	lbs
Wi	Weight fraction	-	

W/S	Wing loading	kg/m^3	lbs/ft^2
V or U	Velocity	m/s or km/hr	ft/s or kt
V_a	Approach speed	m/s or km/hr	ft/s or kt
V_c	Cruise speed	m/s or km/hr	ft/s or kt
V_s	Stall speed	m/s or km/hr	ft/s or kt
V_s	Touchdown speed	m/s or km/hr	ft/s or kt
v	Tail volume	-	
x	Location in the x-axis	m	ft
\bar{x}	Location in the x-axis	% MAC	
Greek Symbols	Definition	Unit (SI)	Unit (Imperial)
α	Angle of attack	deg or rad	
β	Sideslip angle	deg or rad	
Δ	Increment	-	
λ	Taper ratio	-	
ρ	Air density	kg/m^3	slugs/ft ³
Subscripts			
$()_{ac}$	Aerodynamic center		
$()_{alt}$	At altitude		
$()_c$	Canard		
$()_{fus}$	Fuselage		
$()_{lim}$	Limit		
$()_m$	Manufacturing phase		
$()_{max}$	Maximum		
$()_r$	RDTE phase		
$()_{TO}$	Takeoff		
$()_w$	Wing		
$()_{wave}$	Wave drag		
$()_{wf}$	Wing-fuselage		
$()_v$	Vertical stabilizer		
$()_0$	Sea level		
$()_1$	Steady state		
Acronyms			
AOA	Angle of attack		
AC	Alternate current		
CAD	Computer-aided design		
C.G.	Center of gravity		
DC	Direct current		
GPS	Global Positioning System		
MAC	Mean aerodynamic chord		
RDTE	Research, development, test and evaluation		
UAV	Unmanned aerial vehicle		
UCAV	Unmanned combat aerial vehicle		

1. Mission Specification

1.1 Introduction and Motivation

War is a breeding ground for many new and bizarre ideas. However, not many can prove themselves and survive the test of time. The parasite fighter is an example of such an idea. Fighters are fast, agile, and versatile. But they lack the range and payload for any tactical or strategic maneuvers. On the other hand, bombers have the range and payload but not the means to protect themselves against enemy interceptors. If a bomber can carry the fighters with them and deploy them only when needed, it will make for an effective and resilient bomber squadron. But since there are no parasite fighters in service today, it goes without saying that the concept is a failure. More than 60 years have passed since the last major parasite fighter experiment. Technology has advanced considerably since. This project attempts to resurrect this idea, combine it with the newest technology and air force doctrine, and explore the feasibility of this idea on a modern battlefield.

1.2 Literature Review

1.2.1 Parasite Fighter

The concept of carrying an aerial vehicle with another goes as far back as 1852. In an issue of the *Mechanics' Magazine*, British aeronautical pioneer Sir George Cayley first suggested using a balloon to carry a glider to altitude. In 1905, John J. Montgomery became one of the first, if not the first, to employ this tactic in America. The first military application was in WWI. Aviation was still in its infancy. The biplane was the prevailing configuration for a fighter. The role of the bomber was served by airship instead of metallic mono-wing aircraft. The first parasite fighter experiment was launched by the Royal Air Force (RAF). In an attempt to combat German Zeppelin, a Royal Aircraft Factory B.E.2c was to be launched and recovered from an airship. The experiment ended in disaster when the plane was prematurely released in February 1916. The aircraft and both pilots were lost. In 1916, the RAF made another attempt by putting a Bristol Scout on a Porte trimotor seaplane. The British would continue with their experiment even after the war. The Germans made their first and only trial in 1918 when they deployed an Albatross D.III from Zeppelin L35 and landed it successfully.

In America, parasite fighter experiments would not start until after WWI. Between late 1924 and 1926, the U.S. Army Air Service experimented with trying to hook a biplane onto blimp TC-2 and TC-7. The navy would also experiment with their German-built Zeppelin. On July 3rd, 1929, a Vought UO-1 first attempted to hook onto ZR-3 Los Angeles. But the successful hook-on occurred later on the 20th -21st of August after a modification to the hook. The Navy continued

its experiment with different airships and aircraft. By May 1930, the Navy issued a requirement for a new fighter. Curtiss' proposal would eventually become the F9C-2, a purpose-built parasite fighter. The F9C-2 served exclusively on the new Navy airships Akron and Macon. Though they could serve as fighters, they more often served as reconnaissance aircraft, as the two airships were assigned to fleet scouting duty. Unfortunately, Akron and Macon were both lost in accidents within a short period between 1931 and 1933. The age of airships would also end before the outbreak of WWII.

The concept of the parasite fighter experienced a resurgence and advancement in WWII. Large aircraft took over as the new launch platform. Parasite fighters also took on new roles. The Soviet Union had been experimenting with the concept throughout the 1930s. In one experiment in 1935, a TB-3 carried two I-5 fighters above the wing, two I-16s below the wing, and one I-Z on an extended trapeze. All five fighters successfully detached from the mothership [1]. In addition to reconnaissance and bomber escort, the parasite fighter concept was proposed as a way of assisted takeoff. Overloaded dive bombers can get airborne with the help of a mothership [2]. When Nazi Germany invaded in the summer of 1941, the Soviets armed the I-16 with bombs and sent them to battle. One Tb-3 carried two I-16s, each carrying 500 kg of bombs. The I-16 would detach, drop their bombs, and land at the closest friendly airfield. As many as 30 missions were carried out. Despite the occasional success, this tactic was abandoned by 1942. Germany also conducted multiple experiments regarding parasite fighters. In one experiment, reconnaissance aircraft DFS 228 would deploy from a Do-217K bomber. The rocket-powered DFS 228 would then climb to 82,000 feet and make observations above interceptors. In another experiment, fighters were strapped on top of old Ju-88 bombers. The bombers were unmanned and packed with explosives. Instead of releasing a small plane from a large aircraft, the fighter would direct the bomber to the target and release the bomber. From then on, the bomber would function as a glide bomb as the pilot returned to base on the fighter. A few missions were carried out. But with no proper guidance, it inflicted little damage on the enemy. Toward the end of the war, Japan built the Ohka and put it in service. It is a rocket-powered, manned aircraft with an explosive warhead in the fuselage. G4M bombers would bring the Ohka to altitude and release it. The Ohka would then ignite its engines and carry out a kamikaze attack.

The U.S. did not conduct any parasite fighter experiments during the war. But the idea was rekindled towards the end of the war. If there is one lesson the U.S. has learned from WWII, it is that bombers will not always get through, contrary to pre-war doctrine. Lone bombers suffered heavy casualties at the hands of enemy interceptors. Bombers must be escorted. The P-51 Mustang, which was first designed and built for the RAF, turned out to be a remarkable escort fighter. When the Army Air Force was looking for the next escort fighter, the parasite fighter concept was brought back onto the table. McDonnell came forth with the XF-85 Goblin. Designed to fit into the bomb bay of the B-36 Peacemaker, the XF-85 was round and short. It has folding wings and six fins at the back as stabilizers. Two were built for evaluation. During testing, test pilots experienced repeated difficulty hooking on due to turbulence under the bomber. The aircraft, built under heavy restraints, offered lackluster performance. It has been said that the pilot is limited to 5'6" tall and 200 lb heavy, including full equipment [1]. The project was ultimately abandoned in 1949. The purpose-built parasite fighter never once flew from the

intended mothership B-36, as it was not ready when the XF-85 was tested. The XF-85 was tested under a B-29.

The now-independent USAF pressed on with new experiments. Project Tip Tow attempted to dock two EF-84Ds to a B-29 through the wingtips. Each aircraft was modified with a boom in the wingtip, which would be used for docking after airborne. Overall, the initial experiment was a success. Multiple tests were conducted. On one occasion, the three aircraft stayed attached for two and a half hours. Connecting wingtip to wingtip increases the aspect ratio and, therefore, the aerodynamic efficiency. Depending on the optimization of the mission profile, the B-29 suffered between a 2.9% and 7.5% range penalty while enjoying the company and protection from the two F-84s [5]. Because the fighters dock after airborne and generate their lift, the wing of the bomber does not take the load of the fighters. Minimum structural strengthening is needed for the wing. The fighters could contribute to the rolling of the bomber through the use of the elevator. After the fighters were docked, the engine could be shut down and restarted without issue. However, wingtip vortices, wing flex, and vibration caused concerns. And because all three aircraft were controlled separately manually, inputs must be carefully coordinated to avoid stressing the aircraft. In 1953, testing was restarted to develop an electrical autopilot system to control the coupled aircraft. On April 24th, autopilot failure led to one of the F-84s crashing into the B-29, putting an end to project Tip Tow. A similar Project, Project Tom-Tom, was conducted in parallel. A B-36 was used in place of the B-29, while swept-wing RF-84Fs were used in place of the straight-wing EF-84Ds. Both projects faced similar challenges. Project Tom-Tom was also abandoned in 1953.

The FICON Project is the last attempt at the parasite fighter concept from the USAF. The XF-85 concept was recycled. But instead of building a new fighter that can be fitted into a B-36, an F-84 is used. By this time, the focus of the parasite fighter has shifted from bomber escort to attack. The B-36 would bring the F-84 to the enemy while the F-84, using its speed and agility, would serve as the last leg to deliver a tactical nuclear weapon. A trapeze mechanism was used to bring the F-84 into the bomb bay and lower it into the deploy position. Although the F-84 was unable to be fully stowed in the B-36, the F-84 pilot was still able to enter and exit his aircraft, making an extended mission more bearable. When the RF-84F entered service, the focus shifted again from attack to reconnaissance. The FICON Project was completed after seven flights. In March 1955, the USAF took delivery of 10 modified B-36 and 25 RF-84K. The RF-84K was modified to have retractable hookup equipment and retain its four Browning machine guns, allowing it to defend the mothership should the need arise [6]. Their service would be short-lived as the U-2 entered service in 1956.

1.2.2 Unmanned Combat Aerial Vehicle (UCAV)

UCAV is a term used to describe an unmanned aerial vehicle capable of carrying aircraft ordinances such as bombs and missiles. The renowned MQ-1 Predator is an example of a UCAV. A UCAV can still carry out surveillance and reconnaissance missions, making them highly

versatile. Extensive research on UCAV is being conducted at this very moment. In one research, a neural network is used to train the UCAV on how to evade air-to-air missiles successfully [7]. However, much of the research focuses on the control system of the aircraft. While the research is valuable and can be incorporated into the proposed aircraft, the control system is outside the scope of this project.

1.2.3 Comparative Study

Because the concept of a parasite fighter fell out of favor a long time ago, there is no direct comparison to the aircraft proposed here. However, some aircraft are trying to serve a similar, if not the same, objective. Air forces around the world have recognized the advantage of UCAV and are developing autonomous aircraft which support manned fighters in combat. Following are two examples. Unfortunately, information and specifications on them are scarce.

The XQ-58 Valkyrie is a UCAV developed by Kratos Defense & Security Solutions for the USAF. It is 30 ft long and 27 ft wide in wingspan. It has a launch weight of 6,000 lb and a payload of 1,200 lb in two bays. It cruises at Mach 0.72 and has a range of about 3,000 nm [8]. The Airpower Teaming System, also known as the Loyal Wingman project, is a similar aircraft developed by Boeing Australia for the Royal Australian Air Force. Less information is available about this aircraft. According to Boeing, it has a fighter-like performance. It is 38 ft long. It has a range of more than 2,000 nm [9].

These two are similar to the proposed aircraft in this project in that they:

- Carry payload
- Are designed to work together with manned fighter
- Take the incoming fire for the manned fighter if needed

At the same time, they are different in that they:

- Are full-sized aircraft
- Are self-propelled throughout the mission
- Are designed with an emphasis on stealth
- Can conduct surveillance and reconnaissance mission,
- Can also conduct missions on their own or as part of a drone swarm.

1.3 Mission Specification

1.3.1 Project Proposal

This project aims to design a UCAV that is carried and deployed by fighters. It would deploy, conduct its mission, and return to base under its own power. Depending on its payload, the UCAV can carry out an air superiority or ground strike mission.

When carrying air-to-air missiles, the UCAV can provide cover for allied aircraft. The manned fighter can focus on their ground strike mission. If needed, the UCAV can team up with the manned fighter and hunt down enemy aircraft while launching attacks from multiple directions. The mere presence of the UCAV also means that the enemy has more targets to choose from, reducing the chance of a manned fighter getting targeted.

When carrying air-to-ground ordinance, the UCAV can conduct strikes on enemy surface units. The manned fighter and the UCAV can break up and strike different targets simultaneously, minimizing the number of runs the manned fighter must conduct and reducing its time over the combat area and, ultimately, the chance of enemy retaliation.

A manned fighter will carry two of these UCAVs on their wingtips. One lesson learned from the many experiments conducted is that vortices and turbulence make docking extremely dangerous. While the risk can be mitigated through modern sensors and sophisticated autopilot, it is much easier to avoid these challenges entirely. The UCAV would carry enough fuel to loiter and return to base. This design also allows the manned fighter to leave the drones behind to defend other friendly units.

The XQ-58 and the Airpower Teaming System are ways to bring in extra presence and ordinance while maintaining stealth, which is very important in the modern air force doctrine. The proposed UCAV, however, is more of a way to redistribute the existing payload and utilize it differently. While it worsens the stealth and agility of the carrier, with the correct configuration, the UCAV can benefit the manned fighter. If positioned correctly, the manned fighter can use the wing of the UCAV as an extra lifting surface. The engines of the UCAV can potentially serve as thrust vector nozzles for the manned fighter and make up for the lost agility.

1.3.2 Mission Requirement

This project calls for an aircraft with the following requirements:

- Gross weight of no more than 3000 lb.
- Payload of at least 400 lb, with a target of 800 lb.
- Range of 1,500 km
- Loiter time of 30 minutes.

- Cruise Speed of Mach 0.85
- Thrust-to-weight ratio comparable to a manned fighter jet
- The ability to be carried and deployed from a fighter jet (e.g., F-16, F-35)

1.3.3 Project Profile

Because the UCAV would be carried by the manned fighter and deployed before entering battle, there is no takeoff, climbing, and cruising to the target in the first half of the profile. In a way, the mission profile is similar to that of a glider. The aircraft is expected to deploy, initiate combat (loiter), and return to the airfield under its own power.

1.4 Methodology

Roskam's and Raymer's equations and RDS are used to size the aircraft and determine its configuration. XFLR5 is used to determine the performance of the lifting surfaces. Matlab and Excel are used to perform calculations and plot graphs. Finally, Solidworks is used to create a detailed CAD model of the aircraft.

2. Weight Estimate

2.1 Introduction

The weight of the aircraft was estimated using hand calculation, which employed a mix of Raymer's and Roskam's methods, which can be found in [10] and [11], respectively. RDS was then used to verify the results. There was a conflict between the two results. However, an aircraft that satisfies both the performance and weight requirements still appeared plausible.

2.2 Detailed Explanation

2.2.1 Assumptions

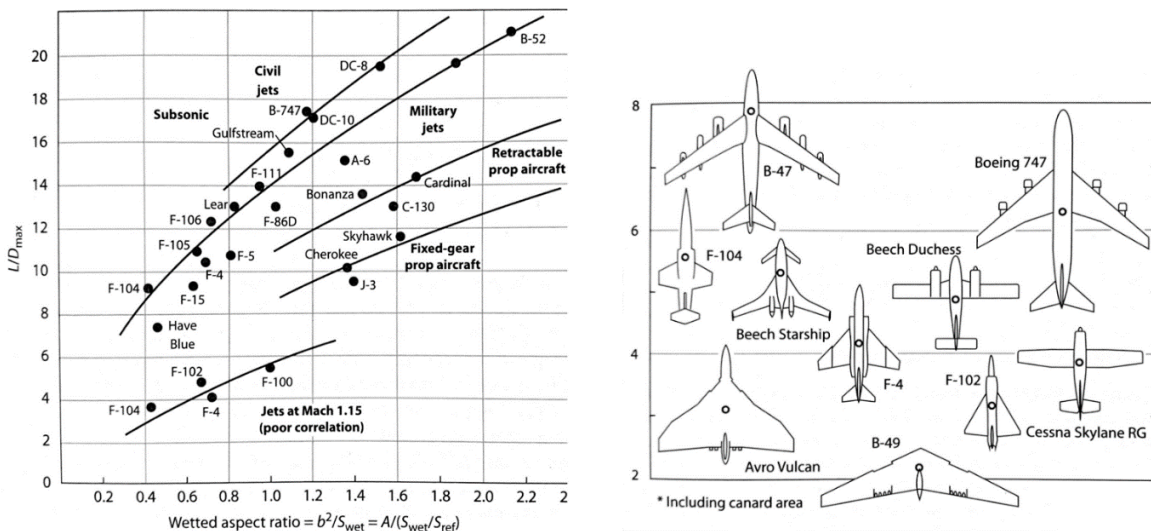


Figure 2.1 - Raymer's lift-to-drag ratio estimation.

Before performing weight sizing, a few values needed to be obtained. Two graphs from Raymer were used to estimate the lift-to-drag ratio of the aircraft. This aircraft was envisioned to have a tailless delta configuration. The closest aircraft on the chart would be the Avro Vulcan. The Avro Vulcan has wetted area ratios of 3. The wetted aspect ratio was found using equation 2.1.

$$\text{Wetted aspect ratio} = \frac{b^2}{S_{Wet}} = \frac{b^2}{S_{ref} * \text{wetted area ratio}} \quad (2.1)$$

With a wing area of 330.2 m² (3,596 ft²) and a span of 30.30 m (100 ft²), the wetted aspect ratio of the Avro Vulcan was calculated to be 0.927. Using the left graph in figure 2.1, following the curve for military jets, the maximum lift coefficient was estimated to be 15. For a jet, the lift-to-drag ratio for loitering is simply the maximum ratio, 15. The lift-to-drag ratio for cruising is 0.866 times the maximum, which is about 13.

2.2.2 Hand Calculation

The total mission weight fraction is the product of the individual weight fractions for each mission segment. For this aircraft, the mission consists of five segments: engine start, combat or loiter, cruise, descend, and land. For engine start, descend, and land, the estimations are fixed. Roskam estimated them to be 0.990, 0.990, and 0.995, respectively.

The weight fraction for loitering can be calculated using

$$\frac{W_i}{W_{i-1}} = e^{-EC_L \left(\frac{L}{D}\right)_L} \quad (2.2)$$

The weight fraction for cruising can be calculated using

$$\frac{W_i}{W_{i-1}} = e^{-\frac{RC_C}{v \left(\frac{L}{D}\right)_c}} \quad (2.3)$$

Table 2.1 shows all the symbols, and their values used to calculate the weight fractions. The engine was assumed to be a pure turbojet. In the end, the weight fractions for loiter and cruise were calculated to be 0.991 and 0.9281. The total weight fraction is 0.8975, meaning the fuel fraction is 0.1025. The calculated fuel fraction was multiplied by 1.06 to account for reserve fuel, bringing the final fuel fraction to 0.10865.

$$W_{0,calculated} = \frac{W_p}{1 - \frac{W_e}{W_{0,guess}} - \frac{W_F}{W_{0,guess}}} \quad (2.4)$$

Equation 2.4 was used to calculate the gross weight of the aircraft. It is an iterative process. The calculated gross weight may not match the guessed gross weight for the first iteration. The

guessed gross weight is adjusted for the following iterations until the two numbers are within a few percent of each other.

Table 2.1 - Variables and values used in weight fraction calculation.

Parameter	Symbol	Metric	Imperial
Cruise Specific Fuel Consumption	C_C	25.5 mg/(Ns)	0.9 hr ⁽⁻¹⁾
Loiter Specific Fuel Consumption	C_L	22.7 mg/(Ns)	0.8 hr ⁽⁻¹⁾
Endurance	E	30 min	
Cruise lift-to-drag ratio	$(L/D)_C$	5	
Loiter lift-to-drag ratio	$(L/D)_L$	6	
Range	R	1,500 km	937 miles
Cruise speed	V_c	980 km/hr	612 mph
Payload weight	W_p	454 kg	1000 lb

2.2.3 RDS

The RDS is very similar to the hand calculation. The underlying equations are the same as Raymer's equations. However, there are some differences in the mission profile. Firstly, there is no engine start segment in RDS. Secondly, when determining the mission profile in RDS, combat was one of the options. In the hand calculation, loiter was used in place of combat. But because combat was available, it was used in RDS. The combat altitude was set at 5,000 m or 16,500 ft. The aircraft would perform six turns in combat. In the end, RDS estimated the weight of the aircraft to be 1,277 kg or 2,809 lb.

2.3 Results

Table 2.2 - Calculated weight fraction.

Parameter	Symbol	Hand calculation	RDS
Engine start	W_1/W_0	0.990	-
Loiter/ combat	W_2/W_1	0.9342	0.9465
Cruise	W_3/W_2	0.7676	0.7132
Descent	W_4/W_3	0.990	0.9900
Landing	W_5/W_4	0.995	0.9950
Fuel with reserve	W_F/W_0	0.3187	0.3552
Aircraft gross weight	W_0	1,122 kg / 2,468 lb	1,277 kg / 2,809 lb

2.4 Discussion

There is a discrepancy between the hand-calculated value and the result from RDS. The first discrepancy exists between the weight fractions for the combat or loiter segment, which was pointed out earlier. This result should not come as a surprise. When loitering, the aircraft flies at the maximum lift-to-drag ratio while the aircraft consistently maneuvers and expends energy in combat. The weight fraction for combat should be smaller than that of loiter.

The second discrepancy exists between the weight fractions for the cruise segment. While the exact cause of this difference is unknown, here are some potential contributing factors. In the earliest sizing, a cruise lift-to-drag ratio of 13 was used. This value would soon be proved to be an extreme overestimate. The drag calculation yielded a mere cruise lift-to-drag ratio of three. This seems to be an unrealistically low estimate. Even the F-104, which has the lowest maximum lift-to-drag ratio in Figure 2.1, has a subsonic cruise lift-to-drag ratio of about 7.8. The drag calculation will be expanded upon in the drag chapter. For the time being, with the given aircraft data, RDS used a cruise lift-to-drag ratio of 6.1 for the calculation.

It also is important to note the configuration used in the RDS calculation. Of the specifications set in the mission requirements, perhaps the payload and the combat radius influence the weight sizing the most. The aircraft is envisioned to be able to conduct both air superiority and ground strike missions. The 1,500 km range set in the mission specification is intended for air superiority missions. For air-to-air combat, there are two main types of ordinances a fighter may carry: AIM-9 and AIM-120. The former is a light, infrared missile with short range, while the latter is a heavy radar-guided missile with beyond visual range capability. A pair of AIM-9 weighs about 400 pounds, while a pair of AIM-120 weighs about 700 pounds. While it would be desirable for the aircraft to be able to carry AIM-120s for as far as possible, RDS was unable to converge to a gross weight under 3,000 lb. However, RDS was able to converge if the aircraft was to carry 500 lb for 1,500 km or 800 lb for 1,000 km.

2.5 Conclusion

There were discrepancies between the hand calculation and the RDS result. However, the result from RDS suggests that the minimum requirement of carrying 400 lb of payload at 1,500 km while maintaining a gross weight of less than 3000 lb, can be met. The aircraft can carry a heavier payload with a compromise in range.

3. Wing and Propulsion Sizing

3.1 Introduction

A matching graph, created in MATLAB, was used to determine the wing loading and thrust-to-weight ratio of the aircraft. The equations used here can be found in [12].

3.2 Detailed Explanation

There are multiple curves on a matching graph, each representing one attribute of the aircraft. Depending on the nature of the aircraft, the matching graph may have a different number of curves. This graph has five curves representing stall speed, cruise speed, landing, climb, and maneuver. The equations used here all originate from Roskam. The code and values used in the calculation can be found in appendix C.

3.2.1 Stall Speed

Stall speed is essential for every aircraft, as they must fly fast enough to stay in the air. After rearranging the equation, the stall speed is only a function of wing loading. The wing loading can be found using equation 3.1.

$$\frac{W}{S} = \frac{1}{2} \rho V_{stall}^2 C_{L_{max}} \quad (3.1)$$

The targeted stall speed is 150 knots.

3.2.2 Cruise Speed

Cruise speed is a function of both thrust-to-weight ratio and wing loading. To plot the curve, the ratio is isolated on the left-hand side and can be found using the equation (3.2). The 0.9^{-1} represents the throttle of the engine. Typically, the wing loading would be multiplied by a factor representing the percentage of gross weight. However, this aircraft would start the mission at gross weight since it will be deployed from a manned fighter in midair. The factor is, therefore, one.

3.2.3 Landing

According to Roskam, the landing sizing can be done using the same equation in 3.2.1. The stall speed is substituted with the approach speed. In a military setting, the approach speed is 1.2 times the stall speed.

$$\frac{T}{W} = \frac{1}{0.9} \left(\frac{\rho_o}{\rho} \right)^{0.75} \left[\frac{C_{D0} \frac{1}{2} \rho V_{cruise}^2}{\frac{W}{S}} + \frac{\frac{W}{S}}{\pi A R e \frac{1}{2} \rho V_{cruise}^2} \right] \quad (3.2)$$

$$\frac{T}{W} = \left(\frac{\rho_o}{\rho} \right)^{0.75} \left(\frac{c}{\sqrt{\frac{2 \frac{W}{S}}{\rho_{sl} C_{L_{climb}}}}} + \frac{C_{D_{climb}}}{C_{L_{climb}}} \right) \quad (3.3)$$

$$\frac{T}{W} = \left(\frac{\rho_o}{\rho} \right)^{0.75} \left[\frac{\left(C_{D0} \frac{1}{2} \rho V^2 \right)}{\frac{W}{S}} + \frac{W}{S} \frac{n_{max}^2}{\pi A R e \frac{1}{2} \rho V^2} \right] \quad (3.4)$$

3.2.4 Climbing

Climbing is a function of both thrust-to-weight ratio and wing loading. Because the aircraft would be deployed in midair near the mission area, climb performance is not as important. However, if it has completed a ground strike mission, the aircraft will be low to the ground and needs to climb to cruising level before returning to base. In this scenario, the aircraft is assumed to climb from 1,000 m (3,300 ft) to 5,000 m (16,500 ft) in three minutes. After arranging the equation, the thrust-to-weight ratio can be found using this equation.

The C_D is assumed to be four times the C_{D0} .

3.2.5 Maneuvering

Maneuvering is also a function of both thrust-to-weight ratio and wing loading. Thrust is especially important since an aircraft constantly loses energy in a maneuver. For a sustained turn, the engine must provide enough thrust. After rearranging the equation, the thrust-to-weight ratio can be found using equation 3.4. The target load factor is 5 g at Mach 0.8.

3.3 Discussion

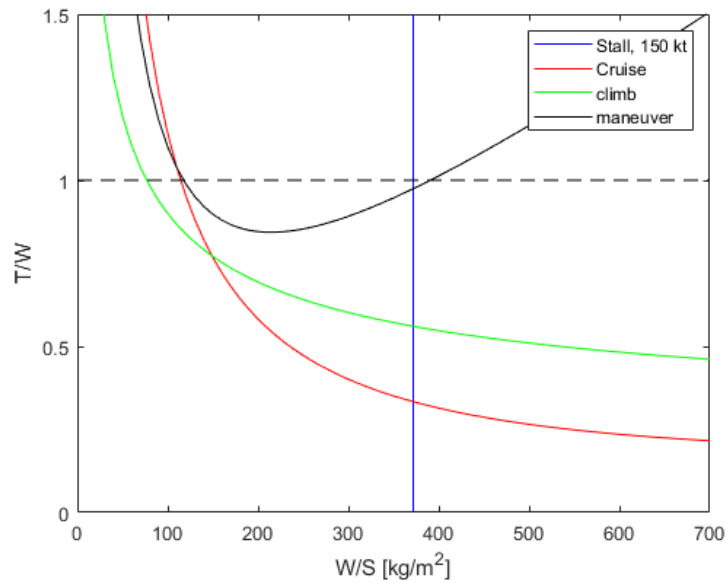


Table 3.1 - Matching graph.

The wing loading requirement is satisfied in the region to the left of the vertical lines. For the thrust-to-weight ratio, the requirement is satisfied in the region above the curve. In this case, the climb and cruise curves do not play a crucial role in determining the minimum cost point. If the target stall speed is 150 knots, the minimum cost point is located at a wing loading of 370 kg/m² (74.5 lb/ft²) and a thrust-to-weight ratio of 0.9725.

In early sizing, a maximum lift coefficient of 0.55 was used. This was due to an incorrect assumption that a delta wing is incapable of generating a high lift coefficient. A highly swept delta wing can also generate a high lift coefficient at a higher angle of attack by taking advantage of vortex lift. With no high-lift devices, a modest lift coefficient value of one was used in the calculation.

3.4 Conclusion

The aircraft would be designed to have a thrust-to-weight ratio of one and a minimum wing loading of 370 kg/m², or 74.5 lb/ft².

4. Configuration Selection

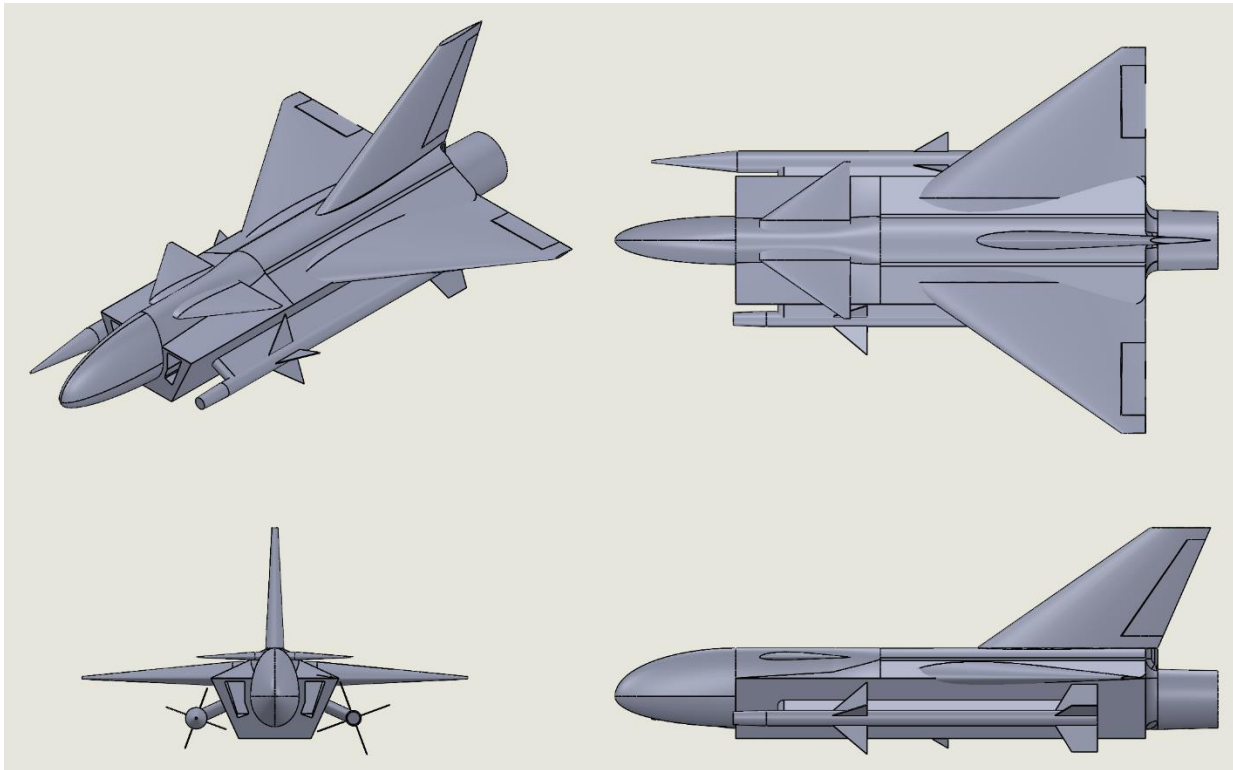


Figure 4.1 - Isometric and three-view drawing of the aircraft.

4.1 Overall Selection

The aircraft has a cropped delta wing in a shoulder mount configuration. A canard and a single-plane vertical stabilizer provide stability to the aircraft. It is powered by a single turbojet engine embedded in the rear of the fuselage. Lastly, the aircraft is supported by a tricycle landing gear system.

4.2 Wing Configuration

Delta wing is a popular configuration for supersonic fighters. But as described in the mission profile, this aircraft will only fly at high subsonic speed. A delta wing configuration was chosen here because of its structural efficiency. With a larger wing area, the wing can also employ an airfoil with a lower lift coefficient. The UAV is designed to be mounted on the wingtips of a manned fighter. When stowed, some of the lift generated is not useful for the manned fighter.

Yet, the aircraft will still experience the full lift-induced drag. Using an airfoil with a lower lift coefficient can mitigate this penalty.

4.3 Empennage Configuration

Initially, the aircraft was envisioned to have a tailless delta configuration. However, without a horizontal stabilizer, it is much more challenging to maintain the stability of the aircraft. While it is possible by carefully incorporating wing sweep and wing twist at the outboard portion of the wing, it is much easier to use a canard or a horizontal stabilizer. Therefore, the aircraft was designed to have a canard. The canard can use a positively cambered airfoil and contribute to the wing area of the aircraft. On a side note, the canard delta is a popular configuration used by highly maneuverable aircraft such as Saab Viggen and Eurofighter Typhoon.

As for the vertical stabilizer, a single-plane stabilizer was chosen for its simplicity and efficiency.

4.4 Propulsion Configuration

The aircraft is powered by a single turbojet engine. The engine is mounted on the rear of the fuselage. Side inlets supply the engine with air. From the front, the engine face is hidden to improve the stealth capability of the aircraft. Although stealth was never a focus, an effort was made to improve it as much as possible.

4.5 Landing Gear Configuration

The landing gear is in a tricycle configuration, which is conventional for jets. A tricycle configuration keeps the aircraft level and the jet blast from impacting the ground. Initially, the aircraft was envisioned to be gearless and land on a retractable skid. Omitting the landing gear could have saved on weight. But considering the UAV would operate at the same airbase and share a runway with other aircraft, landing on a skid may not be the best idea. Other configurations, such as the bicycle configuration on the U-2, were also considered. Ultimately, the tricycle configuration was selected for ease of ground operation and stowage.

The front landing gear has a strut as wide as that of the main gear. It also has two wheels instead of one. This was done because the center of gravity does not sit forward of the main landing gear, requiring the nose gear to bear load. The double wheel is an attempt to reduce tip over.

4.6 Payload Configuration

Since this is a small UCAV carrying ordinances intended for full-size fighter jets, there is no space for a bomb bay. The ordinance is to be carried externally. The aircraft would have two pylons at the side of the fuselage. It would carry a pair of identical missiles to maintain balance. The aircraft is primarily designed to carry AIM-9 or AIM-120, though the newer missiles such as the ASRAAM, meteor, and air-to-ground missiles such as the Hellfire were anticipated.

5. Fuselage Design

5.1 Fuselage Layout

The fuselage is 4.5 m (14.9 ft) long, 0.91 m (3 ft) wide, and 0.85 m (2.8 ft) tall. The shape of the fuselage was inspired by that of the F-22 and F-35. The cross-section of the nose cone is an ellipse that has a dimension of 0.4 m (1.3 ft) wide and 0.5 m (1.7 ft) tall at 1 m (3.3 ft) from the front. The cross-section of the aft fuselage resembles an inverted trapezoid with a curved top for the engine. In Figure 5.2, canals can be observed at the bottom of the fuselage in section view B. Those are for attaching the drone to the wingtip of the manned fighter. The attached drone can be seen later in Figure 18.8.

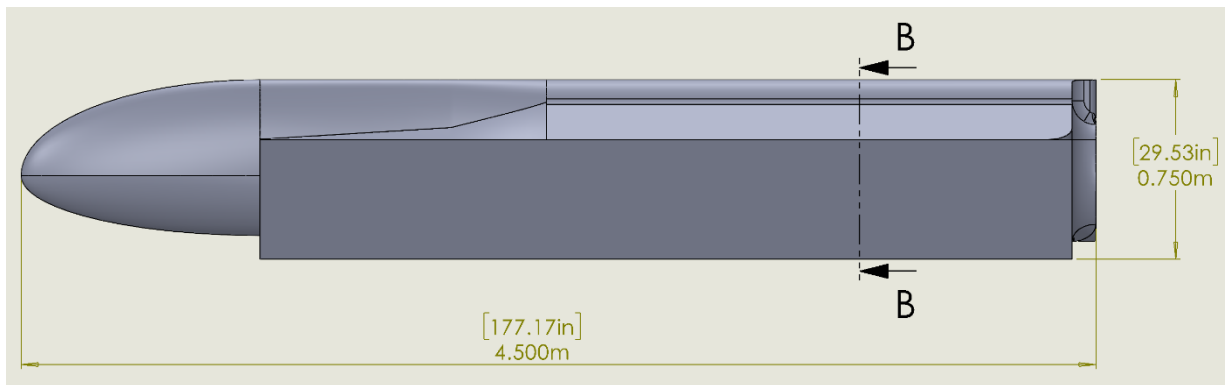


Figure 5.1 - Fuselage dimensions.

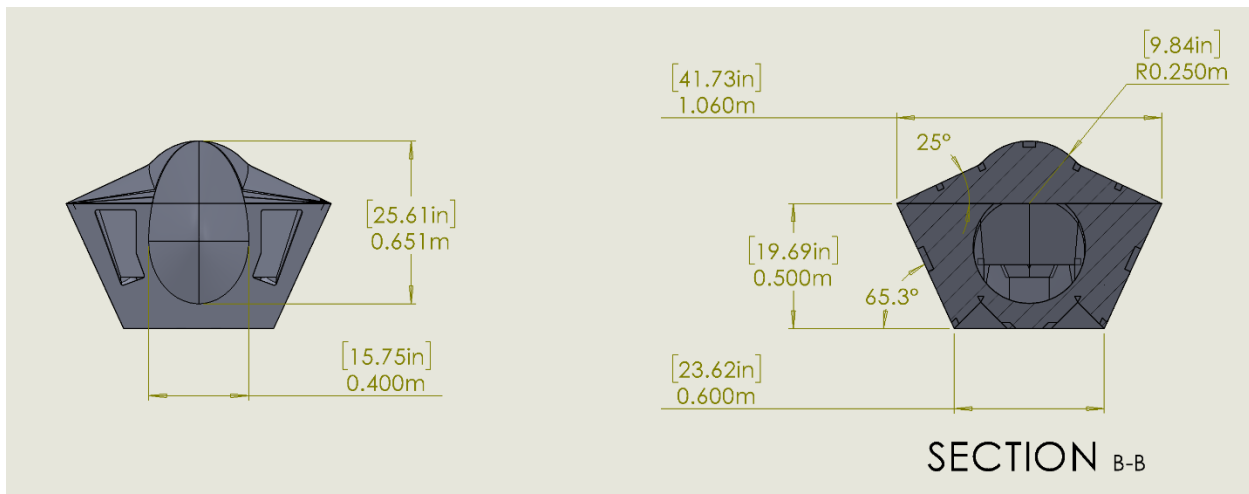


Figure 5.2 - Fuselage cross-section.

The nose and the front of the fuselage body are where the necessary avionics sit. The bottom of the forward fuselage body also houses the front landing gear.

The engine intakes are located next to the nose cone at 1 m (3.3 ft) from the front. The air intakes merge into one single air duct that leads to the engine buried deep inside the fuselage. The engine is 3.2 m (10.6 ft) from the front of the aircraft. The engine nozzle is 0.5 m long, bringing the total length of the aircraft to 5 m (16.5 ft).

The UAV is docked to the wing of the manned fighter through a mounting at the bottom of the fuselage.

5.2 Discussion

On a manned fighter jet, the pilot would typically sit just behind the nose cone and before the main fuselage. Since this is a UAV, a pilot is not needed, and the space typically allocated for them can be relinquished to the avionics and equipment. The absence of a pilot also means that instrument, oxygen, and pressurization equipment can be omitted. However, the size of the avionic is unknown, and the space may not be sufficient.

A concealed engine is the hallmark of a stealth aircraft. Engine blades are significant contributors to the radar cross-section of an aircraft. While this is not a stealth-focused aircraft, measures were still taken to reduce the radar cross-section wherever possible.

This CAD model only provides the general layout and shape of the fuselage. There is certainly room for improvement and optimization. For example, the nose should be pointier. There is too much flat surface at the air inlets. The current design adds unnecessary drag and radar signature. However, these features are outside the scope of this project.

5.3 Conclusion

For now, this fuselage design should provide enough internal volume for the subsystems of the aircraft. While it can be refined for better drag and stealth performance, it is adequate for the scope of this project.

6. Wing Design

6.1 Wing Platform Design

6.1.1 Wing Platform Design Criteria

For this aircraft, there are no hard criteria that drive the wing design. However, there are a few features that may be preferred. Firstly, a shorter wing is more maneuverable for ground operation. When the UAV is docked to the manned fighter, a shorter wing will reduce the chances of ground strike and collision. Secondly, an airfoil with a lower coefficient of lift may be preferred. The higher the lift coefficient of the wing, the more lift-induced drag it produces. When stowed, the wing of the UAV is still producing lift. However, the wing may be orientated in a way that some of the lift produced is not useful to the manned fighter. An airfoil with a lower lift coefficient can reduce the lift-induced drag produced. Such airfoil is often used in a flying wing design.

6.1.2 Wing Platform Design

With the two preferable features in mind, a cropped delta wing with a low-lift airfoil was selected. Figure 6.1 depicts the shape of the wing, while Figure 6.1 and Table 6.1 detail the dimensions of the wing.

Table 6.1 - Wing parameter.

Parameter	Metric	Imperial
Reference Wing Area (S)	4.15 m ²	45.2 ft ²
Aspect Ratio (AR)		2.47
Taper Ratio (λ)		0.10

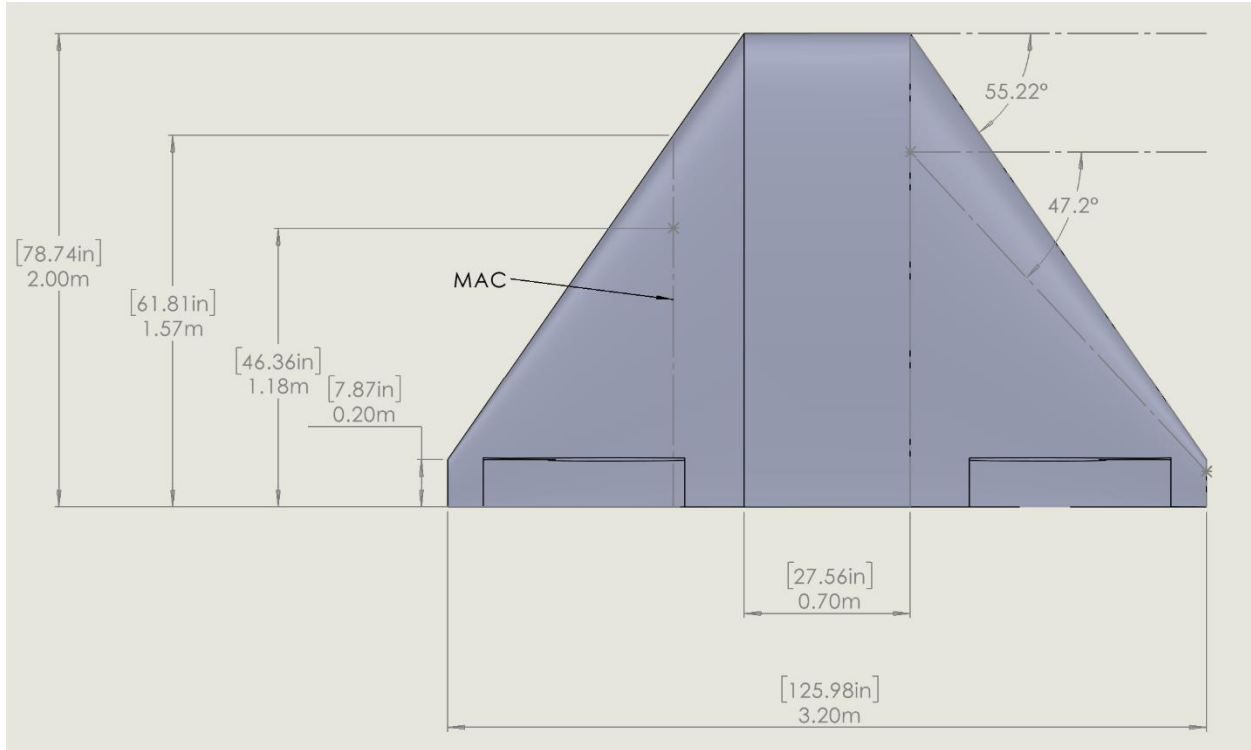


Figure 6.1 - Wing drawing.

6.2 Airfoil Selection

A low-lift airfoil is most often featured on flying wings. Therefore, a series of flying wing airfoils, the MH 60 series, to be specific, was examined. There are four entries in the MH 60 series: 60, 61, 62, and 64. After comparison, the MH 60 was selected. MH 60 has one of the higher thicknesses at 10.1% at 26.9% chord. A thicker wing can produce more internal volume for fuel and higher structural efficiency. And since the aircraft is flying at high subsonic speeds, a thin airfoil is unnecessary. The MH 60 has a maximum camber of 1.7% at 36.6% of the chord. All four airfoils bar MH 61 have comparable performance at low AOA. However, the MH 60 has a better lift-to-drag ratio as the AOA increases. The MH 60 also stalls at a higher angle of attack.



Figure 6.2 - MH 60 airfoil.

6.3 High Lift Devices

There is no plan to fit the wing with any high-lift devices. Without the aid of high lift devices, a delta wing can already sustain a high angle of attack. This aircraft is also extremely light and should not have difficulty coming to a stop on landing. Traditionally, delta-wing aircraft do not have flaps, which can produce pitching moments when deployed. However, with fly-by-wire systems, more and more delta-wing aircraft are fitted with flaperon. There certainly is space for flaperon. However, with the rear of the missile and main gear nearby, the inboard trailing edge of the wing is already very crowded. Therefore, the aircraft would not be fitted with a flaperon.

6.4 Wing Controls

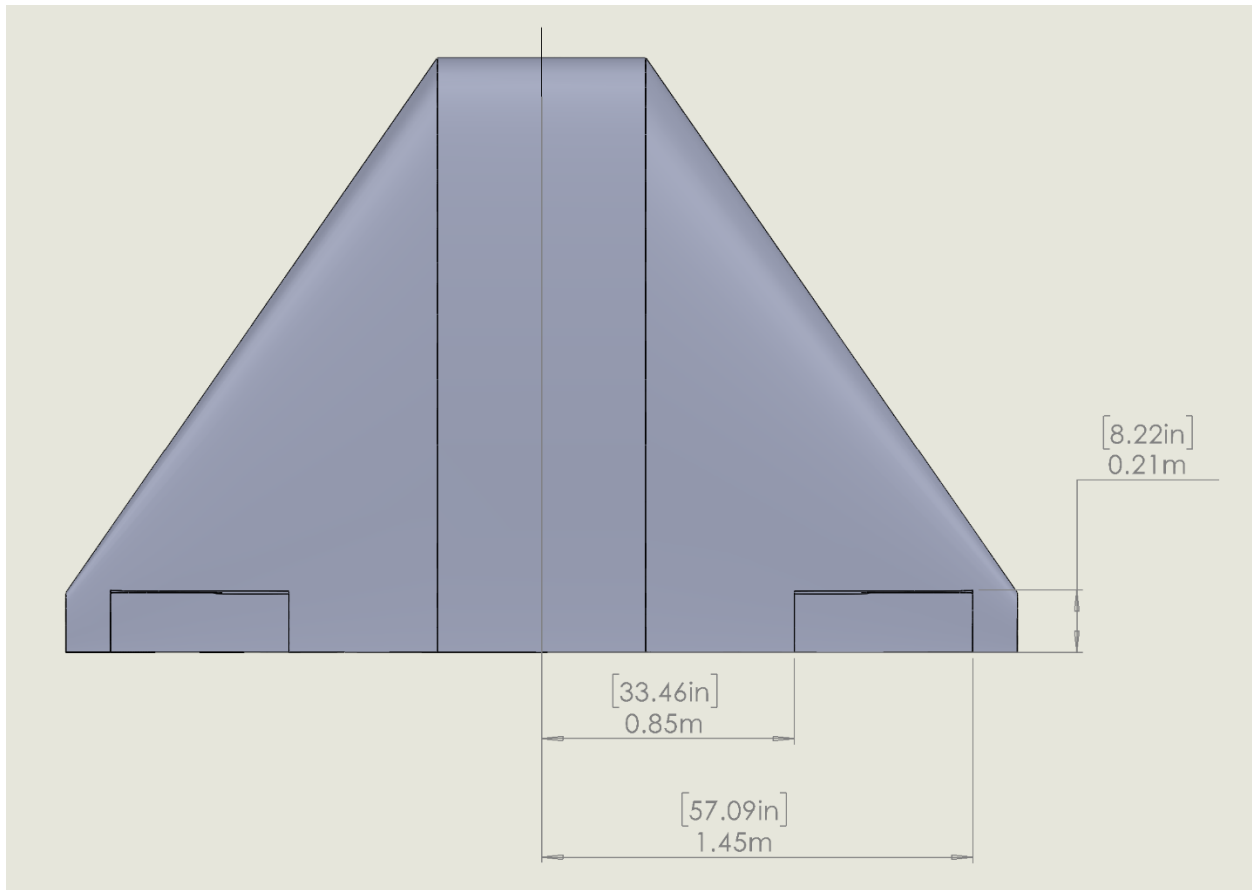


Figure 6.3 - Aileron drawing.

Figure 6.3 shows the dimensions and location of the aileron. The aileron has a constant chord of 0.21 m or 8.22 in. The aileron spans between 0.53 and 0.90 of the wingspan. The aileron stops at 90% of the wingspan because the last 10% has little control effectiveness due to wingtip vortices.

The inboard aileron location is determined using historic aircraft data from Roskam. The aileron chord is set at 0.21 m (0.69 ft), leaving ample space for spars to connect between the wing root ribs.

6.5 Wing Design Analysis

The clean maximum lift coefficient is estimated using the Raymer method [14]. For a low aspect ratio and high sweep wing, the maximum lift coefficient is the sum between $(C_{L_{max}})_{base}$ and $\Delta C_{L_{max}}$, which can both be found in Figure 6.5. Δy is determined by the geometry of the airfoil and can be found in Figure 6.4. Before it can be used in Figure 6.5, it must first be converted to percent of chord length. Δy has a value of 3.607% of the chord. β is a function of the Mach number. To determine the $C_{L_{max}}$ at stall speed, a Mach number of 0.20 was used. C_1 and C_2 are factors determined by the taper ratio of the wing. With a taper ratio of 0.1, C_1 and C_2 both have a value of 0.25. $(C_{L_{max}})_{base}$ and $\Delta C_{L_{max}}$ were calculated to be 0.90 and 0.025, respectively. The wing has a clean $C_{L_{max}}$ of 0.925. On a side note, the angle of attack for maximum $C_{L_{max}}$ was calculated to be 23 degrees.

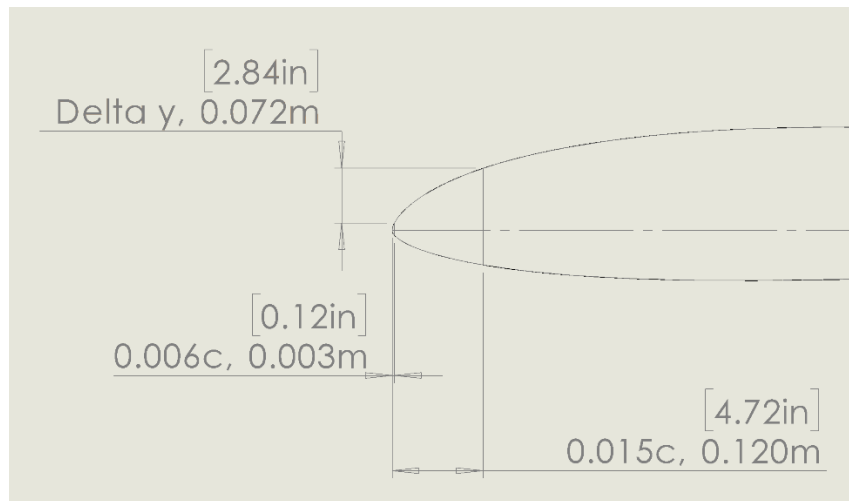


Figure 6.4 - Leading edge of the MH 60 airfoil.

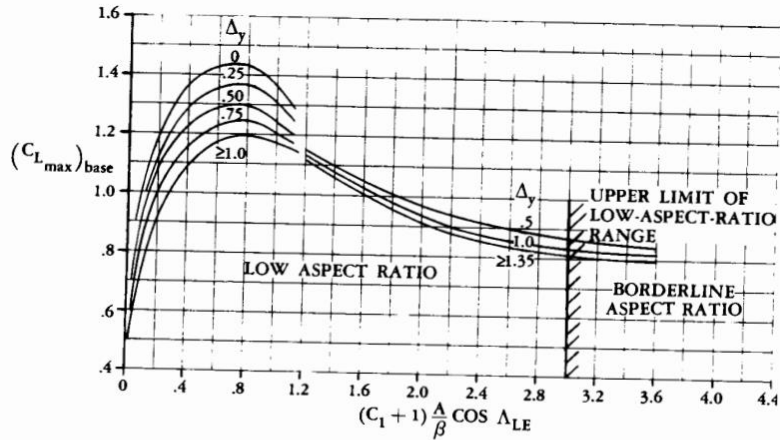


Fig. 12.12 Maximum subsonic lift of low-aspect-ratio wings. (Ref. 37)

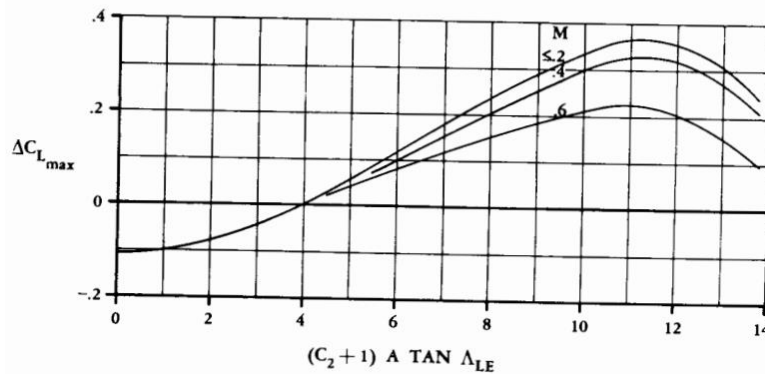


Fig. 12.13 Maximum-lift increment for low-aspect-ratio wings. (Ref. 37)

Figure 6.5 - Graphs to determine $(C_{L_{max}})_{base}$ and $\Delta C_{L_{max}}$.

6.6 Discussion

The calculated $C_{L_{max}}$ falls short of the value used in the wing sizing, 1. The question of whether or not this wing design satisfies the requirements will be further explored in Chapter 17, critical performance requirement.

There was an attempt to calculate the $C_{L_{max}}$ using XFLR5. However, it failed to converge before reaching $C_{L_{max}}$. The last data point is located at 0.904 C_L and 19.5 degrees.

6.7 Conclusion

The performance of the wing will be further explored in Chapter 17, critical performance requirement.

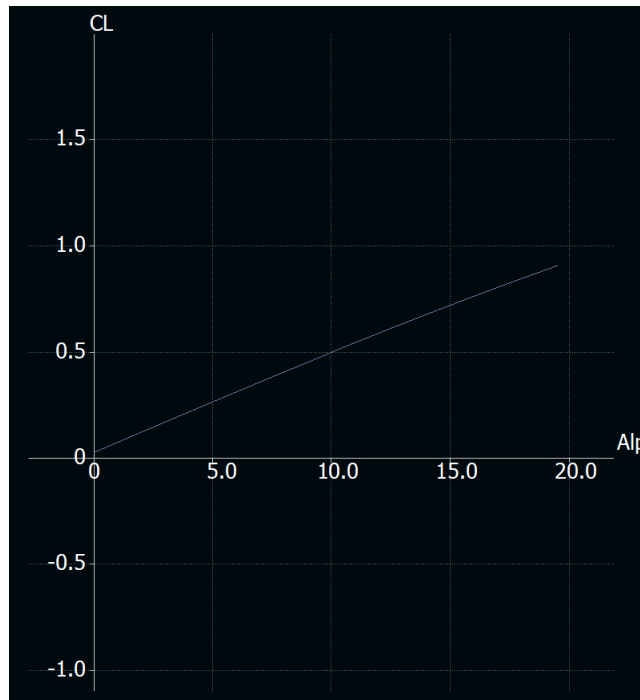


Figure 6.6 - Calculation of $C_{L_{max}}$ using XFRLR5

7. Empennage Design

7.1 Canard Design

7.1.1 Canard Airfoil Selection

On a conventional wing-tail layout, the wing and tail are aft of the CG. To maintain longitudinal stability, the tail must produce a negative lift to counteract the positive lift from the wing. Therefore, symmetric or even negatively cambered airfoil is often used. But on a canard design, the CG is typically between the canard and the wing, meaning a positively cambered airfoil can be used instead.



Figure 7.1 - MH 64 Airfoil.

The MH 60 was selected as the airfoil for the wing. For the canard, the MH 64 was selected instead. For the same reason explained in the wing chapter, a low coefficient of lift airfoil was selected for the canard. But instead of reusing MH 60 for the canard, the MH 64 was chosen because it stalls at a lower AOA compared to the MH 60. Even if the canard is not deflected, the canard will stall first and bring the nose of the aircraft down. The MH 61 stalls even earlier than the MH 64, making it a good candidate. However, it was not selected due to the inferior lift-to-drag performance.

The MH 64 has a maximum thickness of 8.6 % at 26.9% chord and a maximum camber of 1.4 % at 41.8% chord.

7.1.2 Canard Platform Design

In his book, Roskam has not provided a method for canard sizing. And while Raymer provided the method for it, the desired tail volume was not provided. For reference, three different canard delta aircraft were examined. The three aircraft were the Dassault Rafale, Eurofighter Typhoon, and Saab Gripen. The canard and vertical stabilizer of these aircraft were measured and modeled in XFLR5. XFLR5 automatically calculated the tail volume.

In the end, the Saab Gripen was selected as a reference. It has the closest layout, with the trailing edge of the canard sitting just above the leading edge of the wing. This is not a coincidence. Initially, the configuration of this UAV was inspired by the Saab Viggen, which is the earliest canard delta design and also the predecessor of the Saab Gripen. However, the three newest canard delta aircraft moved on and featured a flying canard. The Saab Gripen now serves as the inspiration for the canard design.

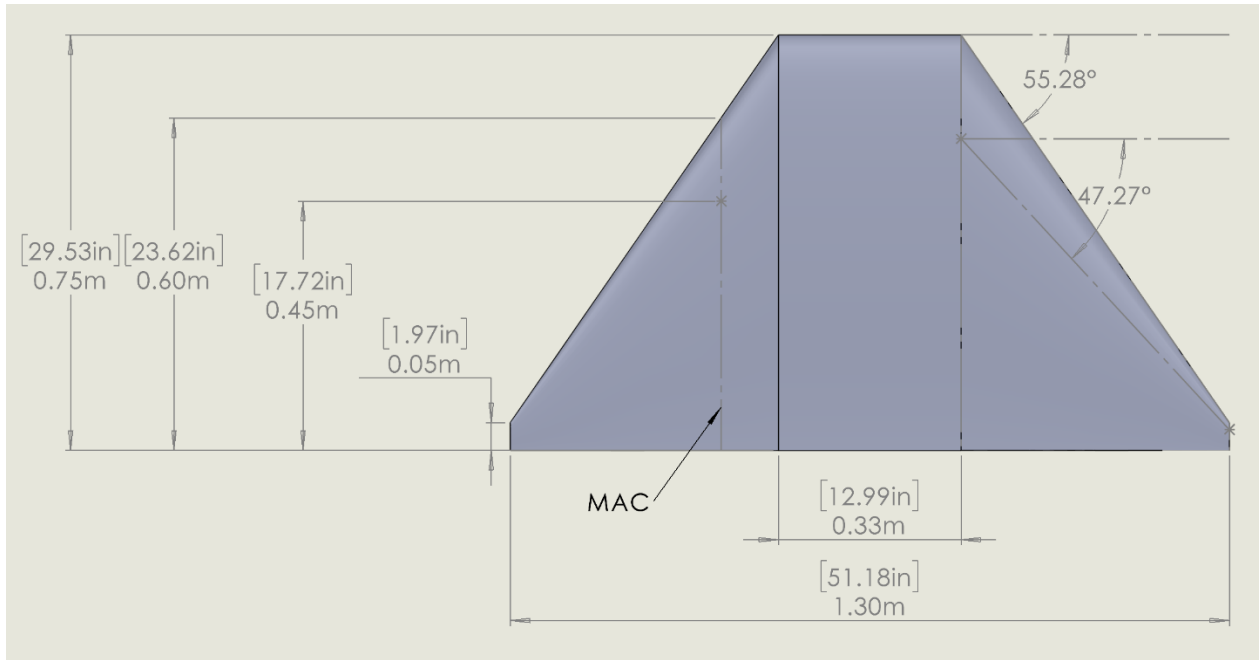


Figure 7.2 - Canard drawing.

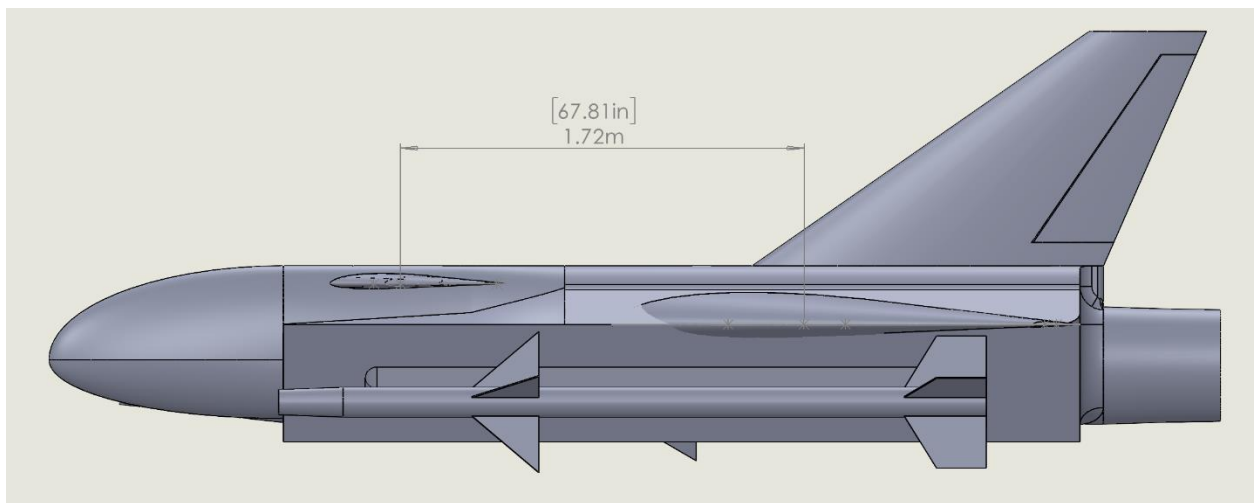


Figure 7.3 - Canard moment arm.

Table 7.1 - Canard parameter.

Parameter	Metric	Imperial
Reference Area (S_c)	0.64 m ²	6.97 ft ²
Aspect Ratio (AR_c)	2.66	
Taper Ratio (λ_c)	0.067	
Tail volume (v_c)	0.13	

The parameters of the canard are shown in Figure 7.2 and Table 7.1. The canard is positioned above the wing to keep the wing away from the downwash from the canard. But because of the clearance of the ordinance, the wing had to be mounted high at the shoulder, reducing the vertical displacement between the wing and the canard. The leading edge of the canard is carefully swept at an angle of 55.28°, very close to the 55.22° sweep of the wing. The parallel leading edge and trailing edge of the wing and stabilizer or canard is another feature of a stealth aircraft.

7.2 Vertical Stabilizer Design

7.2.1 Vertical Stabilizer Airfoil Selection

For the vertical stabilizer, a simple NACA 0010 airfoil was used. Typically, a vertical stabilizer does not require an airfoil with unique features. A simple symmetric one is sufficient.



Figure 7.4 - NACA 0010 airfoil.

7.2.2 Vertical Stabilizer Platform Design

The aircraft has a single-plane vertical stabilizer mounted on the fuselage. Figure 7.4 and Table 7.2 detail the dimensions. Figure 7.5 describes the dimensions of the rudder.

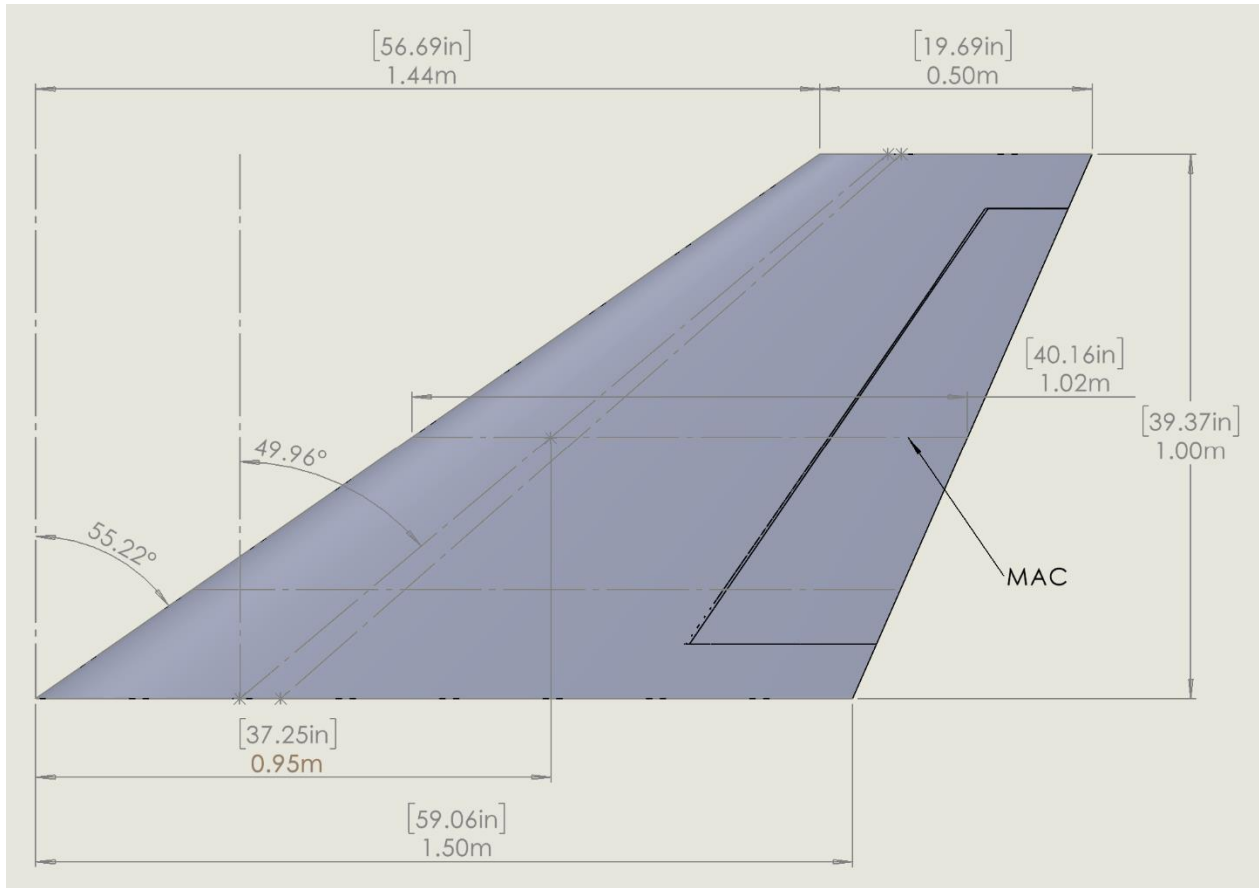


Figure 7.5 - Vertical stabilizer drawing.

Table 7.2 - Vertical stabilizer parameter.

Parameter	Metric	Imperial
Reference Area (S_v)	1 m ²	9.6 ft ²
Aspect Ratio (AR_v)	2.29	
Taper Ratio (λ_v)	0.3333	
Tail volume (v_v)	0.0695	

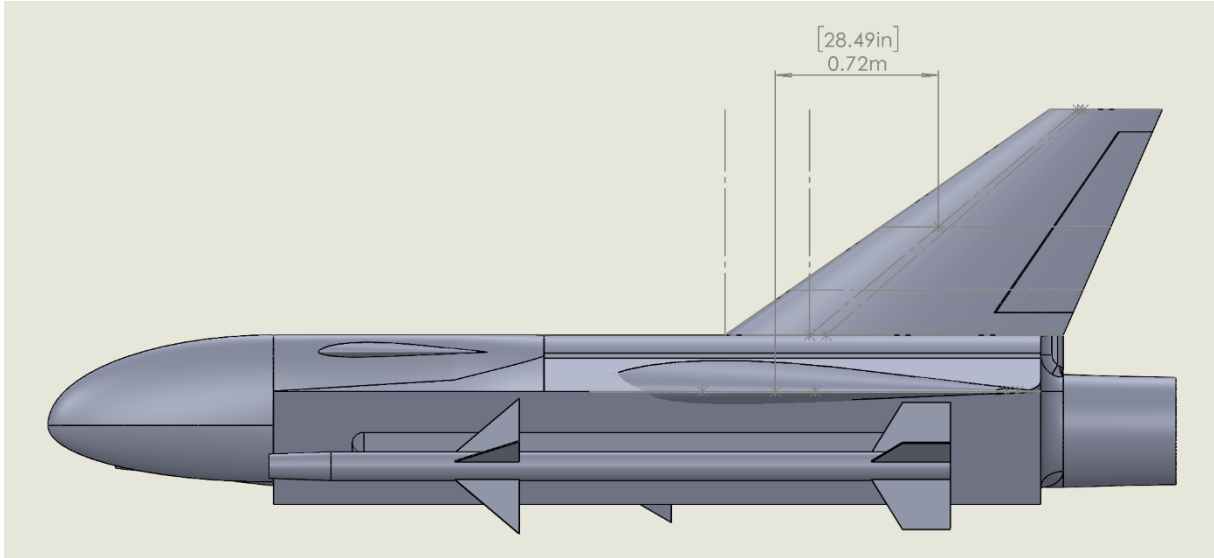


Figure 7.6 - Vertical Stabilizer Moment Arm.

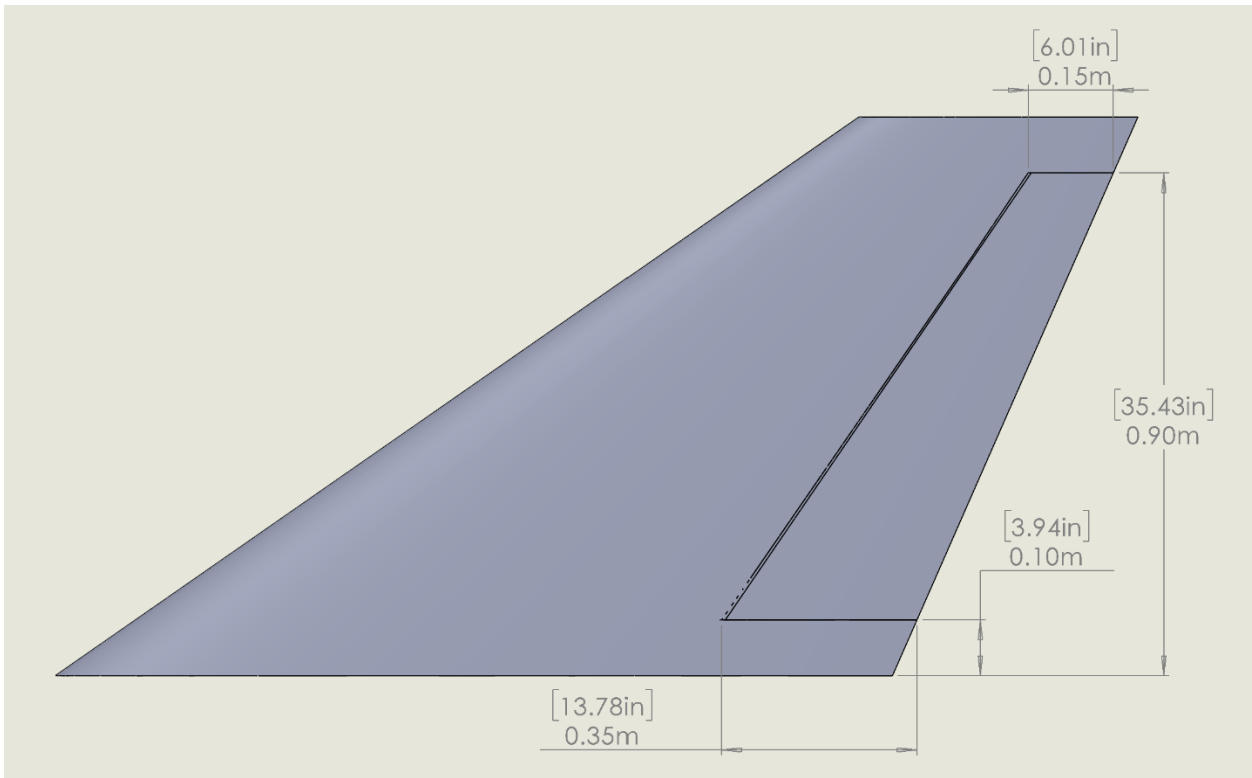


Figure 7.7 - Rudder dimensions

7.3 Discussion

XFLR5 calculated the canard tail volume of the Dassault Rafale, Eurofighter Typhoon, and Saab Gripen to be 0.12, 0.08, and 0.18, respectively. The current canard design yields a tail volume of 0.13, which is within the range of the three.

For the vertical stabilizer, Raymer recommends a tail volume of 0.07 for a fighter. The current vertical stabilizer design yields a tail volume of 0.0695, which is extremely close to the recommendation.

Since the canard also produces positive lift, technically, it contributes to the wing loading. However, it was not accounted for when the wing was designed. The actual wing loading is lower than that stated in the wing chapter. Perhaps the wing and canard can be further optimized.

The measurements used to calculate the tail volumes can be found in appendix D.

7.4 Conclusion

While there is room for optimization, the current empennage design satisfies the requirements and is adequate to proceed.

8. Landing Gear Design

8.1 Landing Gear Layout Design

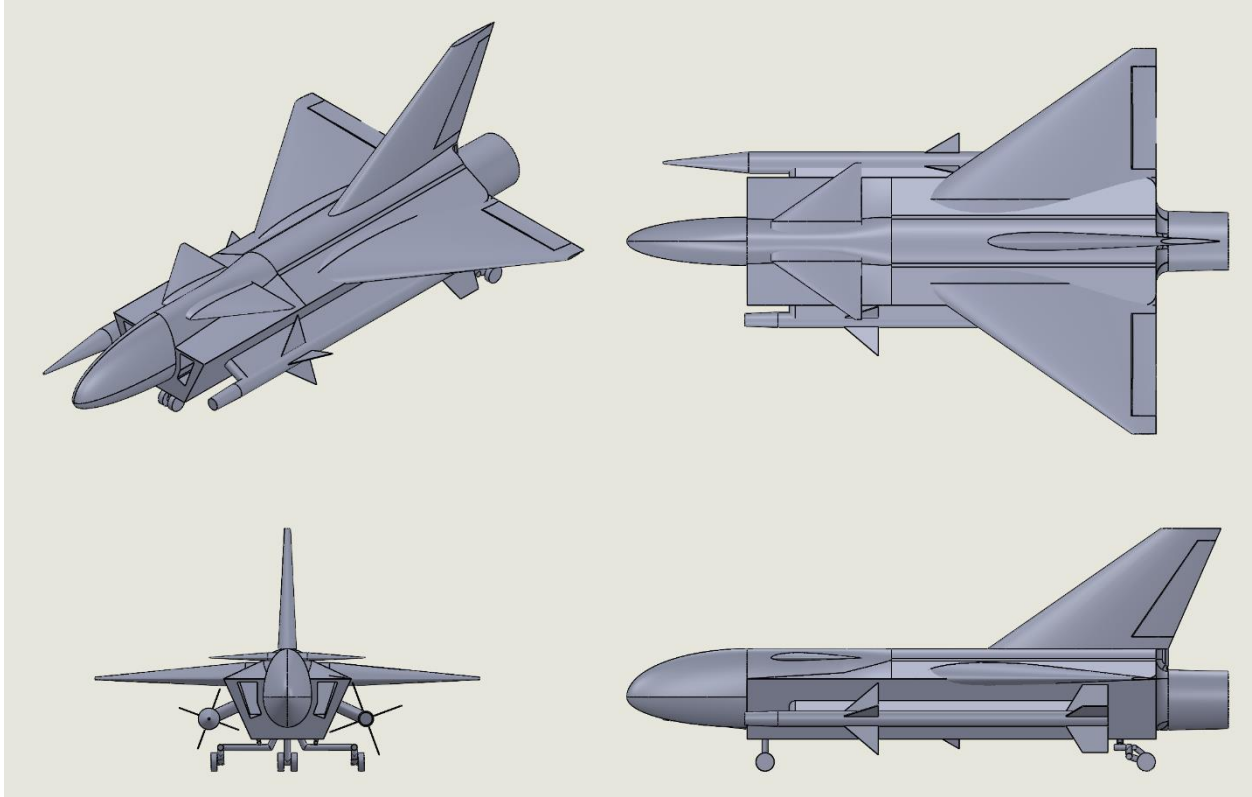


Figure 8.1 - Isometric and three views of the aircraft with extended landing gear.

The landing gear for this aircraft is in a tricycle configuration. Unlike most fighter designs, the main gear is in the rear of the fuselage. When stowed, the main gear strut wraps around the engine, and the tire is parallel to the wall of the fuselage. To deploy the landing gear, a hydraulically powered actuator pushes the main gear strut down so that the strut is parallel with the bottom of the fuselage. A mechanical link underneath the main gear strut, connected between the actuator and the tire section, would align the tire perpendicularly with the ground. Due to its complexity, it is currently omitted in the CAD model. The deployment process of the rear landing gear is shown in Figure 8.2 and 8.3.

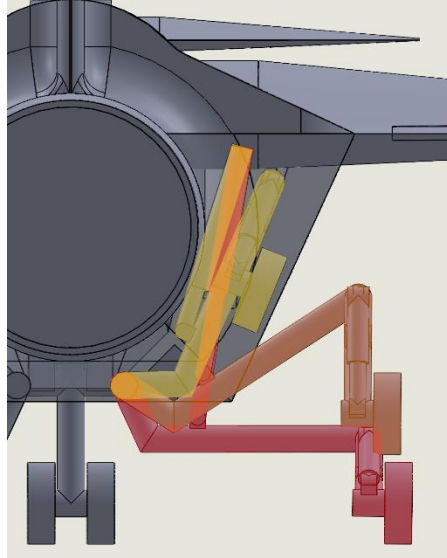


Figure 8.2 - Side view of landing gear deployment.

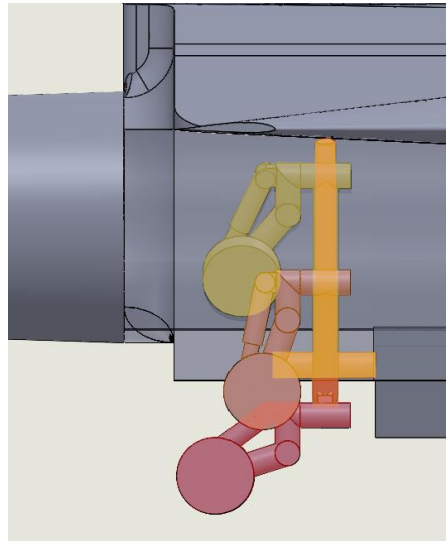


Figure 8.3 - Side view of landing gear deployment.

8.2 Landing Gear Layout Discussion

The design of the landing gear is heavily constrained by its mission profile and other design decisions. Firstly, there is not much space where the landing gear can be stowed. The wing is thin and mounted high. Therefore, a wing-stowed landing gear is unfeasible. They must be stowed in the fuselage instead. While many fighter jets have main landing gear in their fuselage,

the payload configuration causes complications. This tiny UCAV carries ordinances intended for full-size manned fighters. The ordinance is mounted on the side of the fuselage, which offers the most surface area and structural strength. While the design of the pylon is uncertain, it is expected to occupy a large amount of the fuselage area. The bottom of the fuselage is occupied by two long slots where the UCAV connects to the wing tip of the manned fighter. The only location where the landing gear can go is the side of the fuselage aft of the ordinance. However, the limited space means there can be practically no movement in the x-axis. On most fighter jets, the landing gear is stowed in a way that it runs along the length of the fuselage. This is only logical, as there is much more space in the longitudinal direction. But this means that typical landing gear designs will not work on this aircraft.

In the beginning, the F-22-style landing gear was considered. It is straightforward. The landing gear is stowed vertically on the side of the fuselage. To deploy it, the main gear simply pivots down. However, the length of the main gear is constrained by the height of the fuselage under the wing. Furthermore, the width of the base is constrained by the width of the fuselage. A better design is needed.

Fortunately, this is a problem that was tackled before. With a large and heavy engine in the back of the fuselage, fuel tanks in the middle, and variable wings that prohibit the mounting of landing gear on the wing, the Mig-23 faced similar constraints. The solution is a “crab-like” landing gear that rotates about the longitudinal axis. When deployed, the strut of the landing gear sticks out the side of the fuselage and provides a wide base for the main gear. When stowed, it neatly wraps around the engine wall to conserve space.

8.3 Tire Sizing and Discussion

According to Roskam, to determine the size of the tires, the loading and velocity must first be determined. Afterward, tire databooks published by major tire manufacturers are used to look up suitable tires.

Unfortunately, this method may not be adequate for this aircraft. The unique size, weight, and mission profile of this aircraft again causes complications. While loading and tire velocity can be calculated and determined, there is simply no existing tire that fits the parameters perfectly. Military aircraft predominantly use type VII tires. However, most type VII tires are too big for this aircraft. Certain type III tires came close to the designed dimensions. However, type III tires are low-pressure and, according to Roskam, obsolete. But even though type III tires came close, they never fit. On the data book, the minimum tire width found is four inches. The crowded fuselage simply cannot house a four-inch-wide tire. Currently, the UCAV is designed for a two-inch-wide tire that is six inches in diameter. At the very least, the diameter seems reasonable. There are multiple tires with diameters smaller than six inches in the databook. And the UCAV does have the volume to house a larger diameter tire.

To investigate the tires used on other UAVs, the MQ-1 Predator was examined. The predator is a reconnaissance drone which was converted to carry out strike missions. At sub-2,200 lb gross weight, the Predator is light. But it is also very large. Optimized for long-endurance flights, it is long and thin. The tire size on the Predator was estimated using a three-view drawing of the predator. The sizes of the tires in the image are measured and multiplied by a factor to obtain the real dimensions. The nose tire was estimated to be two inches wide and between nine and ten inches in diameter. The main tire was estimated to be four inches wide and between 12 and 13 inches in diameter. The Predator and this UCAV differ in mission, loading, and landing speed. While the result here is not directly transferable, it should at least demonstrate that a sub-four-inch wide tire is possible.

While a four-inch wide and six inches in diameter tire does not exist in the published tire databook, it does not seem completely unrealistic either. This design will continue using said tire size.

8.4 Landing Gear Stability

8.4.1 Tip-back Angle

The tip-back angle is the angle between the tail of the aircraft and the fully extended landing gear. With a typical single-strut landing gear, the tire simply lowers when it is fully extended. With this design, the tire also moves forward when it is fully extended. The tip-back angle is determined when the aircraft flies at an AOA that generates 90% of the maximum lift [15]. In the wing chapter, it is calculated that $C_{L_{max}}$ occupies at 23 degrees. Therefore, the tip-back angle is estimated at about 20.7 degrees AOA. This aircraft has a tip-back angle of 30.88 degrees. To prevent the aircraft from a tail strike, the angle between the C.G. and the vertical axis of the main wheel should be larger than the tip-back angle. In this case, depending on the location of the C.G., the C.G. is between 66.11 degrees and 69.16 degrees away from the vertical axis of the main wheel.

While the tail strike requirement is satisfied, the C.G. is too far forward from the main landing gear. A forward C.G. makes it difficult for the aircraft to rotate on takeoff. An aft C.G. makes it difficult to steer the nose gear. According to Raymer, if the nose gear is carrying over 20% of the aircraft's weight, the main gear is too far aft of the C.G. In this case, the C.G. is close to the midpoint of the wheel base. The nose gear should be carrying close to half the weight of the aircraft. There is no easy solution to this problem since, as mentioned earlier, there is little space for the main landing gear. But since this aircraft is not designed to take off by itself, this may not be a real problem. The nose gear was also designed accordingly to carry the load. The nose gear has two tires that are the same size as the main wheels.

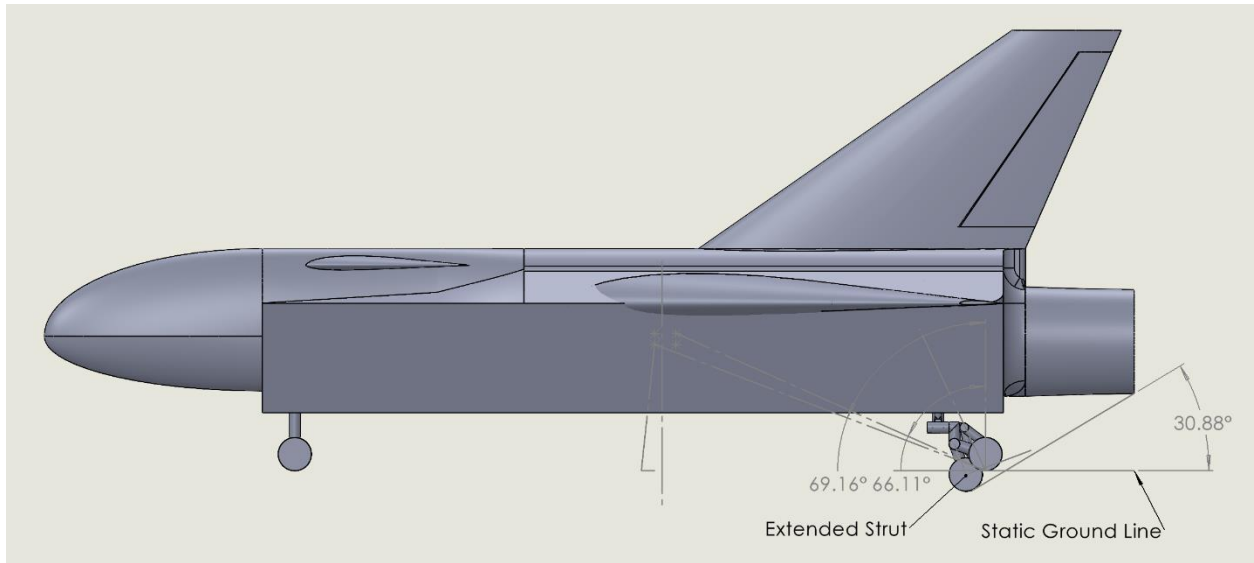


Figure 8.4 - Tip-back angle and C.G. - main gear angle.

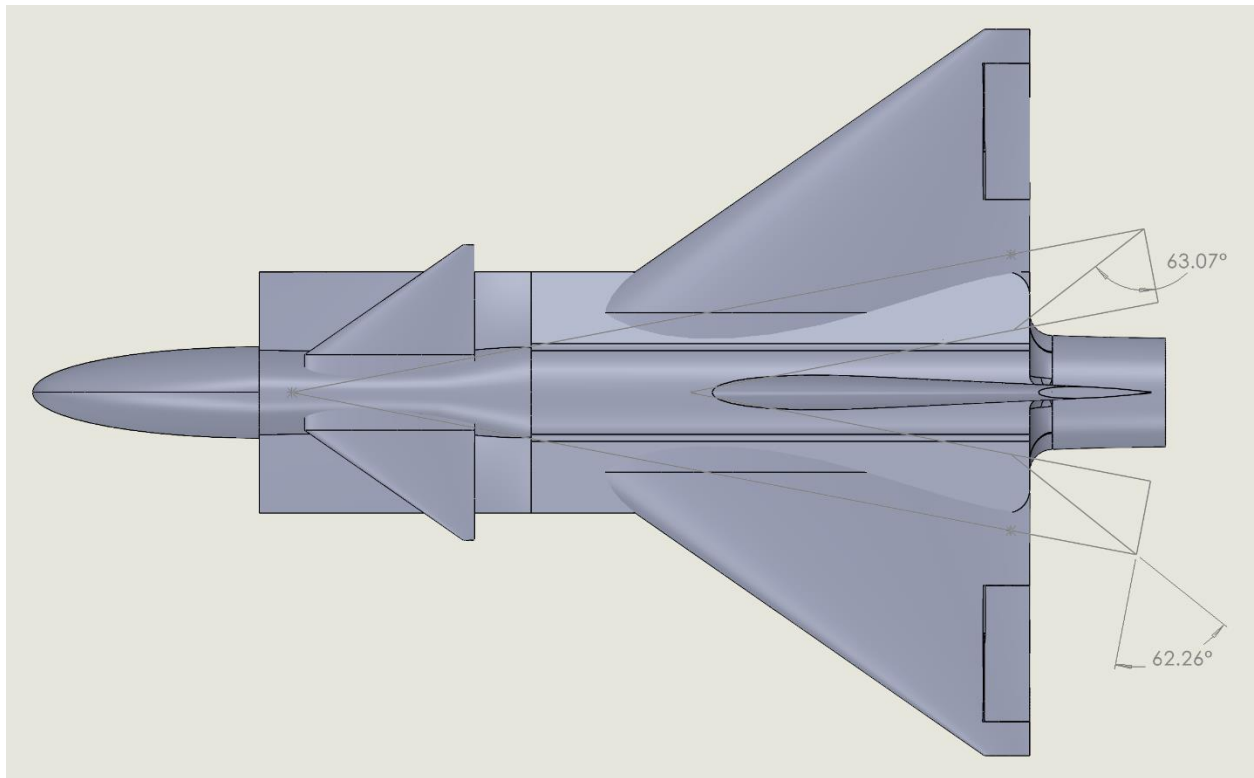


Figure 8.5 - Overturn angle.

8.4.2 Overturn Angle

The overturn angle determines how likely the aircraft tips over when taxiing. Depending on the height of the C.G., the aircraft has an overturn angle between 62.26 degrees and 63.07 degrees. For most aircraft, the overturn angle should not be larger than 63 degrees. This design borderline satisfies the overturn angle requirement.

8.4.3 Wingtip Angle

The wingtip angle determines how likely the aircraft will strike its wingtip on takeoff and landing. Figure 8.6 shows the wingtip angle of the aircraft. The aircraft is loaded with one AIM-9 missile and one AIM-120 missile in this figure. This was only done to demonstrate the wingtip angle with different ordnance. It is not a realistic loadout. With a 38-degree wingtip angle, it is safe to say that the aircraft is extremely unlikely to suffer a wingtip strike.

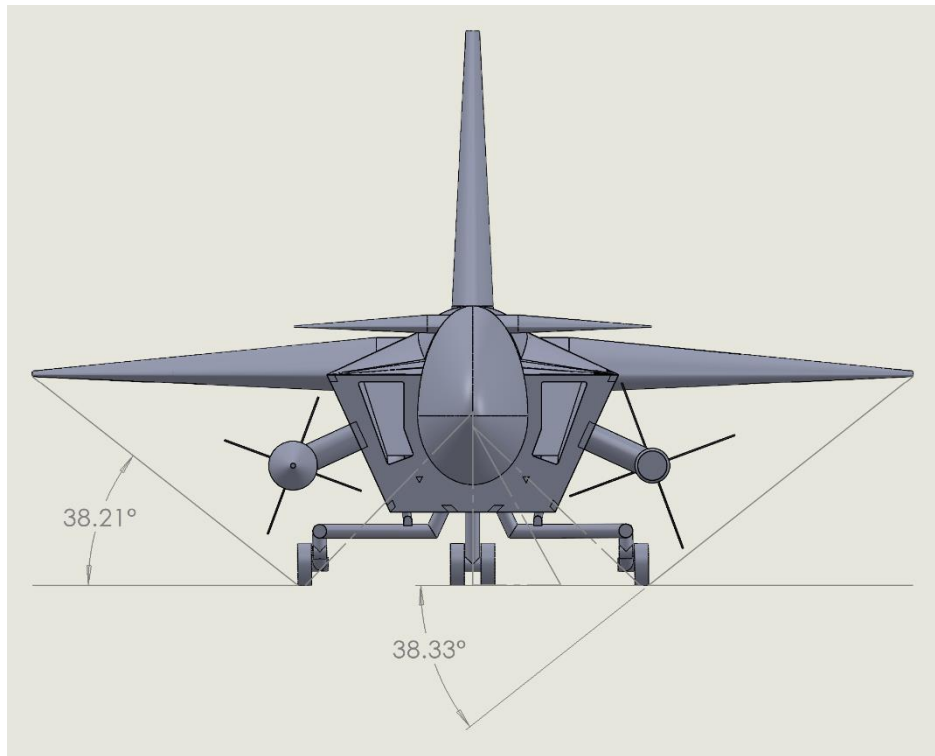


Figure 8.6 - Wingtip angle.

9. Class I Weight and Balance Analysis

9.1 Introduction

The weight of the aircraft and its location are essential in maintaining the balance of the aircraft. It is not uncommon for an aircraft to experience a loss of control and ultimately crash due to an improper center of gravity location. In this chapter, Roskam's Class I method is used to estimate the weight of the components.

9.2 Component Weight Breakdown

A Class I method uses existing aircraft data to estimate the component weight. This is an easy way to provide a preliminary estimate for most aircraft. But for this project, it is not as straightforward. UCAV is a recent development. There is virtually no aircraft that can serve as a reference. Moreover, the weight, size, and mission of this aircraft make it unique from other aircraft. Manual adjustments must be made to provide reasonable results.

The aircraft data used here can be found in appendix A of Roskam's aircraft design Part V. Considering this aircraft will serve primarily as a fighter, the data of the following five aircraft are examined: F-102A, F-16, F-15C, F/A-18A, and AV-8B. None of the five aircraft has the same configuration as this UCAV does. The F-102A is somewhat similar. It has a delta wing near the aft of the aircraft. However, it does not have a canard. It also has a single engine with a split air intake. But it is an old aircraft, meaning the weight would not be a perfect representation of the component weights of a modern aircraft. Over the decades, significant progress has been made in material science and computer electronics. The data of the other four aircraft were used to reflect these changes.

In the original document, the component weights were given in pounds and fractions of the design gross weight. According to the weight sizing chapter results, the UCAV would have a much lower empty weight fraction for it to complete the determined mission than the five fighters. If one multiplies the design gross weight of the UCAV by the given weight fractions, the UCAV will not have enough weight to carry the payload and fuel. Therefore, the weight fractions were adjusted to fractions of the empty weight.

The spreadsheet used to calculate the component weight can be found in appendix E.

Table 9.1 - Component Weight Fractions of different aircraft.

	F-102A	F-16	F-15C	F/A-18A	AV-8B	Dragoon
Wing	0.158	0.090	0.134	0.165	0.113	0.135
Empennage	0.028	0.044	0.041	0.041	0.029	0.045
Fuselage	0.179	0.208	0.230	0.204	0.161	0.205
Engine Section	0.002	0.041	0.004	0.006	0.011	0.010
Landing Gear	0.056	0.059	0.051	0.087	0.079	0.060
Engine	0.263	0.205	0.224	0.187	0.298	0.300
Air Induct System	0.036	-	0.054	0.018	0.018	0.036
Fuel System	0.021	0.024	0.041	0.044	0.042	0.040
Propulsion System	0.015	0.019	0.019	0.024	0.035	0.020
Instrument	0.007	0.012	0.006	0.004	0.006	0.000
Surface Control	0.022	0.049	0.030	0.046	0.055	0.025
Hydraulic Pneumatic	0.017	0.025	0.016	0.016	0.014	0.015
Electrical	0.031	0.026	0.022	0.024	0.033	0.025
Electronics	0.105	0.068	0.066	0.067	0.054	0.075
Armament	0.031	0.038	0.023	0.017	0.012	0.000
Air Conditioning	0.014	0.016	0.025	0.026	0.017	0.005
Anti-Ice	-	-	-	0.001	-	-
Furnishings	0.012	0.040	0.011	0.014	0.023	0.000
Auxiliary Gear	0.004	0.011	0.004	0.008	-	0.004

The weight fractions of the F-102A served as the basis and were adjusted as needed. Most parameters were adjusted to bring them in line with the average values. The wing weight fraction was reduced to account for the increasing use of composites in recent years. The empennage weight fraction was increased to account for the canard. The engine weight fraction was fixed due to the engine selected. There are not too many engines of this weight class and thrust level. Because the F-102A has the identical engine and air intake configuration, the air induct system fraction remained unchanged. The fuel system weight fraction should depend on the amount of fuel carried. Since this aircraft carries quite a lot of fuel for its gross weight, the fuel system fraction was increased. The hydraulic and pneumatic fractions were reduced as the aircraft does not have a lot of hydraulic-powered devices such as leading-edge slats and flaps. Electrical and electronics fractions were reduced to reflect the technological advancements in past decades. As the aircraft is a UAV with no fixed guns, instruments, armament, or furnishings, the corresponding weight fractions were reduced to zero. Air conditioning also includes cockpit pressurization. While this aircraft has no pilot, the air conditioning fraction was reduced but not removed for cooling the avionics.

Table 9.2 - Component weight and location using class I method.

	Empty Weight fraction	Weight (kg)	Weight (lb)	Location (m)	Location (ft)
Wing	0.135	80.5	177	2.9	9.6
Empennage	0.045	26.8	59	3.3	10.8
Fuselage	0.205	122.2	269	2.5	8.2
Engine Section	0.010	6.0	13	3.2	10.6
Landing Gear	0.060	35.8	79	3.0	9.9
Engine	0.300	178.6	393	3.6	11.7
Air Induct System	0.036	21.5	47	2.1	6.9
Fuel System	0.040	23.8	52	2.5	8.3
Propulsion System	0.020	11.9	26	3.2	10.6
Surface Control	0.025	14.9	33	3.3	10.7
Hydraulic Pneumatic	0.015	8.9	20	3.5	11.6
Electrical	0.025	14.9	33	4.0	13.2
Electronics	0.075	44.7	98	1.0	3.3
Air Conditioning	0.005	3.0	7	1.5	5.0
Auxiliary Gear	0.004	2.4	5	1.5	5.0
Payload	-	227.3	500	2.5	8.4
Fuel	-	453.0	997	2.5	8.3
Total empty weight	1.000	595.9	1311	2.9	9.5
Total weight w/ fuel	-	1048.9	2308	2.7	9.0
Total gross weight	-	1276.2	2808	2.7	8.9

9.3 Discussion

Because the weight fractions were adjusted arbitrarily, the results may not be entirely correct. The result also assumes that the empty weight fractions from the weight sizing chapter are correct. An estimation using the class II method should verify this result.

9.4 Conclusion

The class I method provided a simple estimate for the component weight. The accuracy of this result will be verified in the following chapter with the class II method.

10. Class II Weight and Balance Analysis

10.1 Introduction

A class I method estimates the component weight using existing aircraft data. A class II method estimates the weight using the actual parameters of the aircraft. The results from the class II method should verify whether the result obtained using class I method was correct.

10.2 Component Weight Breakdown

Tables 10.1, 10.2, and 10.3 show the result from Roskam’s fighter equation, RDS fighter/attacker equation, and RDS general aviation equation, respectively. The results vary significantly between the different methods. The x location of the component is also defined differently, with it being the center of gravity for Roskam’s and the location of the leading edge for RDS’. The Roskam fighter equation code can be found in appendix F, while the RDS result for fighters and general aviation aircraft can be found in appendix G and H, respectively.

Table 10.1 - Roskam’s fighter equation result.

Component	Weight		x Location	
	Metric (kg)	Imperial (lb)	Metric (m)	Imperial (ft)
Wing	30.8	67.8	2.9	9.6
Canard	8.9	19.5	1.3	4.3
Vertical Stabilizer	27.8	61.2	3.9	12.9
Fuselage	119.9	263.7	2.5	8.3
Landing Gear	71.2	156.5	3.0	9.9
Air Induction	13.4	29.6	2.1	6.9
Fuel System	74.0	162.9	2.5	8.3
Engine	178.6	393.0	3.6	11.9
Propulsion System	10.6	23.3	3.2	10.6
Flight Control	118.8	261.3	3.3	10.9
Instrumentation, Avionics and Electronics	18.8	41.5	3.3	10.9
Electrical System	85.3	187.7	4.0	13.2
Fuel	453.0	996.6	2.5	8.3
Payload	227.3	500	2.5	8.3
Total	1385.9	3164.6	2.8	9.2

It should also be pointed out that all three results indicate that the aircraft is overweight. The Roskam equation resulted in a total weight beyond the weight requirement of 3,000 lb. In the two RDS results, the total weights are exactly 3,000 lb because RDS automatically reduces fuel weight to maintain the gross weight of the aircraft.

Table 10.2 - RDS fighter equation result.

Component	Weight		x Location	
	Metric (kg)	Imperial (lb)	Metric (m)	Imperial (ft)
Wing	56.9	125.2	2.000	6.600
Canard	5.8	12.8	1.000	3.300
Vertical Stabilizer	67.7	148.9	3.000	9.900
Fuselage	69.6	153.1	0.000	0.000
Main Gear	41.5	91.3	4.250	14.025
Nose Gear	18.9	41.6	0.000	0.000
Engine Mount	6.9	15.2	3.200	10.560
Engine Section	3.8	8.4	3.200	10.560
Air Induction	55.4	121.9	1.000	3.300
Engine	189.0	415.8	3.200	10.560
Tail pipe	3.8	8.4	4.500	14.850
Oil Cooling	17.2	37.8	4.500	14.850
Starter	5.2	11.4	4.500	14.850
Fuel System	54.9	120.8	3.000	9.900
Flight Controls	140.1	308.2	4.000	1.320
Hydraulic	49.2	108.2	4.000	1.320
Electrical	187.3	412.1	4.000	1.320
Air Conditioning	16.8	37.0	0.000	0.000
Handling Gear	0.4	0.9	0.000	0.000
Fuel	146.1	321.4	3.000	9.900
Payload	227.3	500.1	2.500	8.300
Total	1363.6	2999.9	2.9	9.6

Table 10.3 - RDS general aviation equation result.

Component	Weight		x Location	
	Metric (kg)	Imperial (lb)	Metric (m)	Imperial (ft)
Wing	54.7	120.3	2.000	6.600
Canard	22.7	49.9	1.000	3.300
Vertical Stabilizer	25.7	56.54	3.000	9.900
Fuselage	208.0	457.6	0.000	0.000
Main Gear	58.7	129.1	4.250	14.025
Nose Gear	13.4	29.5	1.000	3.300
Engine	189.0	415.8	3.200	10.560
Engine Installation	115.0	253.0	3.200	10.560
Fuel System	32.9	72.4	3.000	9.900
Flight Controls	10.2	22.4	3.000	9.900
Hydraulics	146.1	321.4	4.000	13.200
Electrical	50.7	111.5	4.000	13.200
Fuel	209.3	460.5	3.000	9.900
Payload	227.3	500.1	2.500	8.300
Total	1363.6	2999.9	2.6	8.6

10.3 Center of Gravity Location of Various Loading Scenarios

Table 10.4 lists the longitudinal center of gravity under different conditions. Of the three methods, Roskam's and RDS' fighter equations gave results which generally agree with each other.

Table 10.4 - Center of gravity location variation for different estimations.

Method	Condition	Center of Gravity in x Axis	
		Metric (m)	Imperial (ft)
Roskam's Fighter Equation	Empty	3.1	10.2
	Loaded No fuel	3.0	9.9
	Gross Weight	2.8	9.2
RDS Fighter Equation	Empty	3.0	9.9
	Loaded No fuel	2.9	9.6
	Gross Weight	2.9	9.6
RDS General Aviation Equation	Empty	2.5	8.3
	Loaded No fuel	2.5	8.3
	Gross Weight	2.6	8.6

10.4 Discussion

The first calculation was carried out using Roskam's equation for fighters. However, the result was unsatisfactory. The weight of the vertical stabilizer is calculated to be the same as that of the wing, while the wing is much bigger and would be subjected to much larger aerodynamic forces, requiring more structure. The calculation was later done again in RDS using fighter equations. While the two produced a similar center of gravity, the weight of the individual component differs greatly. The mismatch between the role and the weight of this aircraft is suspected to be the cause of the discrepancies. A typical fighter jet is large and heavy, while this aircraft is small and light. This aircraft is only about one-tenth the weight of an empty F-4 Phantom. The last calculation was done with the general aviation equation hoping it would yield better results for a lighter aircraft. However, these equations do not describe this aircraft perfectly. It does not consider the effect of a delta wing, nor does it include a scenario of a jet engine mounted in the fuselage with air ducts. Therefore, the three results cannot produce an agreeable estimate.

Contrary to the original expectation, the class II method of weight estimation has failed to verify the result obtained in the previous chapter. A second way to verify the previous results would be determining specific components to be used in the design and comparing the weight from the manufacturer with the weight calculated. But for now, the result from the previous chapter will continue to be used for calculation in other chapters.

10.5 Conclusion

The class II method was proven ineffective in estimating the component weights for this aircraft. Results from the previous chapter would continue to be used for other calculations.

11. Drag Polar

11.1 Introduction

In this chapter, the class II method was used to determine the drag performance of the aircraft. The drag for each component of the aircraft is calculated and then added together for the total drag of the aircraft. This method should provide an accurate estimate of the drag of the aircraft. The equations used can be found in [17], while the code can be found in appendix I.

11.2 Breakdown and Calculation

The drag is broken up into four main components: wing, fuselage, empennage, and payload. There is also landing gear. But it is only significant at low speeds. The trim drag is accounted for in the empennage section, as this design features a flying canard. The lift and drag coefficients were calculated at different airspeeds and plotted together to obtain the drag polar graph.

The drag was calculated between Mach 0.25 and 0.85 at 0.5 increments. It was also calculated at two different densities: sea level and cruise altitude, which is 5000 m. The data point for Mach 0.25 at the cruise altitude was omitted since it is under the stall speed at altitude.

There are two components to the drag of each part of the aircraft: the zero-lift drag and the lift-induced drag. Each component is calculated differently for different speed regimes.

11.2.1 Coefficient of Drag of Wing

At subsonic speed, the zero-lift coefficient of drag of the wing can be calculated with equation 11.1

$$C_{D_{0W}} = R_{wf} R_{LS} C_{fW} \left(1 + L' \left(\frac{t}{c} \right) + 100 \left(\frac{t}{c} \right)^4 \right) \frac{S_{wetW}}{S} \quad (11.1)$$

At transonic speed, the $C_{D_{0W}}$ is the sum of the zero-lift drag, evaluated using equation 11.1 at Mach 0.6, and the wing wave drag, $C_{D_{Wwave}}$. The wing wave drag is dependent on the flying condition of the aircraft and the geometry of the wing. Figure 11.1 was constructed to determine the wave drag.

The curve in the figure represents the wing design with zero quarter chord sweep. The M_{DD} is defined as the Mach number when $C_{D_{wave}}$ has a value of 0.002. Using equation 11.2, the M_{DD} was corrected for the sweep angle and has a value of 0.9705. With a 47.2 degree of quarter chord sweep, the $C_{D_{wave}}$ has a value of 0.002 at Mach 0.97, which is much higher than the intended cruise speed of 0.85. Therefore, the wave drag is considered to be negligible.

$$C_{DD\Delta_{.25c}} = \frac{M_{DD}}{(\cos \Delta_{0.25c})^{0.5}} \quad (11.2)$$

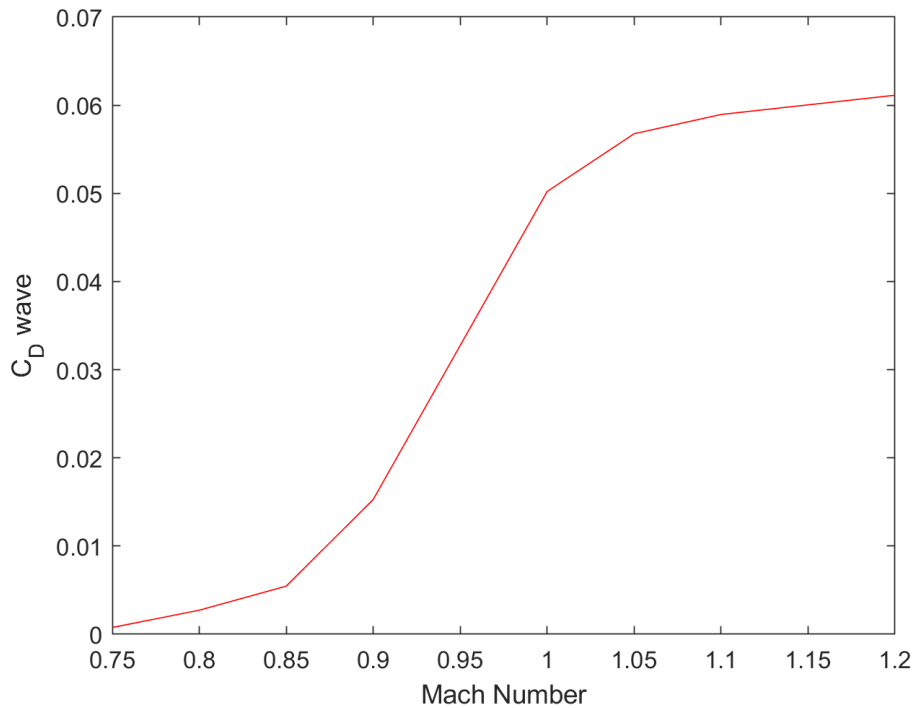


Figure 11.1 - Wave divergence diagram

At subsonic speed, the lift-induced drag coefficient can be calculated using equation 11.3. This equation was simplified due to the lack of wing twist.

$$C_{D_{Lw}} = \frac{C_{Lw}^2}{\pi e AR} \quad (11.3)$$

At transonic speed, $C_{D_{Lw}}$ is simply the product between the induced drag ratio, obtained through Roskam, and the square of C_{Lw} .

11.2.2 Coefficient of Drag for Empennage

The drag coefficient for each empennage surface can be calculated using the method from Chapter 11.2.1 with the corresponding substitutes. To arrive at the final value, the calculated coefficient of drag is then multiplied by a factor of S_i/S , where S_i is the area of the empennage surface and S is the area of the wing.

11.2.3 Coefficient of Drag for Fuselage

The subsonic zero-lift drag coefficient for the fuselage can be calculated using equation 11.4.

$$C_{D_{0fus}} = R_{wf} C_{ffus} \left(1 + \frac{60}{(l_f/d_f)^3} + 0.0025 \frac{l_f}{d_f} \right) \frac{S_{wetfus}}{S} + C_{D_{bfus}} \quad (11.4)$$

The transonic zero-lift drag coefficient for the fuselage can be calculated using equation 11.5.

$$C_{D_{0fus}} = R_{wf} (C_{D_{ffus}} + C_{D_{pfus}}) + C_{D_{pfus}} + C_{D_{wavefus}} \frac{S_{wetfus}}{S} \quad (11.5)$$

Similar to the wing, $C_{D_{ffus}}$ and $C_{D_{pfus}}$ are parameters evaluated at 0.6 Mach. The wave drag is addressed with the last term in the equation.

The subsonic lift-induced drag coefficient can be calculated using equation 11.6, while the transonic lift-induced drag coefficient can be calculated using the more straightforward equation 11.7.

$$C_{D_{Lfus}} = 2\alpha^2 \frac{S_{bfus}}{S} + \eta c_{dc} |\alpha|^3 \frac{S_{plffus}}{S} \quad (11.6)$$

$$C_{D_{Lfus}} = \alpha^2 \frac{S_{bfus}}{S} \quad (11.7)$$

11.2.5 Coefficient of Drag for Payload

The payload can be treated as a fuselage. Therefore, the coefficient of drag can be calculated using the equations from 11.2.4 with the corresponding substitutes.

11.3 Results

Figure 11.2 shows the drag polar of the aircraft. The lift-to-drag ratio falls short of expectations. At cruise altitude, the maximum lift-to-drag ratio is 8.658 at Mach 0.5. This is even less than that of the F-104 in Figure 2.1. For the subsonic regime, the shape of the drag polar is as expected. However, problems arise in the transonic regime. The drag coefficient surges at Mach 0.6 before decreasing again. This sharp increase is irregular. Figure 11.4 shows the drag polar if the lift-induced drag in the transonic regime is omitted. Omitting the transonic drag, the lift-to-drag ratio at Mach 0.65 is higher than that at Mach 0.60, which should not be the case. Omitting the transonic drag did not solve the problem. Interestingly, omitting the transonic drag produces the most discrepancy at the beginning of the transonic regime. The drag performance at Mach 0.85 with and without transonic drag is relatively close. When cruising at altitude with payload, the lift-to-drag ratio in Figures 11.3 and 11.5 are 2.926 and 3.335, respectively.

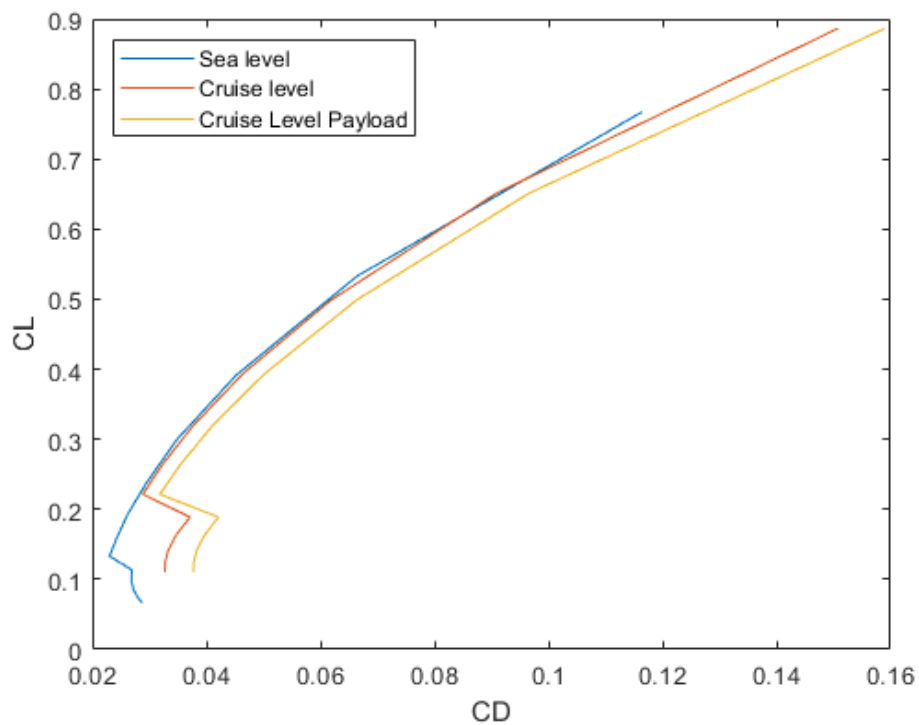


Figure 11.2 - Drag polar of the aircraft.

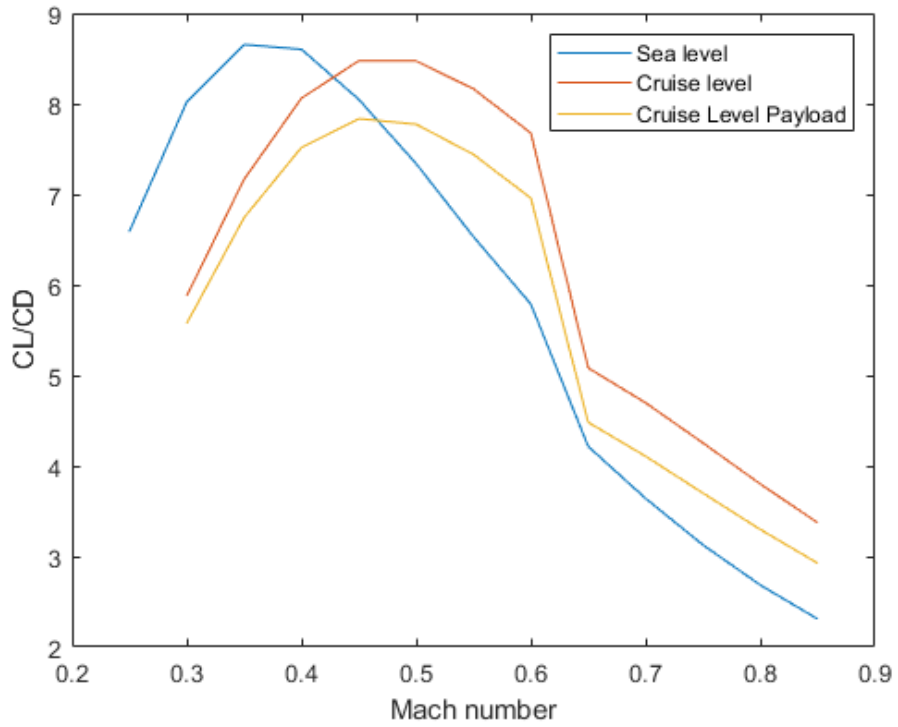


Figure 11.3 - Lift-to-drag ratio of the aircraft at different Mach numbers

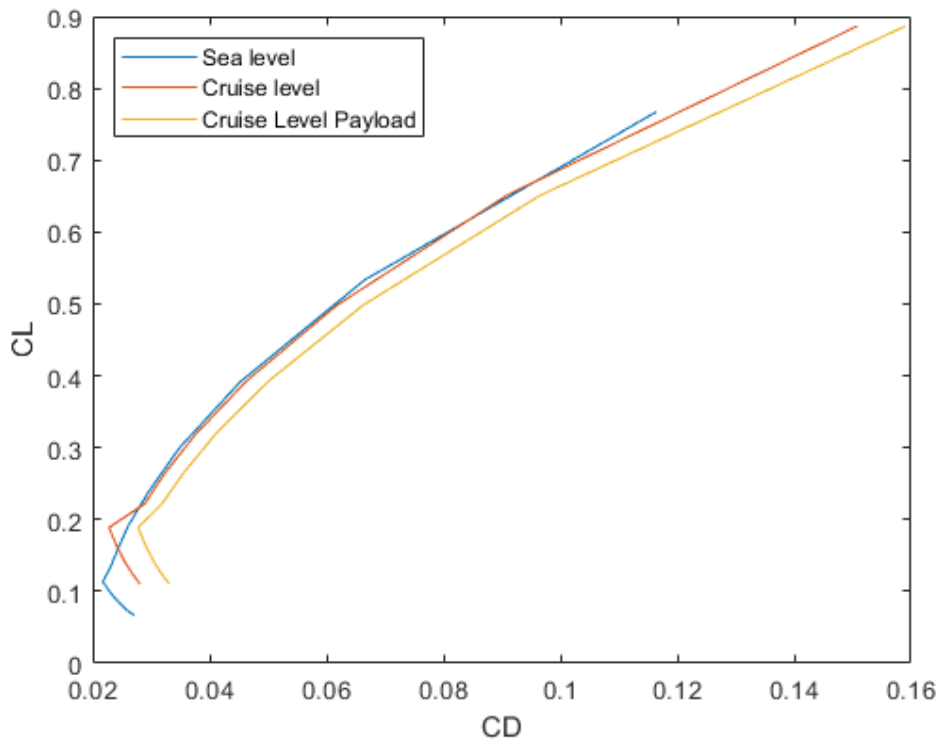


Figure 11.4 - Drag polar of the aircraft without transonic lift-induced drag.

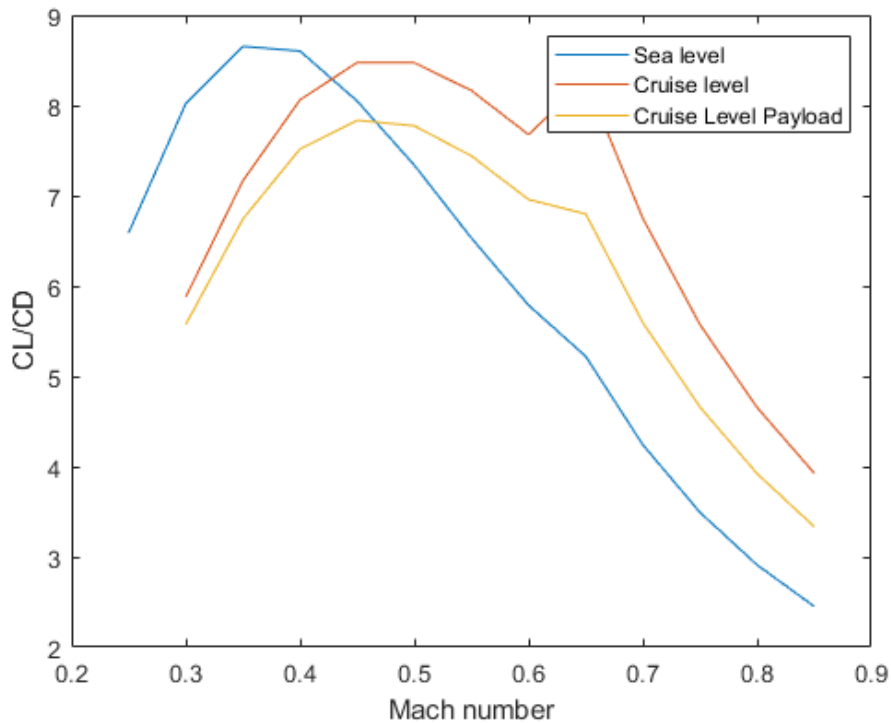


Figure 11.5 - Lift-to-drag ratio of the aircraft at different Mach numbers without transonic lift-induced drag

11.4 Discussion

Considering Roskam's equations, the low lift-to-drag ratios at high Mach numbers may make sense. The zero-lift drag stagnates at Mach 0.6, and wave drag increases. But as the aircraft flies faster and faster, the dynamic pressure also increases, meaning the lift coefficient decreases. Even if there is no lift-induced drag and the total drag stagnates, the lift-to-drag ratio will still decrease. This rules out a coding error.

As to the reason for the poor drag performance, perhaps this can be attributed to the small size and weight of the aircraft. During the calculation for the zero-lift drag, the parameter C_f was used. C_f is the turbulent mean skin-friction coefficient. It was obtained by calculating the Reynolds number of each component and using the Reynolds number to look up the corresponding C_f in Figure 4.3 of Roskam's Part VI. The curves in the figure are parabolic. The coefficient of friction decreases as the Reynolds number increases. It also means that if velocity and viscosity are to stay constant, increasing the chord length decreases the coefficient of drag.

In Roskam's book, a subchapter is dedicated to trim drag estimation. After consideration, it is determined that the trim drag has been accounted for in the empennage subchapter. This design

has a flying canard, meaning the whole canard is a moving surface with no other control surface on the canard. There are two components to the trim drag: trim drag due to lift and trim drag due to profile drag. To calculate the trim drag due to lift, a ΔC_{L_c} is needed. ΔC_{L_c} is the change in the lift coefficient of the canard needed to trim the aircraft. However, in the canard drag calculation, the lift coefficient of the canard used should have included this ΔC_{L_c} . The trim drag due to profile drag accounts for the additional profile drag caused by the deflected canard flap. In the calculation, it is treated as a plain flap. However, there is no canard flap on this design. The trimmed flying canard should be no different than a regular canard with no flap deflection at an incidence angle.

12. Subsystem Arrangement

12.1 Introduction

The unique role and size of the aircraft make it challenging to design detailed subsystems at this phase of the project. The following subchapters are general overviews of each subsystem.

12.2 Flight Control Subsystem

Without a pilot onboard, there is no cockpit or instruments. The forward fuselage, where the pilot would sit, is instead occupied by avionics. Without a flight stick and pedals, there is no need for any mechanical flight control. The UCAV will be entirely fly-by-wire. The control surfaces will be hydraulically powered and electrically controlled. Because the wires are relatively small and can run between the structure, the arrangements of the electrical wires are omitted.

12.2 Avionics Subsystem

Because UCAV is still a developing concept, there are no guidelines on what avionics a UCAV should have. The UCAV would also be using military-grade avionics. The size, weight, and capability of these avionics are closely guarded secrets, making it difficult to design a detailed avionics subsystem. Here is a rough list of what kind of avionics are needed.

Firstly, the aircraft would have a transponder. A transponder is essential for any aircraft, commercial or military. A Military transponder also provides a friend-and-foe identification function. An inertial navigation system and GPS would help the autopilot navigate and control the aircraft. Radio and satellite antennas are needed to exchange information with other aircraft and controllers on the ground.

As for the fire control system, although this UCAV is carrying full-size aircraft missiles, it cannot carry the necessary avionics system to acquire a lock on target. A modern fighter jet radar weighs hundreds of pounds. From the class I weight and balance chapter, the total weight allocated to the electronics is only about 100 pounds. Therefore, the aircraft will need external help acquiring a lock on for its missiles. However, this may not be a big problem. Having one aircraft providing targeting data to another is not unheard of. In fact, this is what has been actively pursued. There has been development of linking up the F-35 with other fighters, often even fourth gen ones, so that non-stealth fighters can fire off beyond visual range missiles safely in stand-off range. The F-35 would have more ordinance at its disposal, minimizing the time wasted returning to base and rearming. In that case, this UCAV can take the role of missile

carrier. Given the nature of a UCAV, it can bring the missiles inside stand-in range, increasing the effective range of the missiles.

Outside of Pulse-doppler radar, perhaps the UCAV can be fitted with an Infrared Search and Track system instead. Those appear to be much smaller in size. However, the specification of such a system is still not well published.

12.3 Electrical Subsystem

Redundancy is critical in aircraft design. Without redundancy, aircraft can easily fail and cause damage or casualty. Fighter jets, which are expected to take damage in their missions, are often triple or sometimes quadruple redundant to maximize the chance of bringing the aircraft and its pilot back home safely. On the other hand, UAVs are meant to be cheap and expandable. For a minimum amount of redundancy, this aircraft would have two electrical systems. The electrical power is provided by two engine-driven generators, which are located near the engine compressor on both sides of the aircraft. The generator would provide AC power while Transformer Rectifier Units will convert some of that AC power to DC power. Although the two generators guarantee that the aircraft will still have electrical power should one of the generators fail, they are both powered by the same engine. And with only one engine, the engine is now the single point of failure. Batteries between the avionics and the integral fuel tank will provide emergency electrical power to the aircraft. The locations of the major electrical components can be seen in Figure 12.1.

12.4 Hydraulic Subsystem

The hydraulic system is another major subsystem where redundancy is paramount. A hydraulic system is essential for high-speed aircraft, as the force needed to actuate the control surfaces increases as speed increases. Similar to the electrical system, there are two separate hydraulic systems for minimal redundancy. Each system has its own engine-driven pump and reservoir near the front of the engine. Because the hydraulic lines are much bigger than electrical wires and, therefore, cannot run through the aircraft structure as easily, the simplified arrangement of the hydraulic lines, the location of the pump, and the location of the reservoir can be observed in Figure 12.2.

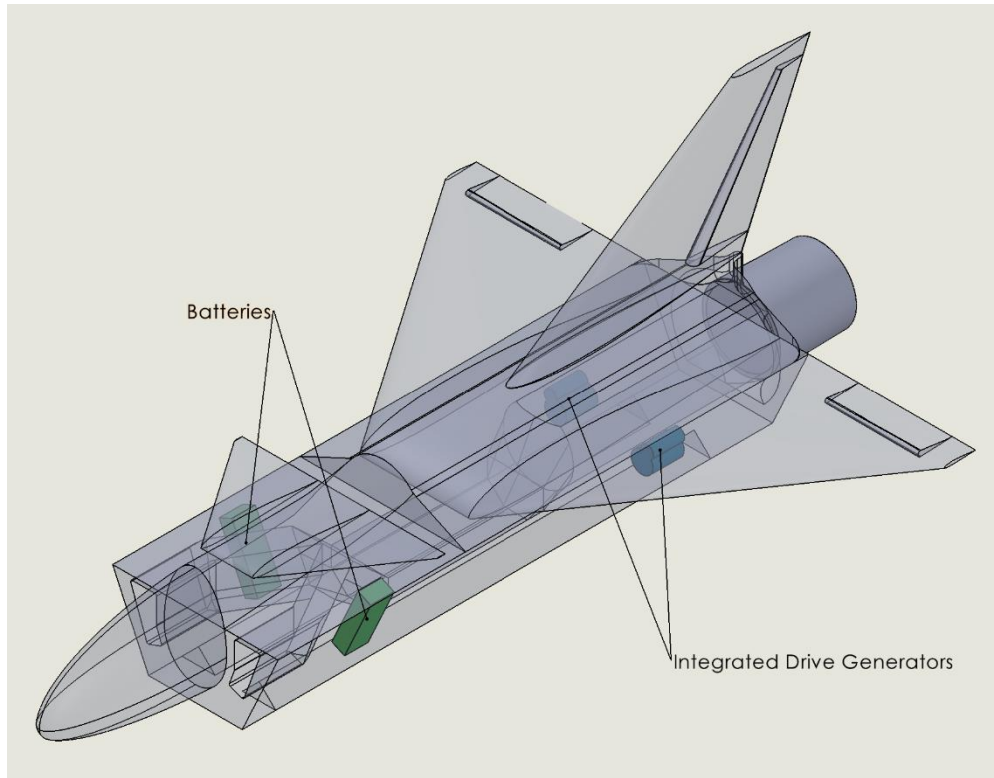


Figure 12.1 - Electrical system components

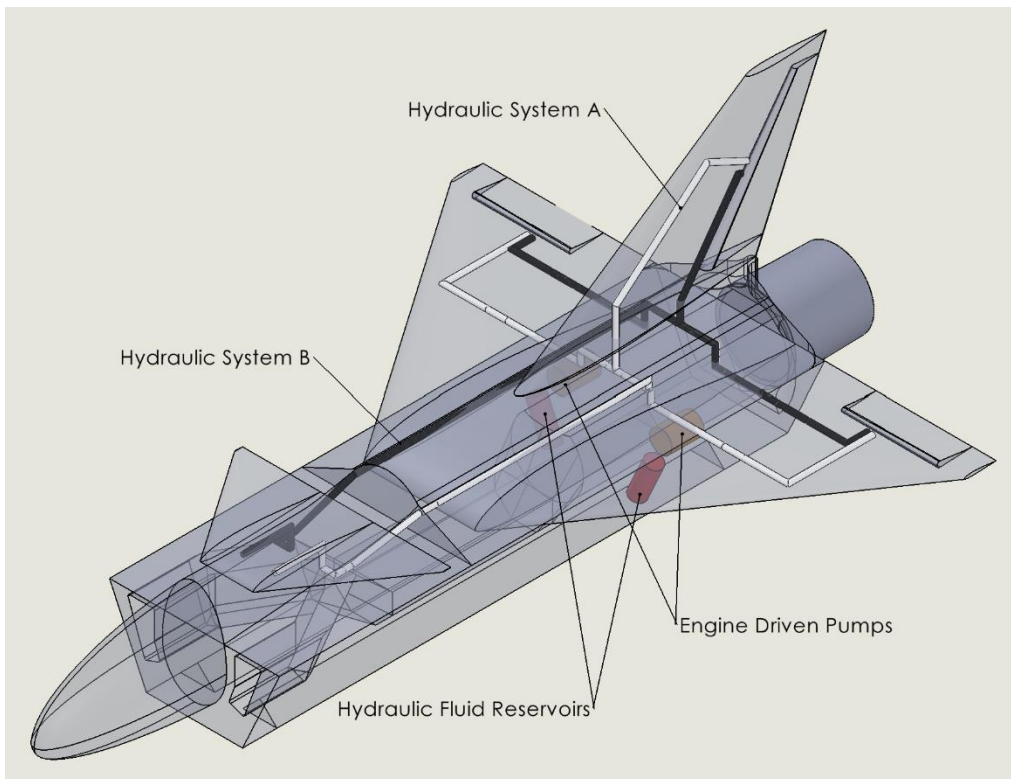


Figure 12.2 - Hydraulic system components.

12.5 Fuel Subsystem

The fuel system is comprised of one main tank in the fuselage and many smaller tanks in the wing. The main tank in the center of the fuselage wraps around the air duct for the engine. The wing spars and wing ribs enclose the wing tanks. The wing tanks only occupy the forward cells, which have the most volume and give a more favorable center of gravity than the aft cells. The fuel is pumped into the engine from the bottom of the main tank. Fuel in the wing tanks is pumped to the main tank before being sent to the engine. The location of the fuel tanks can be seen in Figure 12.3. The fuel tanks have a total volume of 0.596 m^3 (21.4 ft^3). According to the weight sizing chapter, the aircraft requires 453.6 kg (998 lb) of fuel for the mission. JP-8 has a density range of 0.775 kg/L to 0.840 kg/L ($6.47 - 7.01 \text{ lb/gal}$). Therefore, the required fuel has a volume between 0.540 m^3 and 0.585 m^3 ($142 - 154 \text{ ft}^3$). The designed fuel subsystem should have enough volume to house the required fuel.

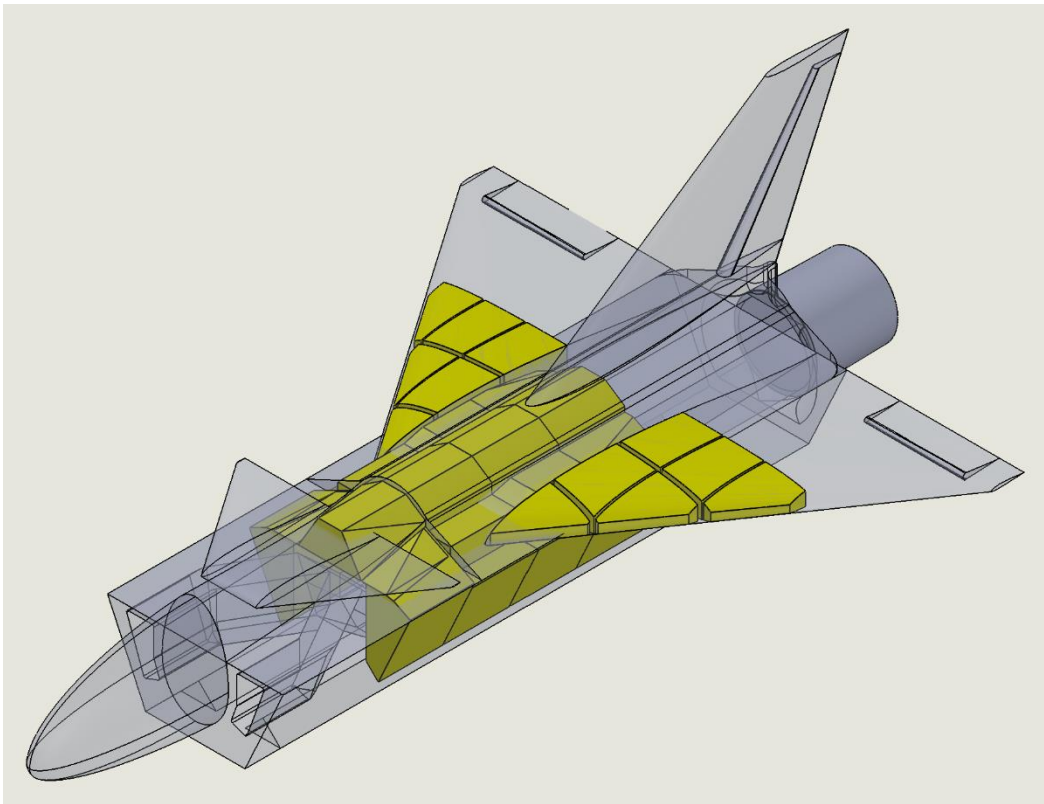


Figure 12.3 - Fuel System.

12.6 Docking system

The UCAV is docked to the manned fighter through the slots at the bottom of the fuselage. Figure 12.4 shows the UCAV docked to the right wing of an F-16. An F-16 is used here as it is one of the few modern fighters with wingtip pylons. The slots in the fuselage have the width and length of the wingtip pylon. However, the heaviest ordinance observed on the wingtip pylon is the AIM-120 AMRAAM missile, which is about one-tenth the weight of this UCAV. The existing pylon and wing are unlikely to be able to carry the UCAV without modification.

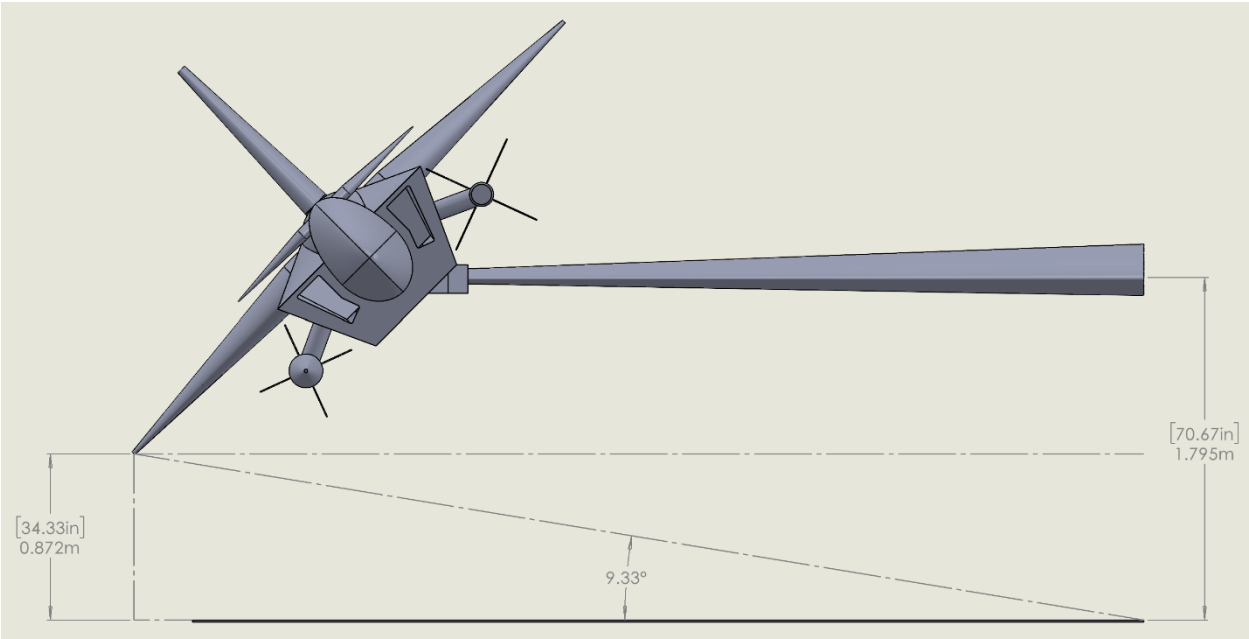


Figure 12.4 - Wingtip clearance when docked.

13. Structure

13.1 Fuselage Structure

13.1.1 Fuselage Structure Design

The main fuselage structure is composed of ten frames, each 25 mm or 0.98 inches thick. Typically, the centerlines for each frame are 400 mm or 15.75 inches apart. The detailed location of each frame can be found in Figure 13.1. The frames are connected by longerons, which run through the longitudinal direction of the aircraft. The locations for the longerons can be found in Figure 13.2

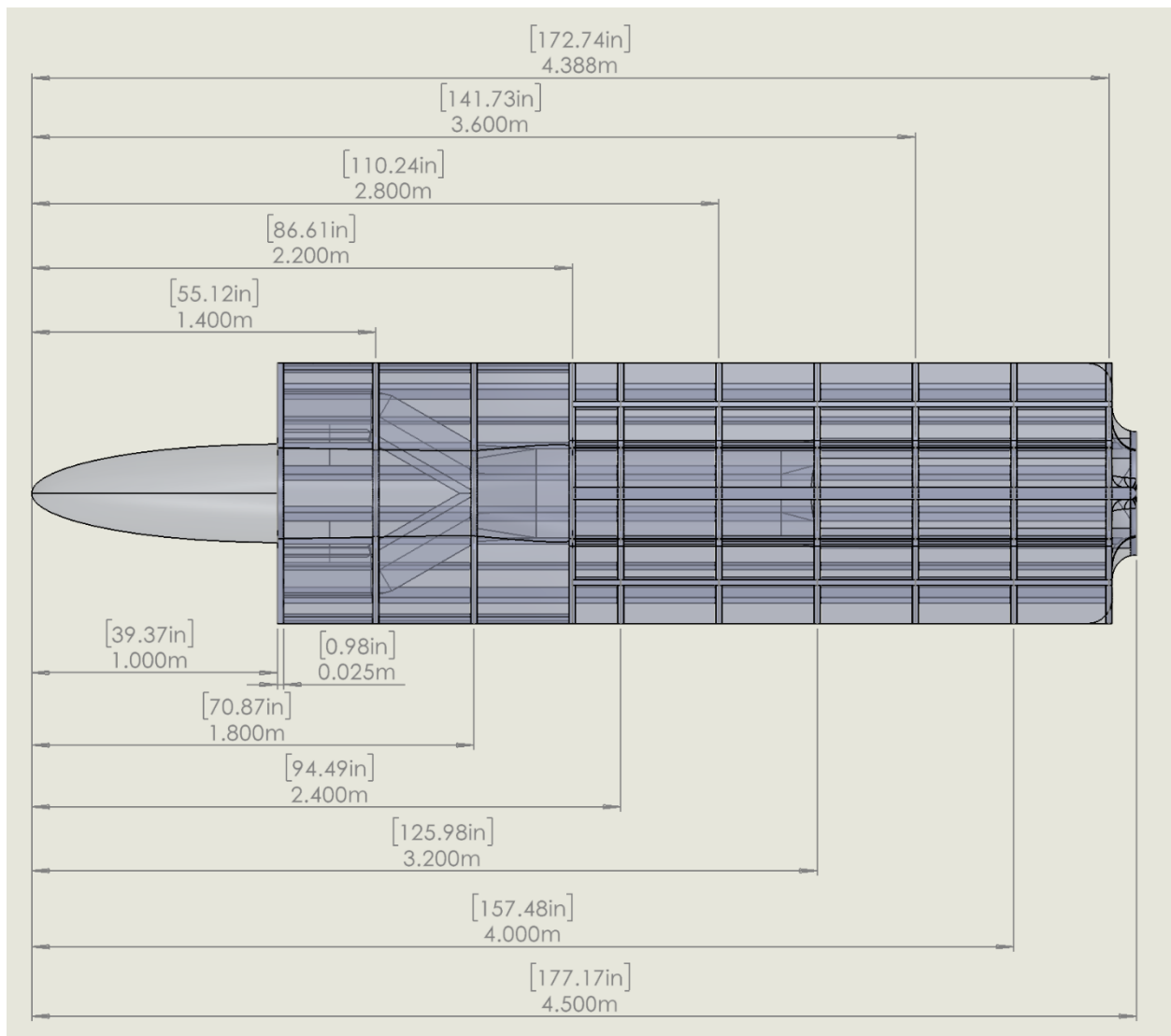


Figure 13.1 - Top view of fuselage structure layout.

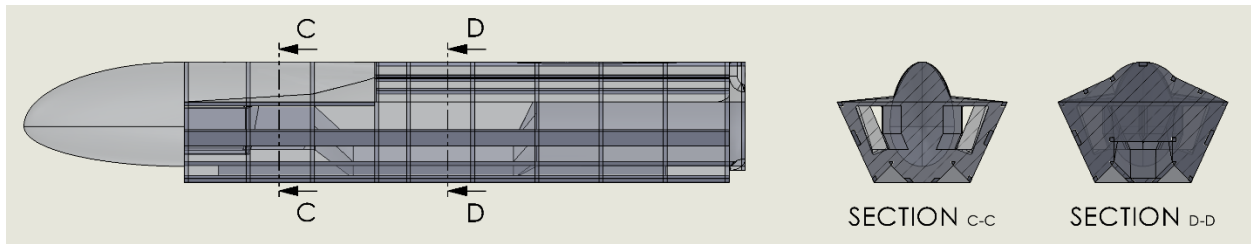


Figure 13.2 - Side and section view of fuselage structure layout.

Most of the longerons are 25 mm or 0.98 in thick. They are generally located at the corners of the fuselage cross-section. Most of them run through the whole main fuselage. However, some are shorter to avoid intruding on other components or to provide extra structural strength where it is needed. Section D shows two such longerons at the upper corners of the air duct. Finally, the longerons in the middle of the side fuselage walls are 100 mm (3.94 in) wide and 25 mm (0.98 in) thick. These reinforced longerons underneath the pylons would distribute the load of the ordinances to the rest of the structure.

13.1.2 Fuselage Structure Discussion

For a fighter, Roskam suggests a frame depth of 2.0 inches and a frame spacing of between 15 and 20 inches [18]. However, these parameters are intended for conventional materials. Given the size of the aircraft and the increasing use of composite material in aircraft design, a frame depth of 0.98 inches, or 25 mm, was chosen.

13.2 Wing Structure

13.2.1 Wing Structure Design

The wing structure is grid-like, with four spars and 14 ribs. The width and spacing of the spar are identical to those of the fuselage frames. There is also a spar at the leading edge of the wing. However, it is mainly intended to maintain the shape of the wing. It only takes on the role of spar near the wing tip. The ribs are 10 mm (0.39 in) thick and 250 mm (9.84 in) apart between the centerlines. Additional ribs and partial spars are added near the wingtip and aileron to maintain the structural integrity. The location of the ribs and spars can be observed in Figure 13.3.

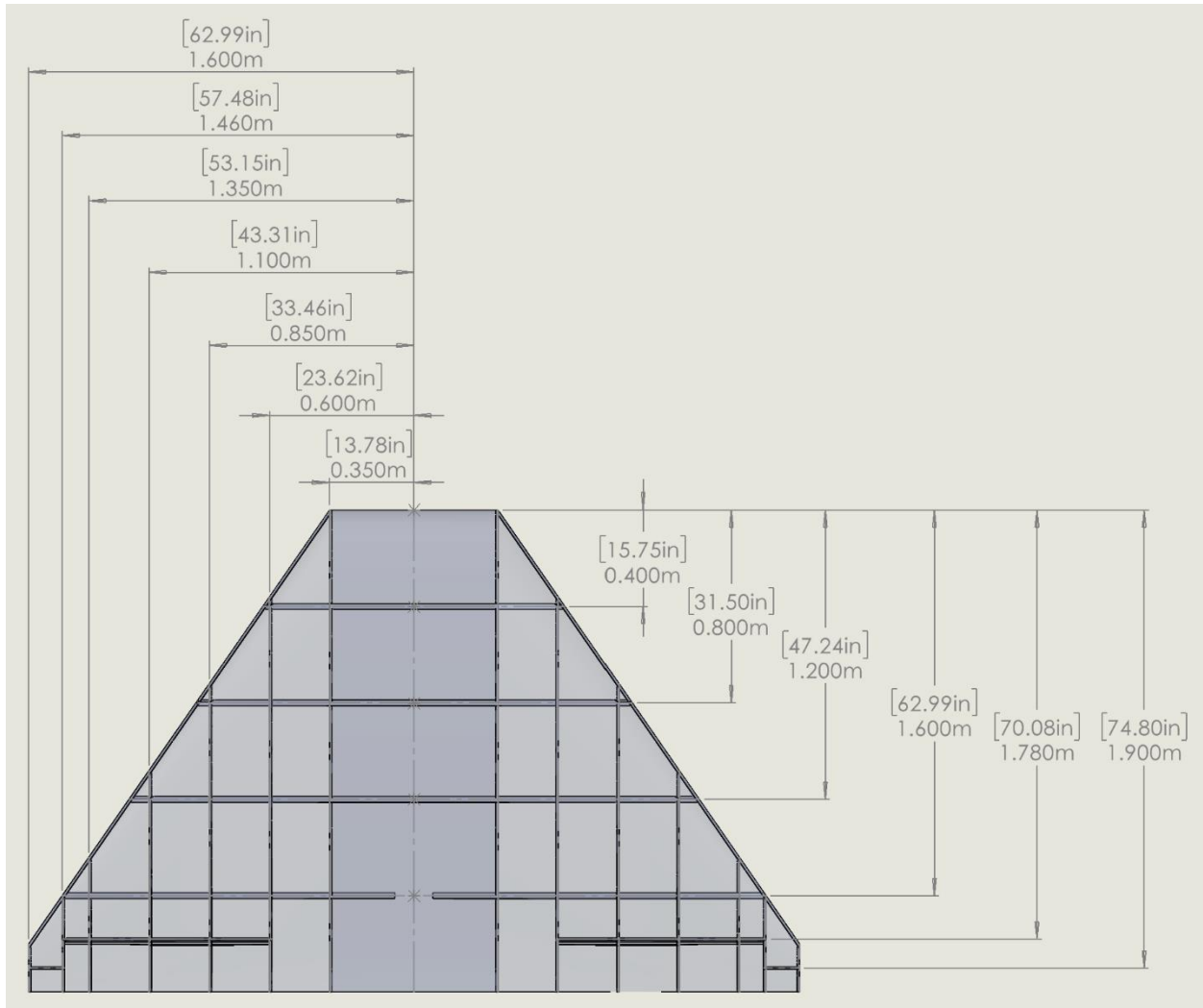


Figure 13.3 - Wing structure.

13.2.2 Wing Structure Discussion

A wing typically has two spars. The wing of a fighter has even more. Given the size of the wing and the unmanned nature of the aircraft, four spars would offer a good balance between safety and cost. The shape of the wing very often decides the orientation of the spars. Since this aircraft has a delta wing with a perfectly straight trailing edge, the spars are designed to parallel the trailing edge.

Unlike the fuselage structure, Roskam gives no suggested thickness and spacing. Therefore, this is only a rough design of the wing structure.

13.3 Canard Structure

13.1.1 Canard Structure Design

The canard has a geometry similar to that of the wing. However, the canard is a flying canard, meaning there are no other control surfaces on it. This allows its structure to be simpler. The two main spars are horizontal at and near the wing box but swept near the wingtip. Figure 13.4 shows the detailed structure of the canard.

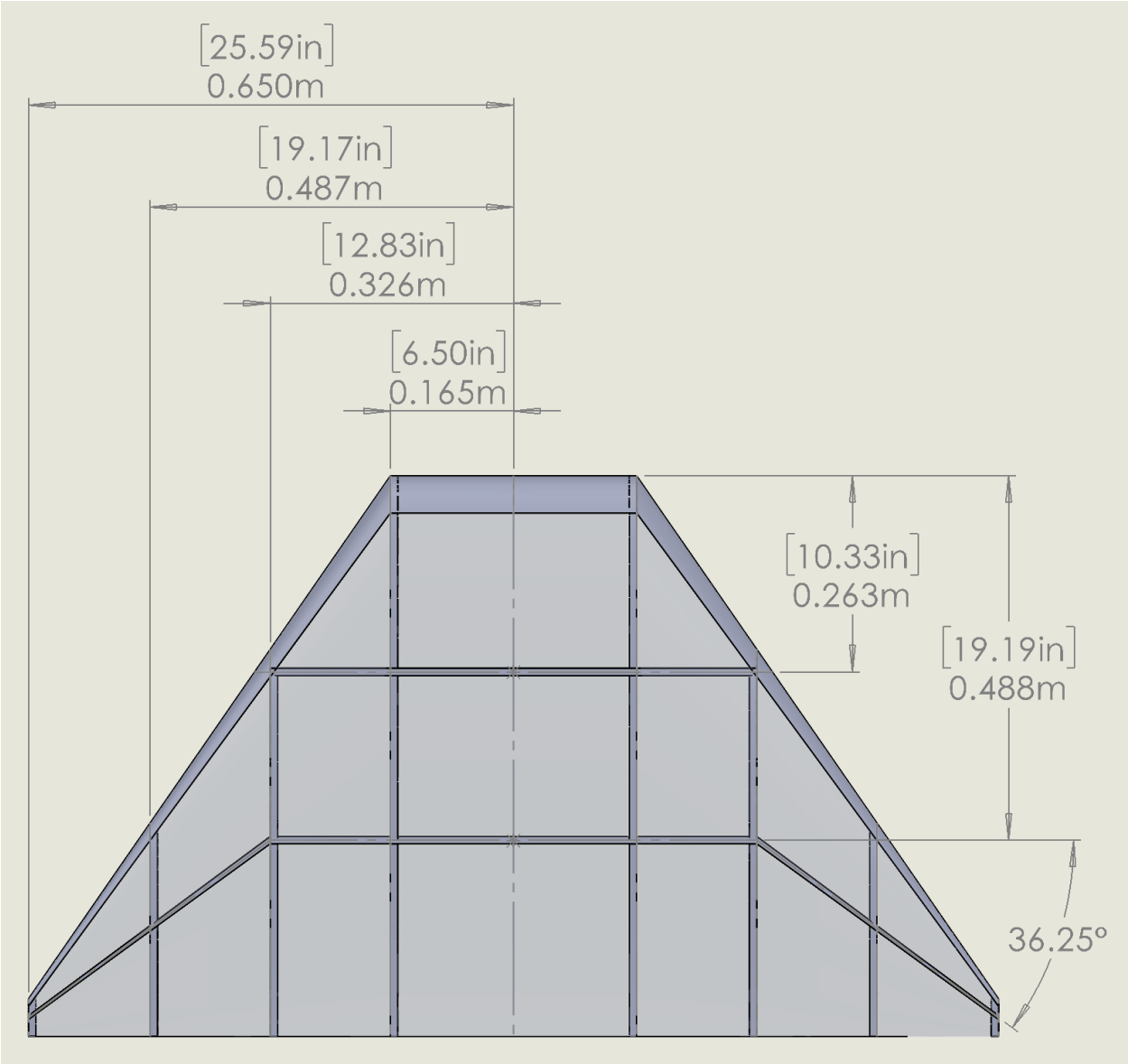


Figure 13.4 - Canard structure.

13.1.2 Canard Structure Discussion

This design seems to satisfy the minimum requirement. However, it does seem flimsy at times. At the first rib, the three spars merge to become two. While this may be adequate for such a small unmanned drone, more redundancy is certainly welcomed.

13.4 Vertical Stabilizer Structure

13.1.1 Vertical stabilizer structure Design

Unlike the wing and canard, the vertical stabilizer has a swept trailing edge. The rudder also occupies a large part of the wingspan. Therefore, it has a more complex design for the structure. The vertical stabilizer has two spars that occupy the thicker parts of the stabilizer. There are two ribs at the root and tip of the vertical stabilizer, with two more sandwiching the rudder. The mid-section of the vertical stabilizer is supported by four angled ribs. Between the first and second ribs, there are two vertical studs as mounting points to secure the vertical stabilizer to the fuselage.

13.1.2 Vertical stabilizer Structure Discussion

Compared to the canard and the wing, which both have a grid pattern, the design for the vertical stabilizer is more complicated. As mentioned early, there is no guideline from Roskam for the design of the structure for the lifting surfaces. One can only study cutaway drawings of other aircraft for guidance. The vertical stabilizer of the F-16 inspires the use of angled ribs. The angled ribs should be more structurally efficient and provide better compression resistance to the air hitting the leading edge of the vertical stabilizer.

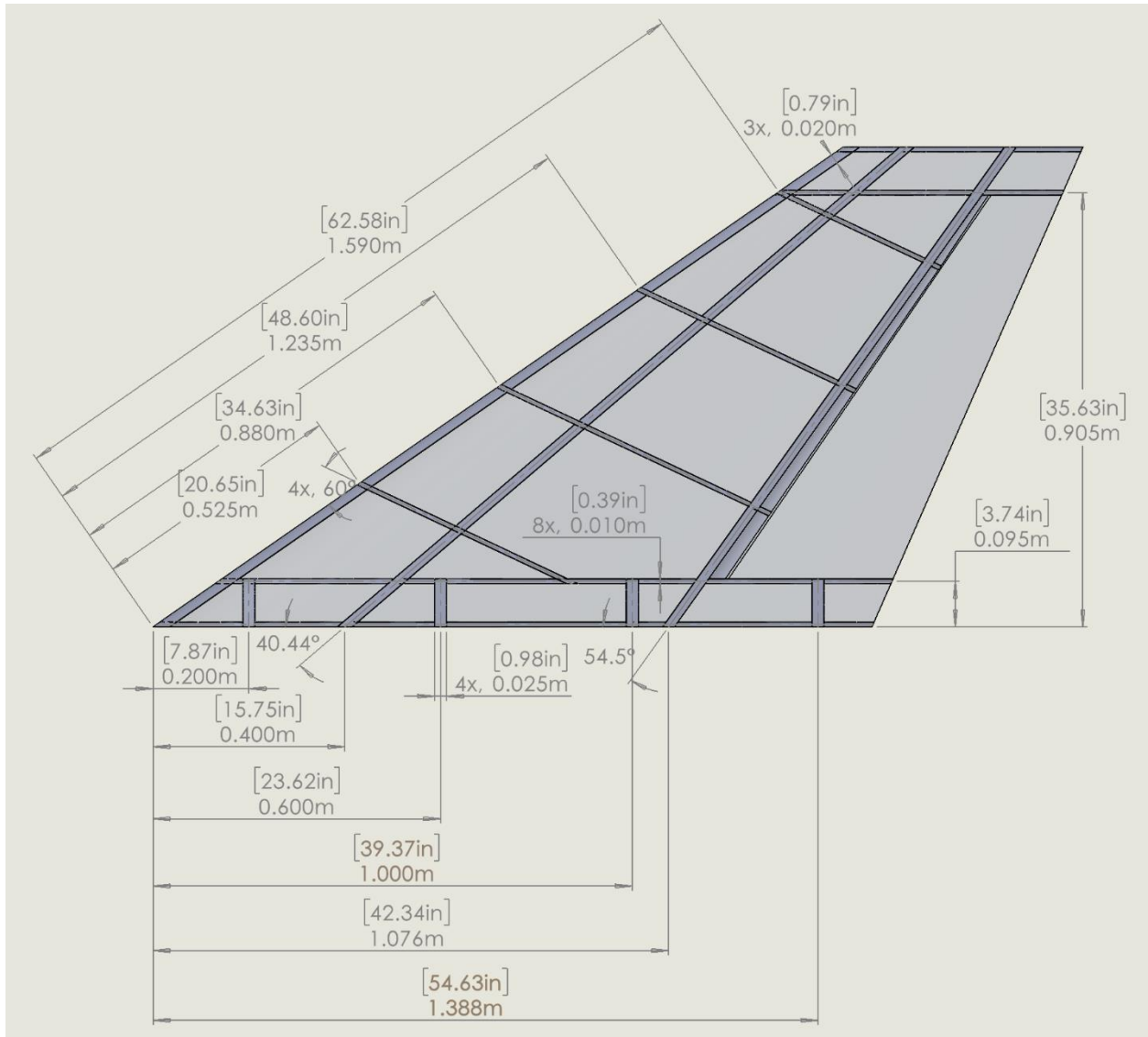


Figure 13.5 - Vertical stabilizer structure.

14. V-n Diagram

14.1 Introduction

The V-n diagram shows the load factor of the aircraft at different speeds. The load factor determines the design of the aircraft structure.

14.2 Results

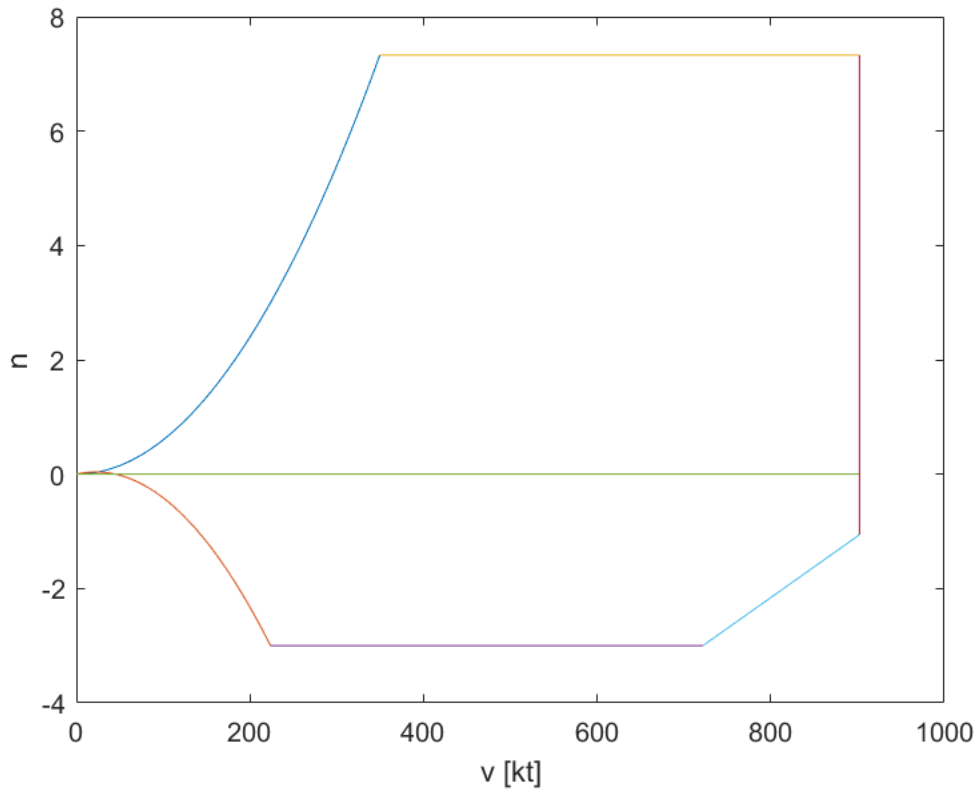


Figure 14.1 - V-n diagram for sea level conditions.

14.3 Detailed Explanation

The diagram was created following [19] and the code can be found in appendix J. The maximum positive and negative limit load factors for military aircraft are determined by their role. While this UAV is intended to take the role of a fighter attacker, it is not exactly the same as traditional

fighters, as it is never intended for dogfight combat. This UAV would be a missile slinger at best. Therefore, the attacker type under the USAF would best describe the role of this UAV. Following the USAF attacker type, the positive and negative limit load factors were determined to be 7.33 and -3.00, respectively. The maximum level speed was calculated to be 568 knots, assuming the thrust of the aircraft equals drag. The maximum dive speed was calculated to be 710 knots, which is 1.25 times the maximum level speed.

The positive and negative stall curves were each calculated using three points. The first point, (0,0), is known. The second point can be calculated using the following equation

$$V_S = \left(\frac{2 \left(\frac{GW}{S} \right)}{\rho C_{N,max}} \right)^{0.5} \quad (14.1)$$

$$V \geq V_S n_{lim}^{0.5} \quad (14.2)$$

With $n = \pm 1$, the stall speed can be calculated. The last point can be calculated using equation 14.2 using the determined maximum positive and negative limit load factors. With three points, excel is used to find the best-fit curve. The last curve at a negative load factor can be determined using two points. With the determined maximum level speed and maximum negative limit load factor, the first point is known. The load factor for the second point can be determined using the gust load factor equation

$$n_{lim} = 1 + \frac{(K_g U_{de} V C L_\alpha)}{498 \left(\frac{GW}{S} \right)} \quad (14.3)$$

14.4 Discussion

The diagram was created using air density at sea level. The maximum level speed at sea level is about the same as the design cruise speed at altitude, Mach 0.85. The dive speed corresponds to 1.05, well into the transonic territory. At this speed, the aircraft will be subjected to wave drag. However, this was not accounted for in the drag coefficient used.

15. Stability and Control Analysis

15.1 Longitudinal Stability

The longitudinal stability can be determined using an x-plot. On a longitudinal x-plot, there are two lines. One represents the location of the aerodynamic center, while the other represents the location of the center of gravity. The x-axis represents the surface area of the canard, while the y-axis represents the two locations. Simply speaking, the curves represent how much the locations of the aerodynamic center and center of gravity move as the canard area increases.

The location of the center of gravity can be calculated using the component weight from Chapter 9. The location of the aerodynamic center for a canard aircraft can be calculated using equation 15.1, which can be found in [20]. The locations are expressed in terms of percents of the mean aerodynamic chord of the wing from the leading edge of the wing.

$$\bar{x}_{acA} = \frac{\left[\bar{x}_{acwf} - \left(\frac{C_{L\alpha c} \left(1 + \frac{d\epsilon_c}{d\alpha} \right) \bar{x}_{acc} \left(\frac{S_c}{S} \right)}{C_{L\alpha wf}} \right) \right]}{\left[1 + \left(\frac{C_{L\alpha c} \left(1 + \frac{d\epsilon_c}{d\alpha} \right) \left(\frac{S_c}{S} \right)}{C_{L\alpha wf}} \right) \right]} \quad (15.1)$$

The code used to construct the x-plot can be found in appendix K.

15.2 Longitudinal Stability Discussion

Figure 15.1 shows the resulting x-plot. Typically, an x-plot would only have one curve for the center of gravity. The most aft center of gravity would be used for the calculation. But to determine the static margin at different configurations, the center of gravity at gross weight is also shown in Figure 15.1.

The static margin is the difference between the center of gravity curve and the aerodynamic center curve. The area to the left of the cross-over signifies the aircraft has positive longitudinal stability, while the area to the right signifies the opposite. The current design has a canard area of 0.64 m² or 6.97 ft². At gross weight, the static margin is -8.52%. At empty weight, the static margin grows to -19.73%.

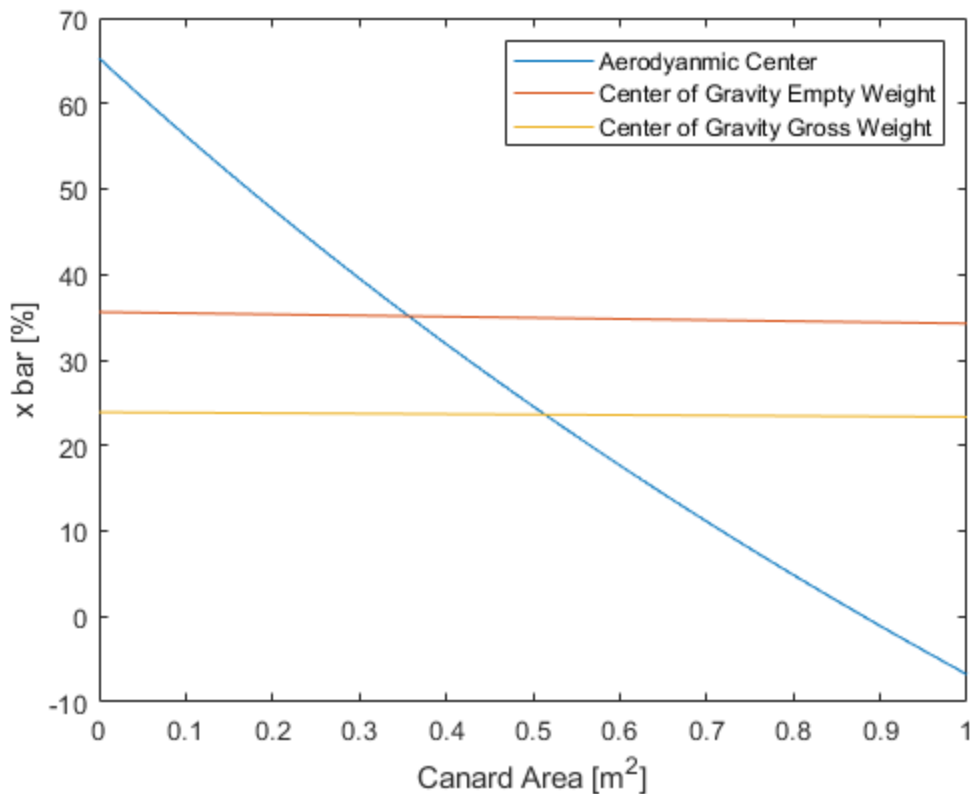


Figure 15.1 - Directional x-plot.

For a modern fighter, a negative longitudinal static margin is desired, as it would allow the aircraft to maneuver better. The stability would be provided by the flight computer instead. But just how large can a negative static margin be before it is unacceptable? For comparison, the widely in-service F-16 has a static margin of only -5%. The technology demonstrator, F-16 Advanced Fighter Technology Integration, has a static margin of -8%, only marginally larger than the regular F-16. The experimental X-29 has a static margin of nearly -40% [21].

While a -8.52% static margin at gross weight seems somewhat acceptable, the -19.73% static margin at empty weight may be potentially problematic. It may only be half of that of the X-29. But the X-29 is an experimental fighter built solely for maneuverability and, therefore, should not be taken as the norm. Per the mission profile, this aircraft would detach from the manned fighter at gross weight, conduct its mission, and return to base. The aircraft would only engage in combat near gross weight with a -8.52% static margin. The -19.73% static margin would only occur near the end of the mission, in a rare situation, should all ordinance and every single drop of fuel be expended. Ultimately, it is difficult to state that this canard design would not work. An unstable aircraft also requires flight control computers to maintain stability. Given the unmanned nature of the aircraft, such features should be easily incorporated into the flight computer.

Early on in the design, a tailless delta design was considered. The idea was quickly abandoned as it would be difficult to control the pitch of the aircraft. Later, the weight and balance revealed that a tailless canard would provide better longitudinal stability. While this aircraft is very tail-heavy, the center of gravity is still located before the aerodynamic center of the wing. The presence of the canard moves the overall aerodynamic center forward past the center of gravity. However, the low controllability of a tailless design still stands. And there is little space on the wing for elevons.

15.3 Directional Stability

There is also an x-plot for directional stability. In a directional x-plot, there is only one curve. The x-axis represents the surface area of the vertical stabilizer, while the y-axis represents the directional stability coefficient. The curve represents how much the coefficient changes as the surface of the vertical stabilizer changes. The directional stability coefficient can be calculated using equation 18.2.

$$C_{n_\beta} = C_{n_{\beta_{wf}}} + C_{L_{\alpha_v}} \frac{S_v x_v}{S b} \quad (15.2)$$

$$k_\beta = \frac{\Delta C_{n_\beta}}{C_{n_{\delta_r}}} \quad (15.3)$$

The aircraft can either be ‘inherently’ stable or ‘de facto’ stable, which means stability is augmented using flight computers. If an aircraft is ‘de facto’ stable, the sideslip to rudder feedback gain, or k_β must be determined using equation 15.3.

15.4 Directional Stability Discussion

Figure 15.2 shows the resulting x-plot. The current design has a vertical stabilizer area of 1 m² or 10.89 ft². According to the figure, this would yield a directional stability coefficient of -0.000284 deg⁻¹. According to Roskam, an ‘inherently’ stable aircraft would have a coefficient of 0.0010 deg⁻¹. The current design is insufficient for the aircraft to be ‘inherently’ stable. For a ‘de facto’ stability, the k_β must be no larger than 5 deg per deg. The calculated k_β has a value of 0.6974 deg per deg. The vertical stabilizer design satisfies the directional stability requirement.

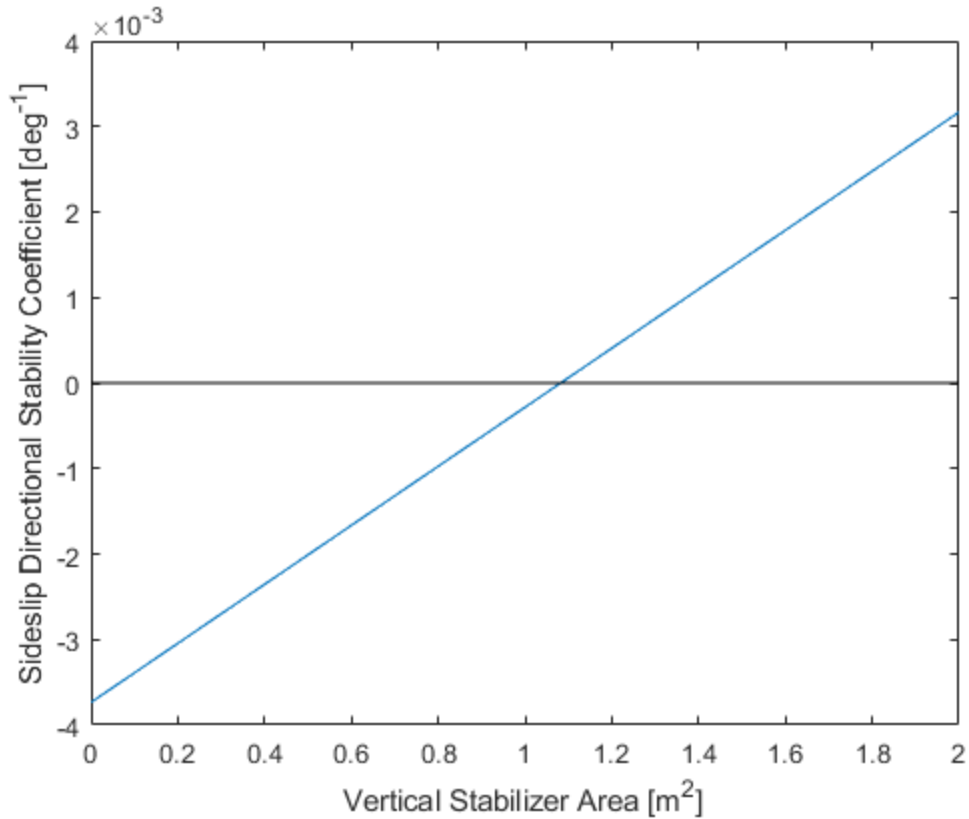


Figure 15.2 - Directional x-plot.

15.5 Trim Diagram

A trim diagram demonstrates the control area deflection needed to trim an aircraft at a specific flight condition. Here, a Raymer-style trim diagram is constructed. However, the equations and qualities used can also be found in Roskam's book. In a Raymer-style trim diagram, the x-axis represents the lift coefficient of the aircraft, while the y-axis represents the pitching moment coefficient. Arbitrary angles of attack are selected and used to calculate the lift coefficients. The multiple curves represent the control surfaces deflected at certain angles. Equation 15.4 is used to calculate the corresponding pitching moment coefficient.

Because this design features a flying canard, the deflection angle of the elevator is replaced by the incident angle of the canard. The total pitching moment coefficient can be estimated using equation 15.4 [22].

$$C_m = C_{m_0} + \frac{dC_m}{dC_L} * C_L + C_{m_{i_c}} * i_c \quad (15.4)$$

15.6 Trim Diagram Discussion

Figure 15.3 shows the resulting trim diagram. At cruise conditions, the aircraft flies at a lift coefficient of 0.1104. This aircraft has a flying canard design. The canard needs to deflect 2 degrees to trim the aircraft at cruise. At sea level and Mach 0.25, the aircraft flies at a lift coefficient of 0.7673. The canard needs to deflect about 11 degrees to trim the aircraft.

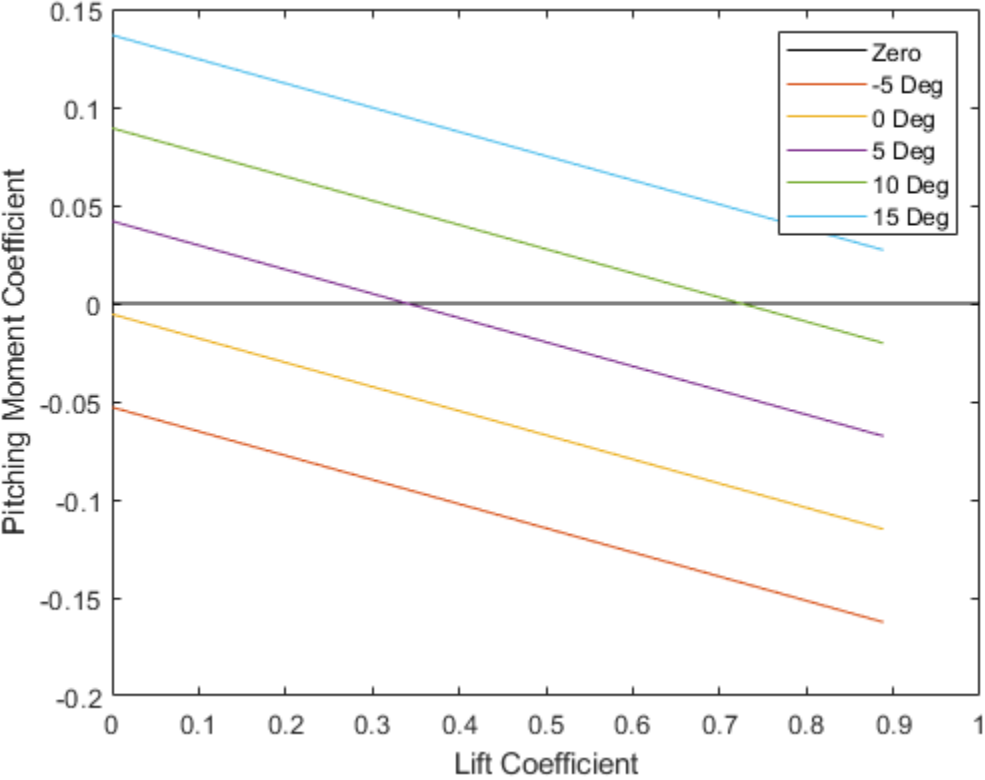


Figure 15.3 - Trim diagram.

16. Installed Power and Thrust Characteristics

16.1 Inlet Sizing

The equations used here can be found in [23], while the code can be found in appendix L.

The required inlet area for a subsonic jet can be calculated using the following equation.

$$A_c = \frac{\dot{m}_a}{\rho U_1} \quad (16.1)$$

The total mass flow rate, \dot{m}_a , can be calculated using equation 16.2.

$$\dot{m}_a = \dot{m}_{gas} + \dot{m}_{cool} \quad (16.2)$$

The mass flow rate for the engine, \dot{m}_{gas} , can be estimated using equation 16.3, while the mass flow rate for cooling is simply assumed to be 6% of the mass flow rate for the engine.

$$\dot{m}_{gas} = k_{gas} T_{TO} \quad (16.3)$$

16.2 Inlet Sizing Discussion

For equation 16.3, k_{gas} is a factor that depends on the bypass ratio of the engine. A turbojet engine is used in this design, meaning the bypass ratio is 0. Therefore, a value of 0.0003 was used for k_{gas} .

The required inlet area was calculated to be 0.0649 m² or 0.7073 ft².

16.3 Inlet Design

Figure 16.1 shows the dimension of the engine inlet, while Figure 16.2 shows the internal layout of the air duct. The current design has an inlet area of 0.07186 m² or 0.7826 ft².

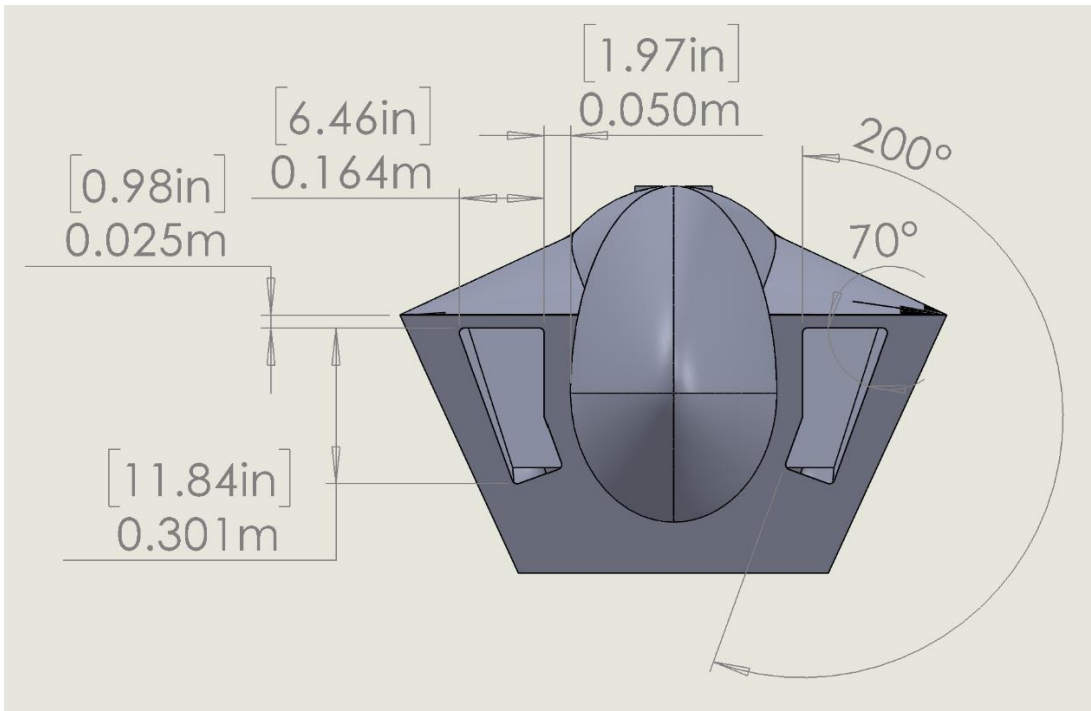


Figure 16.1 - Engine inlet dimension.

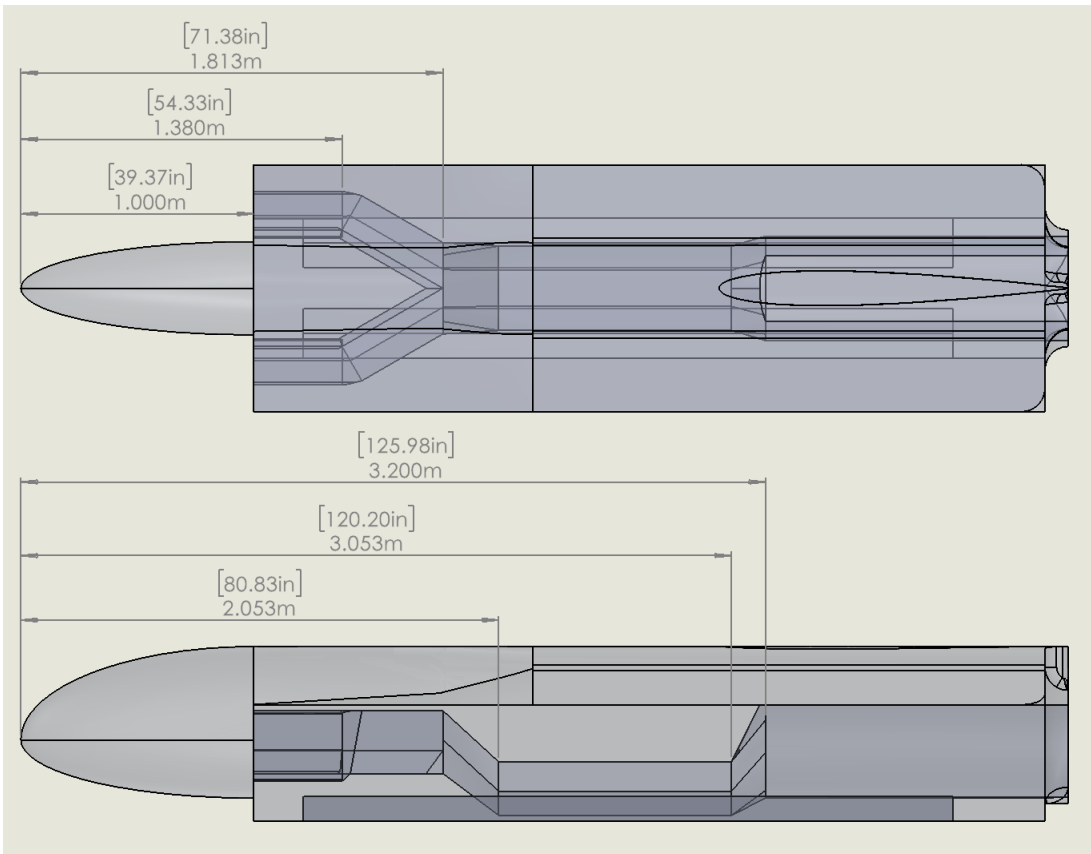


Figure 16.2 - Engine air duct.

16.4 Inlet Design Discussion

There is a 0.050 m, or 6.46 in, space between the nose of the aircraft and the engine inlet. The purpose of it is to reduce the interference on the inlet caused by the boundary layer of the nose. While not modeled here, the aircraft is intended to be fitted with a boundary layer diverter.

The location and shape of the inlet may appear strange. The inlet is located high. However, after the inlets converge, the air duct tunnels down before rising again shortly before the engine face. The bottom of the inlet is also angled. The explanation is that this inlet and air duct were designed for an older iteration of the fuselage. After the modeling of the inlet was complete, the fuselage was widened and heightened. The forward section of the air duct was left as is. It still provides the aircraft with an adequate inlet area. While there is ample space underneath the inlet, having the inlet located high up also helps prevent foreign debris from entering the engine. The air duct near the middle of the fuselage was shifted further down to create continuous internal volume for the fuel tanks. While the inlet can be optimized or redesigned, the current design would function fine.

16.5 Prediction of Installed Power and Thrust

The thrust of a turbine engine depends on the air density or the altitude the engine is operating at. The available installed thrust, T_{av} , can be calculated using equation 16.4. The calculation for the available installed thrust requires the available uninstalled thrust, or $T_{tst/av}$. Supposedly, this data is provided by the engine manufacturer. While there was an attempt to request the data from General Electric, the manufacturer of the CJ 610 engine, the engine manufacturer did not produce a response. At the same time, the data is also not readily available online. Therefore, equation 16.5 was used to approximate the uninstalled engine performance at altitude.

$$T_{av} = T_{tst/av} [1 - 0.35K_t M_1 (1 - \eta_{inl/inc})] - 550 \left(\frac{P_{extr}}{U_1} \right) \quad (16.4)$$

$$T_{tst/av} = T \frac{P_{alt}}{P_0} \sqrt{\frac{T_{alt}}{T_0}} \quad (16.5)$$

$$\eta_{inl/inc} = 1 - \frac{\Delta p_{inl}}{p_{tot\infty}} \quad (16.5)$$

$$\frac{\Delta p_{tot}}{\bar{q}_{\infty}} = \frac{I C_{Fd}}{\mu_{inl}^2} + H C_{Fa} \mu_{inl} \quad (16.6)$$

The inlet efficiency for compressible flow can be estimated using equation 16.5. The pressure loss of the inlet can be estimated using equation 16.6. If the aircraft is fitted with a boundary layer diverter, equation 16.6 can be simplified by eliminating the second term.

$$I = \int_{l_c}^{l_f} \left(\frac{A_c}{A}\right)^2 \left(\frac{p_{eA}}{A}\right) dl \quad (16.7)$$

16.6 Prediction of Installed Power and Thrust Discussion

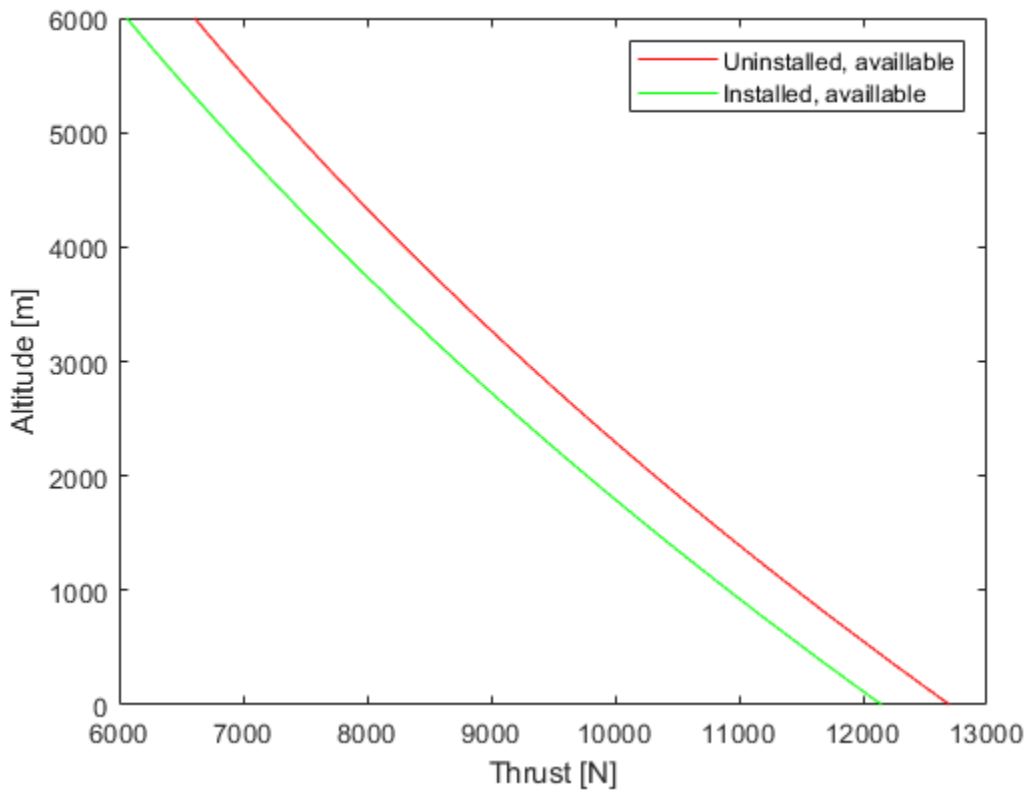


Figure 16.3 - Available installed and uninstalled thrust at altitude.

The result can be seen in Figure 16.1. For comparison, both the uninstalled and installed thrust were plotted. On average, the installed thrust is about 93.5% of the uninstalled thrust. The inlet efficiency is relatively high. The boundary layer diverter may contribute part of it. While not modeled in the CAD model, the aircraft is indeed designed to have one. There is already space

reserved for it between the side of the nose and the air inlet. The estimated power extraction requirement is another factor that may affect the result. Suggested values for fighter jets from Roskam were used to calculate the required power extraction. The traditional fighter jet role does not perfectly describe this UCAV. But it is unlikely that a small UCAV draws significantly more electricity and mechanical power from an engine than a manned fighter. A better power extraction requirement may still be unable to address the high installed thrust efficiency.

17. Critical Performance Requirements

17.1 Introduction

In this chapter, the performance of the aircraft is calculated and compared to the requirements. Given the mission profile, only the stall, cruise, and maneuvering requirements are critical. However, the climb and landing performance are calculated and presented as they are still crucial in the operation of the aircraft.

The equations used can be found in [24], while the code can be found in appendix M.

17.2 Stall Performance

17.2.1 Stall Performance Equations

The stall speed of an aircraft can be calculated using the following equation.

$$V_S = \sqrt{\frac{2(W - T \sin(\alpha_{C_{L_{max}}} + \theta_T))}{\rho C_{L_{max}} S}} \quad (17.1)$$

If thrust and thrust line inclination is zero, equation 17.1 can be simplified to

$$V_S = \sqrt{\frac{2W}{\rho C_{L_{max}} S}} \quad (17.2)$$

17.2.2 Stall Performance Result

Figure 17.1 shows the stall speed of the aircraft at altitude. The aircraft has a stall speed of 66.09 m/s or 128.5 knots without payload. With fuel and payload, the aircraft has a stall speed of 72.90 m/s or 141.7 knots. The 150 knots stall speed target is satisfied, despite the actual $C_{L_{max}}$ being lower than the $C_{L_{max}}$ used in the sizing calculation.

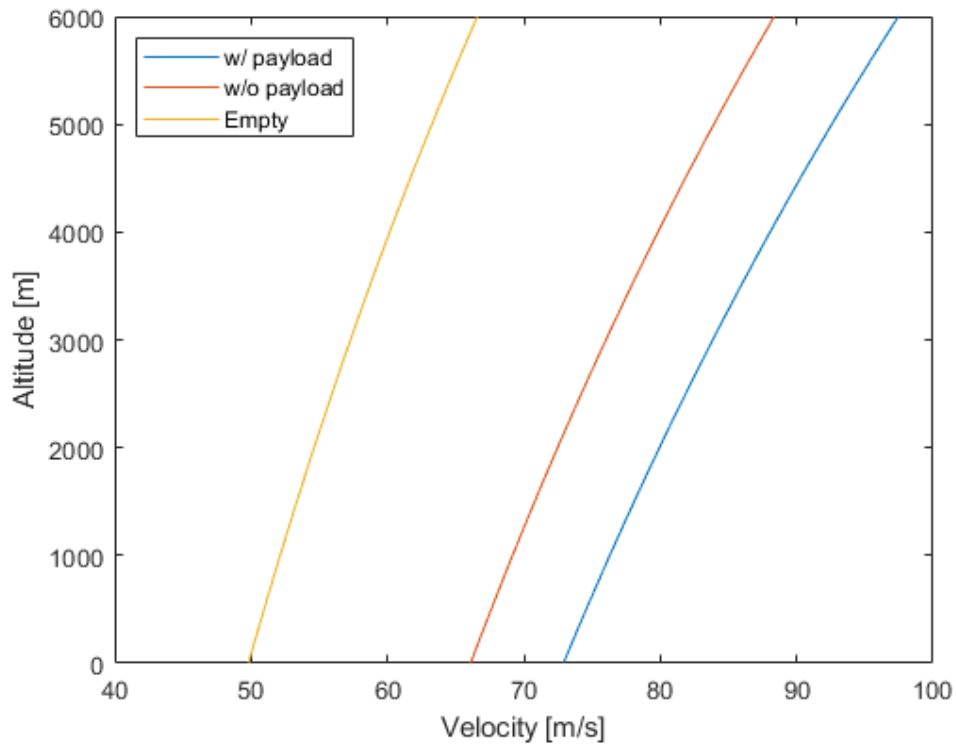


Figure 17.1 - Stall speed at altitude.

17.3 Cruise and Range Performance

17.3.1 Cruise and Range Performance Equations

The cruise range performance can be calculated using Breguet equations. The range of the aircraft cruising at constant altitude can be calculated using equation 17.3, while the range of an aircraft cruising at constant speed can be calculated using equation 17.4.

$$R = \frac{1.677}{c_j} \sqrt{\rho S} \left(\frac{\sqrt{C_L}}{C_D} \right) (\sqrt{W_{initial}} - \sqrt{W_{end}}) \quad (17.3)$$

$$R = \frac{V}{c_j} \sqrt{\rho S} \left(\frac{L}{D} \right) \ln \frac{W_{initial}}{W_{end}} \quad (17.4)$$

17.3.2 Cruise and Range Performance Result

In the mission requirement, the aircraft would carry 400 lb payload, cruise at Mach 0.85, and have a range of 1,500. Unfortunately, according to the result in Table 17.1, the range of the aircraft falls short of expectations. Given the poor drag performance shown in Chapter 11, this should be expected. Figure 17.2 shows the range of the aircraft traveling at different Mach numbers. For it to have the full 1,500 km range while carrying payload, the aircraft must fly at Mach 0.6 at a constant altitude.

Table 17.1 - Range of the aircraft traveling at Mach 0.85

Condition	Condition	Range (km)	Range (nm)
Constant Altitude	With payload	776.2	419.1
	Without payload	904.2	488.2
Constant Speed	With payload	997.8	538.8
	Without payload	1190	642.5

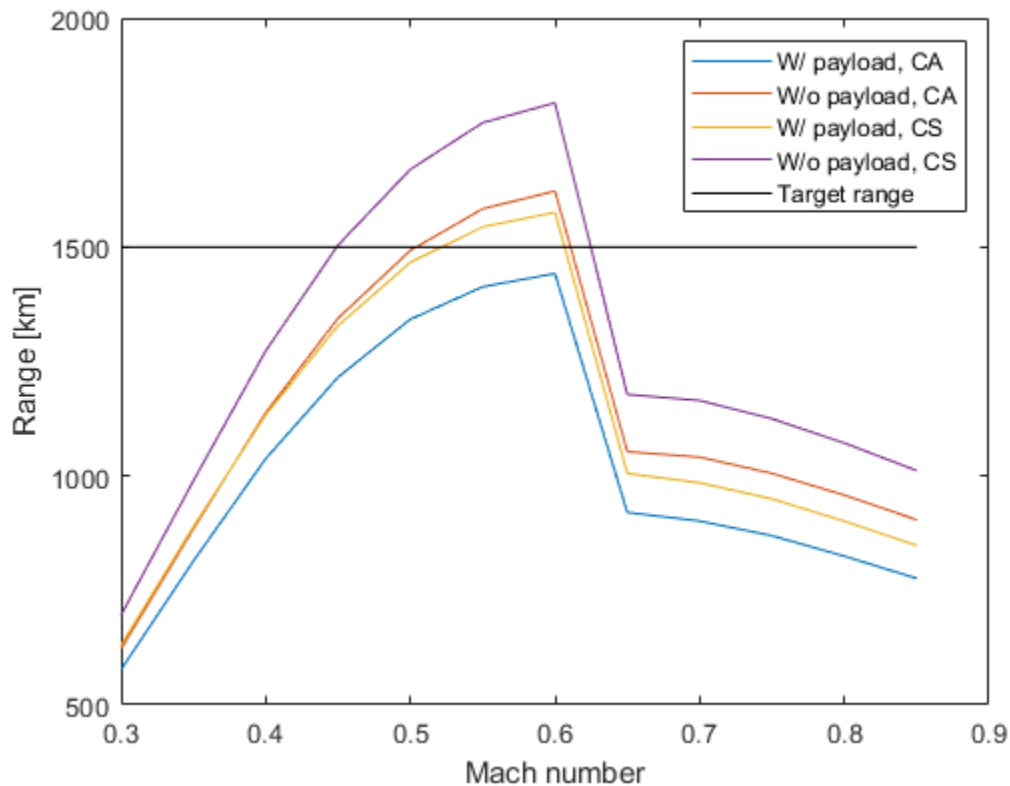


Figure 17.2 - Range of the aircraft traveling at different Mach numbers.

17.4 Maneuvering Performance

17.4.1 Maneuvering Performance Equations

While there is no mission requirement on the maneuverability of the aircraft, a target of 5-G sustained turn at Mach 0.85 was set in Chapter 3. The maneuverability of an aircraft depends heavily on wing loading and available thrust. The thrust required for a sustained turn can be calculated using the following equation.

$$T_{reqd} = \frac{C_{D_0} + C_{L_{man}}^2}{\pi A e} \bar{q} S \quad (17.5)$$

For an aircraft to sustain a turn, the required thrust must be smaller than the available installed thrust. If the required thrust is larger than the available installed thrust, the aircraft will lose speed in the maneuver.

17.4.2 Maneuvering Performance Result

Figure 17.3 shows the required and available installed thrust at sea level and cruise altitude. At sea level, the aircraft has enough thrust for a 5-G sustained turn between Mach 0.475 and 0.85. But at cruise altitude, the engine cannot produce enough thrust for the aircraft at any Mach number. Curiously, the required thrust at the two altitudes appears to converge at Mach 0.85. The required thrust at Mach 0.85 is about 9,320 N, or 2,090 lb. If the required thrust is constant between sea level and 5,000 m (16,500 ft), the highest altitude at which the aircraft can complete a 5-G sustained turn at Mach 0.85 is 2,420 m or 7,986 ft.

Figure 17.3 only shows the thrust required for the sustained turn. Figure 17.4 shows the lift coefficient required instead. In Chapter 6.5, the maximum lift coefficient of the wing was calculated to be 0.904. Since the engine cannot produce enough thrust at cruise level, the lift coefficient is a non-factor. But for sea level, the required lift coefficient reaches the maximum lift coefficient at around Mach 0.525. Therefore, at sea level, the aircraft can only sustain a 5-G turn between Mach 0.525 and 0.85.

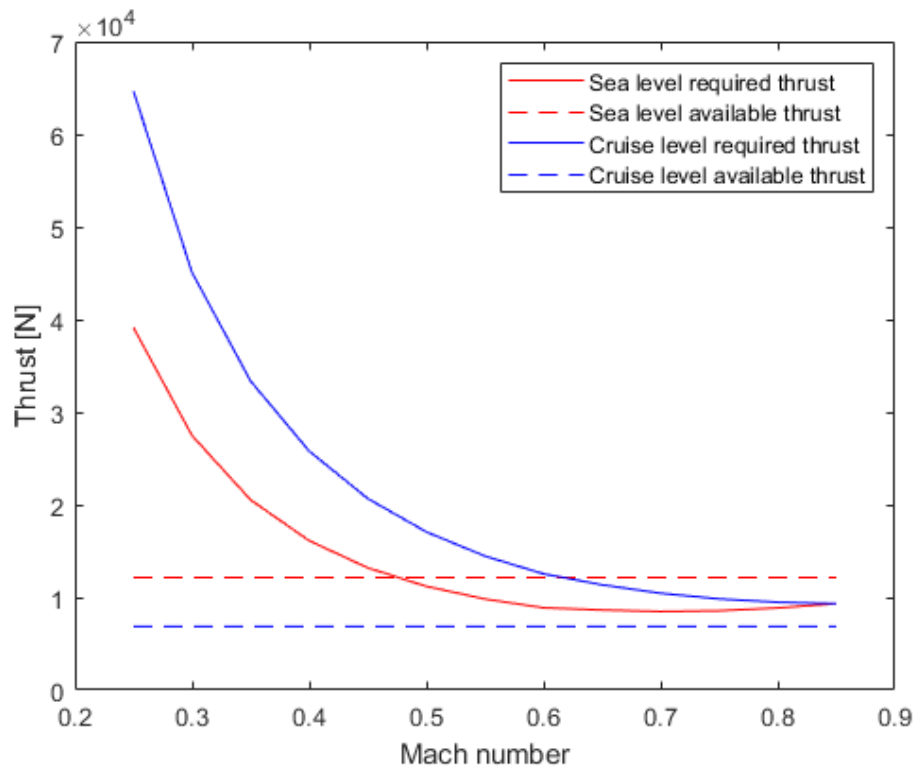


Figure 17.3 - Required and available thrust in a 5-G sustained turn.

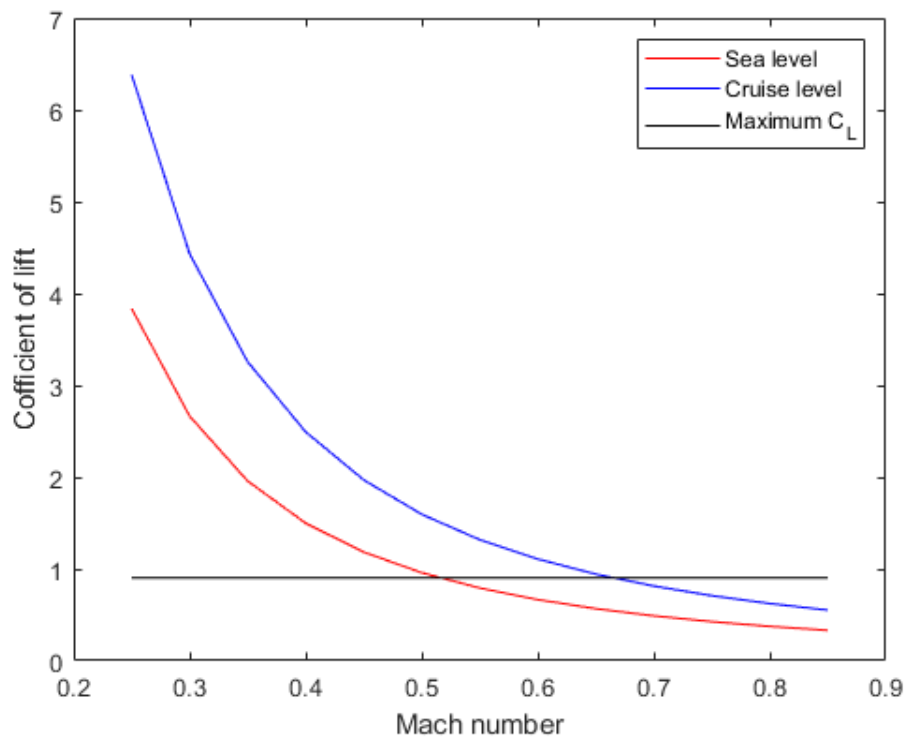


Figure 17.4 - Coefficient of lift in a 5-G sustained turn.

17.5 Climbing Performance

17.5.1 Climbing Performance Equations

The rate of climb and the climb gradient of an aircraft can be calculated using equations 17.6 and 17.7, respectively.

$$RC = 60U_1 \left(\frac{T}{W} - \left(\frac{L}{D} \right)^{-1} \right) \quad (17.6)$$

$$CGR = \frac{T}{W} - \left(\frac{L}{D} \right)^{-1} \quad (17.7)$$

17.5.2 Climbing Performance Result

The rate of climb and climb gradient of the aircraft at altitude are shown in Figures 17.5 and 17.6, respectively. In the mission profile, the UCAV is expected to detach from the mothership, conduct its mission and cruise back to base at 5,000 m. Therefore, there is not much climbing in the mission profile. Even when carrying its payload at 5,000 m, the UCAV still has a rate of climb of 1,000 fpm, which is unsurprising given the high thrust-to-weight ratio of the aircraft.

The rate of climb also indicates the altitude ceiling of the aircraft. A military aircraft must have a minimum climb rate of 100 fpm at maximum power at the service ceiling. It is clear that the service ceiling of this aircraft far exceeds the altitude it is expected to operate at.

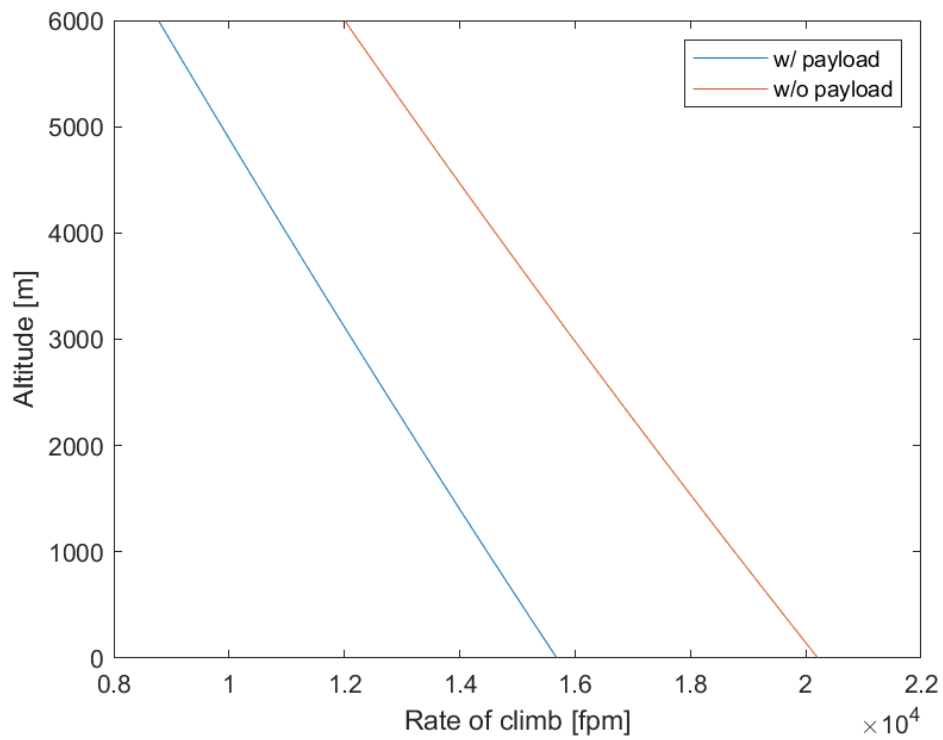


Figure 17.5 - Rate of climb at altitude.

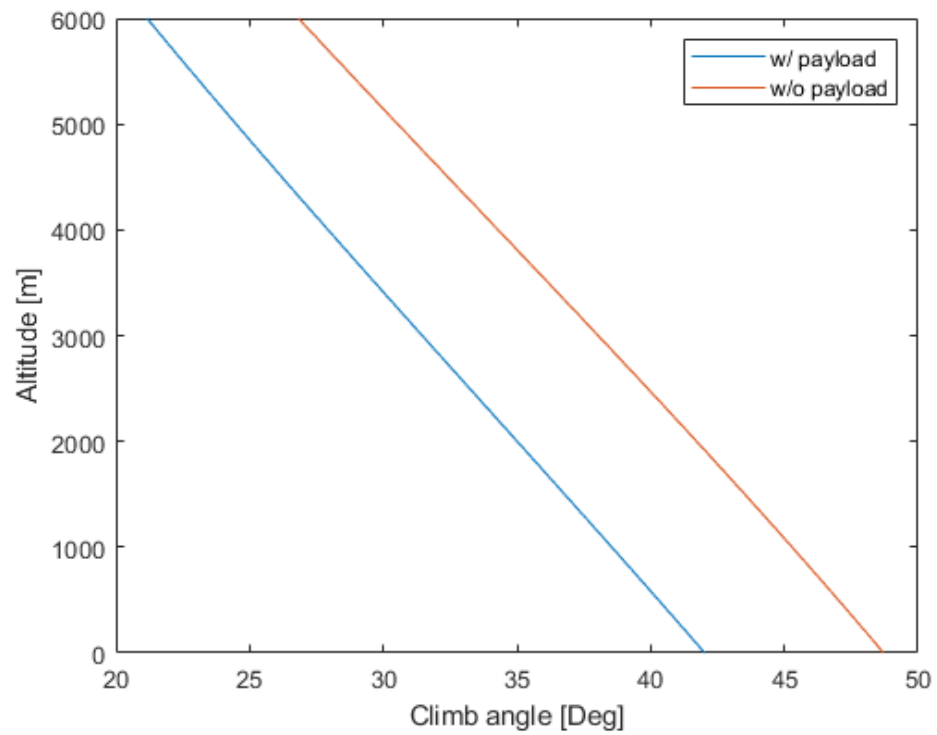


Figure 17.6 - Climb angle at altitude.

17.6 Landing Performance

17.6.1 Landing Performance Equations

The total landing distance, s_L is the sum of s_{AIR} and s_{LG} . s_{AIR} is the distance between a 50 ft obstacle and the point of touch down, while s_{LG} is the distance it takes for the aircraft to come to a complete stop after touching down. The two parameters can be calculated using the respective equations.

$$s_{AIR} = \frac{1}{\bar{\gamma}} \left(\frac{V_A^2 - V_{TD}^2}{2g} + h_L \right) \tag{17.7}$$

$$s_{LG} = \frac{V_{TD}^2}{2\bar{a}} \tag{17.7}$$

17.6.2 Landing Performance Result

Table 17.2 shows the landing distance of different configurations and segments. The maximum landing distance is 1,419 m or 4,684 ft. The landing distance is dependent on the stall speed of the aircraft. The maximum landing distance is calculated using the stall speed of the aircraft at gross weight. This is not a typical configuration the aircraft would land in. Therefore, the 1,419 m is the absolute maximum landing distance of the aircraft. It certainly takes some distance for the aircraft to stop without flaps to raise the stall speed, spoiler, and speed brake to slow it down. However, given that most airbases have at least one runway that is at least 2,000 m (6,600 ft) long, a maximum landing distance of 1,419 m is still acceptable.

Table 17.2 - Landing distances of the aircraft.

Configuration	Unit	S _{air}	S _{LG}	S _L
Full Fuel With payload	Metric (m)	541.6	877.7	1,419
	Imperial (ft)	1,787	2,896	4,684
Empty Fuel With payload	Metric (m)	472.1	721.4	1,194
	Imperial (ft)	1,558	2,381	4,225
Empty Fuel Without payload	Metric (m)	333.6	409.8	743.4
	Imperial (ft)	1,101	1,352	2,453

18. Final 3 View and Subsystem Drawings

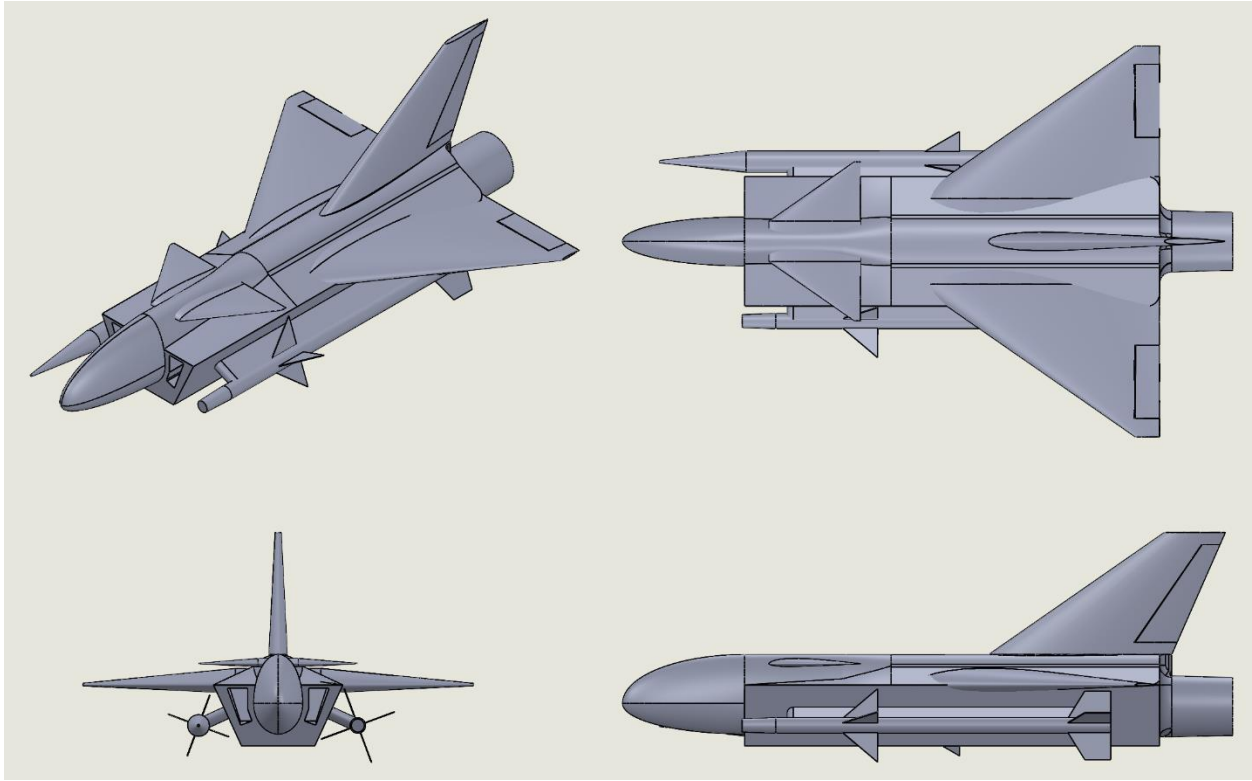


Figure 18.1 - Drawing of the aircraft with landing gear up.

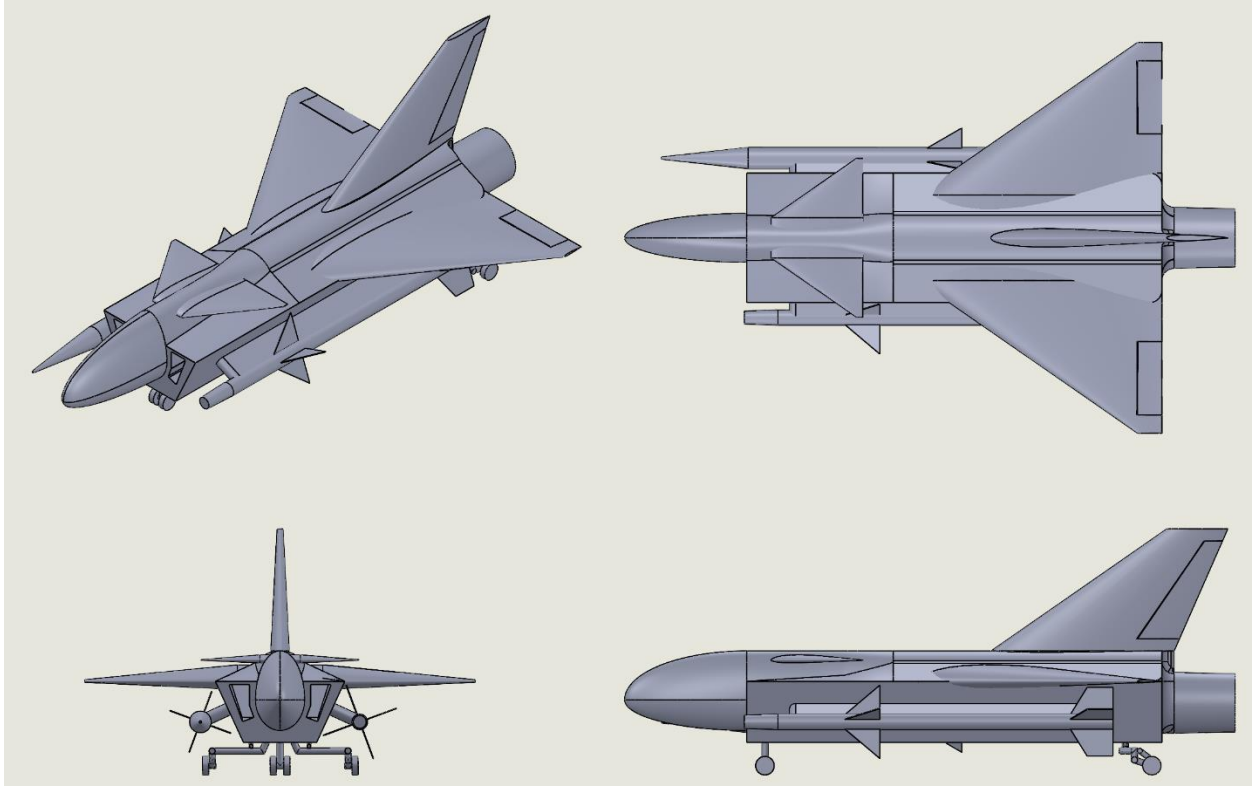


Figure 18.2 - Drawing of the aircraft with landing gear down.

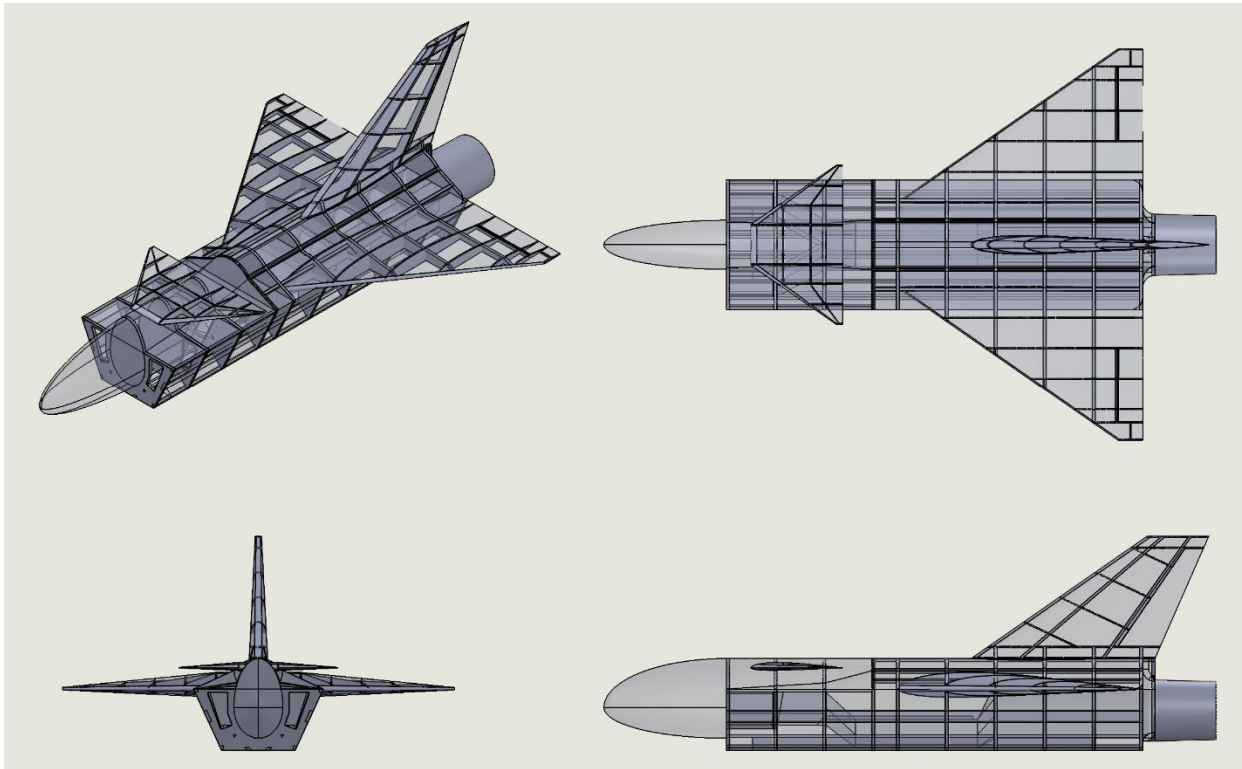


Figure 18.3 - Drawing of the aircraft structure.

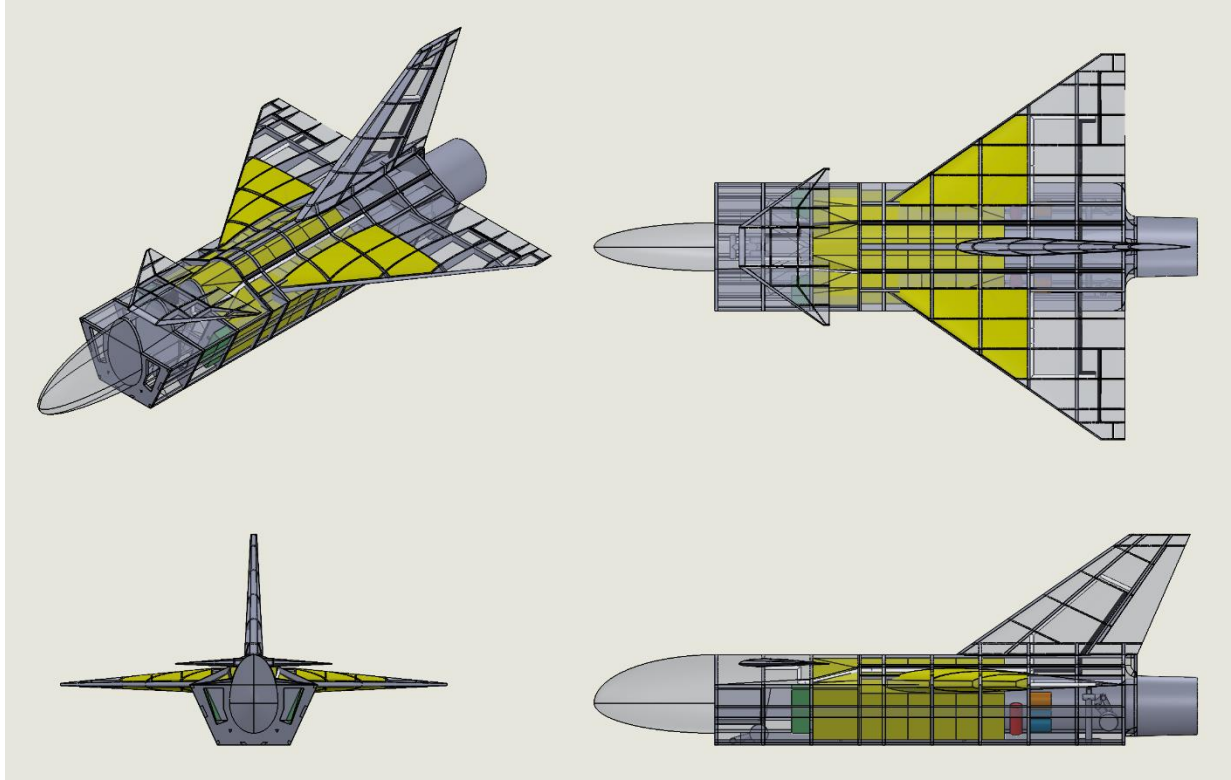


Figure 18.4 - Drawing of subsystems and structure.

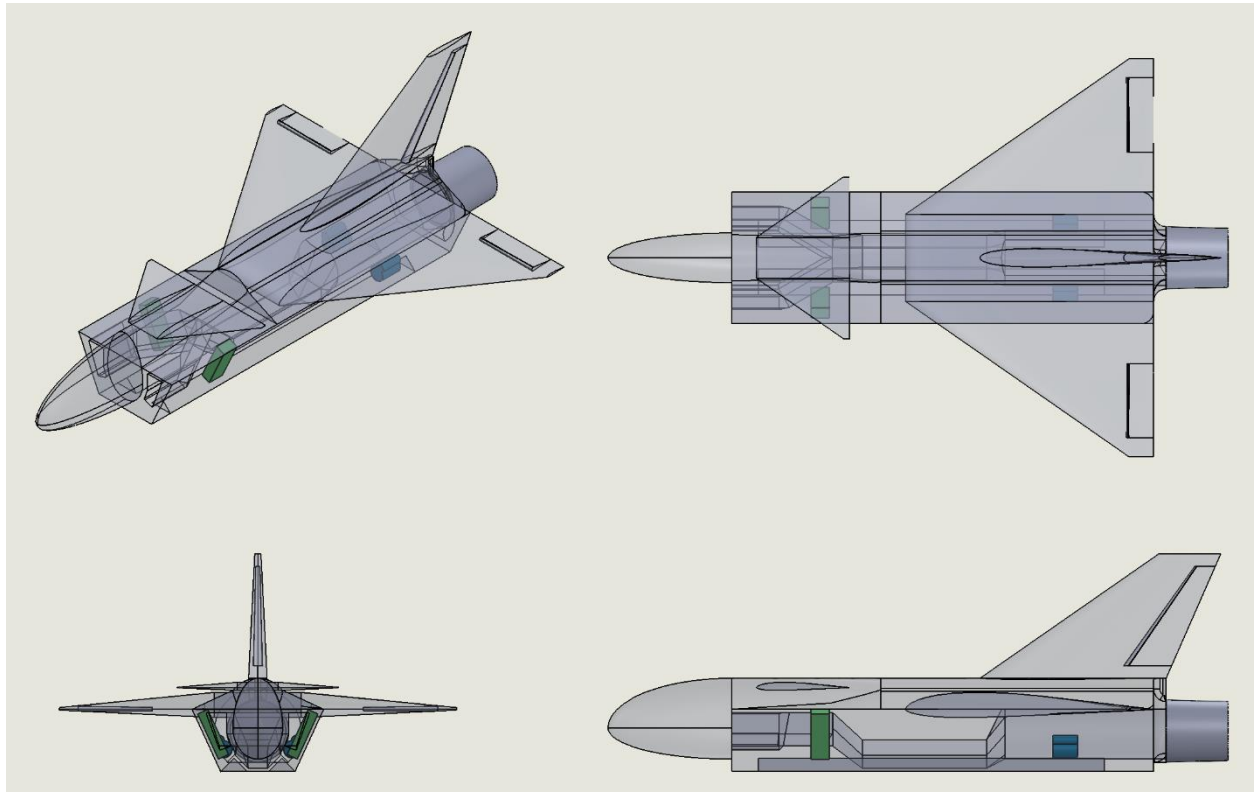


Figure 18.5 - Drawing of the electrical system.

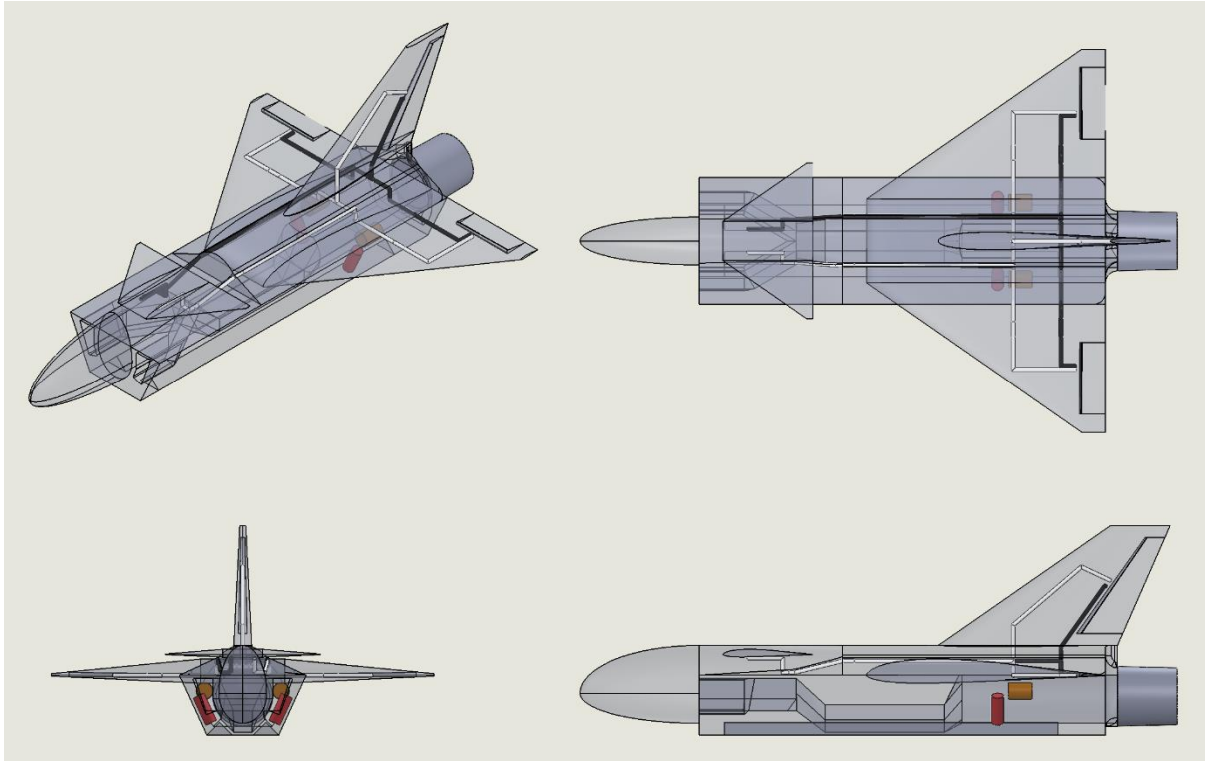


Figure 18.6 - Drawing of the hydraulic system.

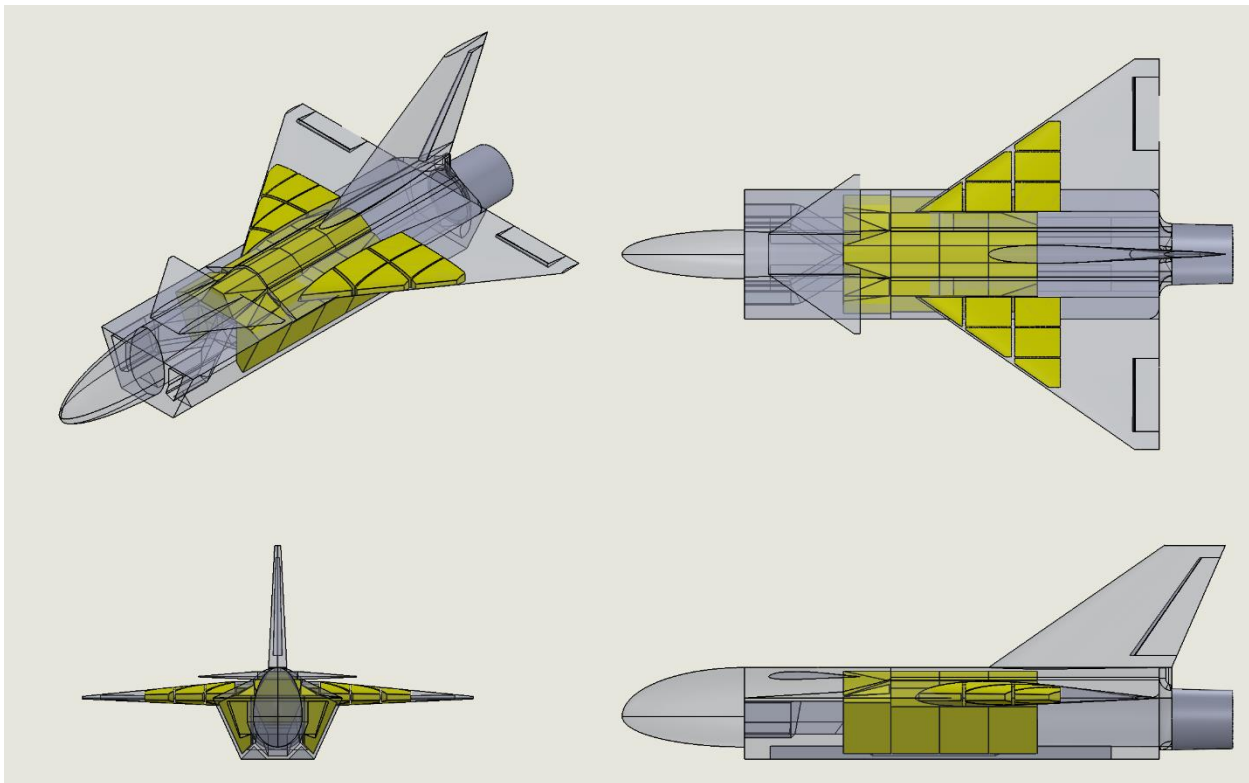


Figure 18.7 - Drawing of the fuel system.

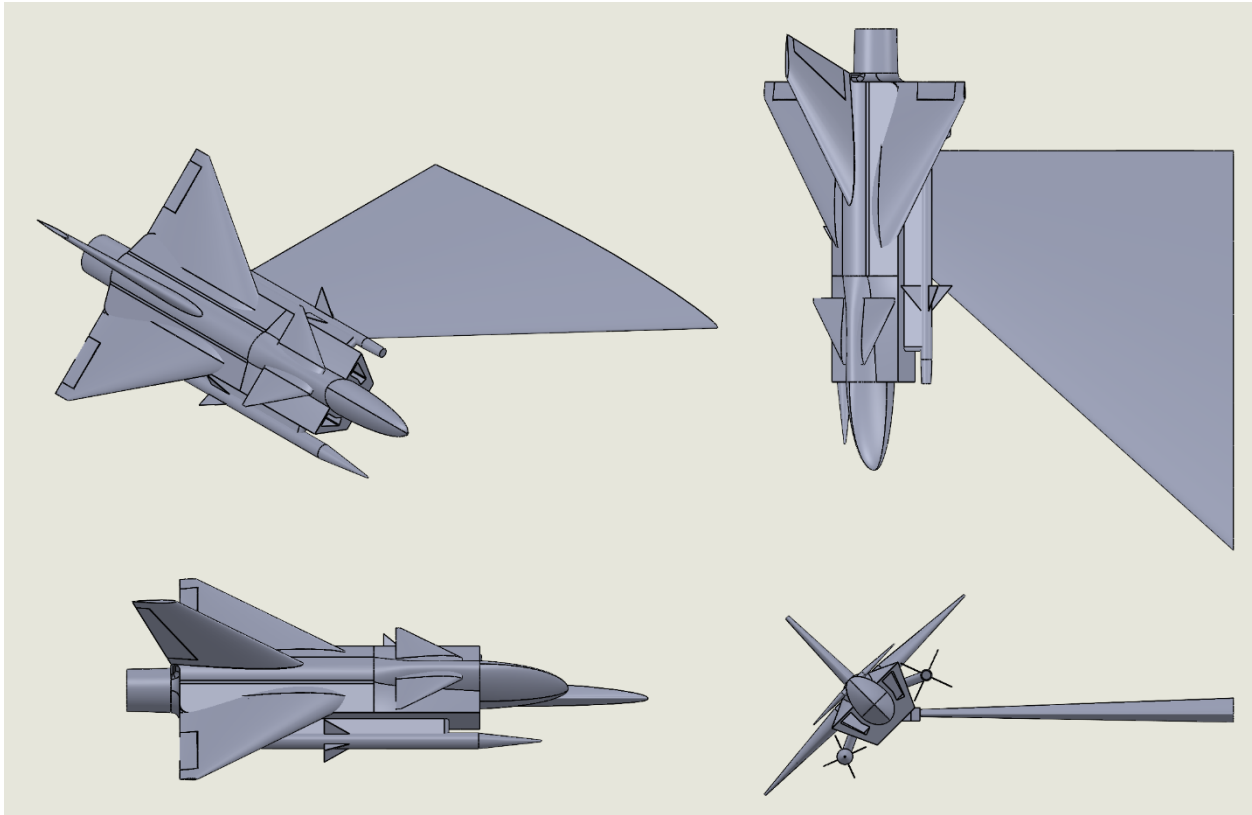


Figure 18.8 - Drawing of the UCAV docked to the right wing of F-16.

19. Cost Analysis

19.1 Introduction

The length of the life cycle of an aircraft depends on the nature of the program. For an experimental plane, the life cycle is short, ending with the testing of the prototype aircraft. For most production aircraft, the entire life cycle can be divided into four main sections: RDTE, acquisition, operation, and disposal. RDTE stands for research, development, test, and evaluation. In order to estimate the cost of the entire program, the cost of each part of the development must be calculated and summed.

The cost was calculated using equations from [25].

19.2 Research, Development, Test, and Evaluation Cost for Prototype Estimation

The total research, development, test, and evaluation cost, or C_{RDTE} , is the sum of seven components and can be calculated using the following equation.

$$C_{RDTE} = C_{aed_r} + C_{dst_r} + C_{fta_r} + C_{fto_r} + C_{tsf_r} + C_{pro_r} + C_{fin_r} \quad (19.1)$$

19.3 Manufacturing and Acquisition Cost Estimation

The manufacturing cost can be calculated using equation 19.2.

$$C_{MAN} = C_{aed_m} + C_{apc_m} + C_{fto_m} + C_{fin_m} \quad (19.2)$$

The airplane program production cost can be calculated using equation 19.3

$$C_{apc_m} = C_{(e+a)_m} + C_{int_m} + C_{man_m} + C_{tool_m} + C_{qc_m} \quad (19.3)$$

The acquisition cost is simply the sum of the manufacturing cost and the profit made by the manufacturer. The unit price per airplane is an important metric and can be calculated using equation 19.4.

$$AEP = \frac{(C_{MAN} + C_{PRO} + C_{RDTE})}{N_m} \quad (19.4)$$

19.4 Operating Cost Estimation

The operating cost for military aircraft can be calculated using equation 19.5.

$$C_{OPS} = C_{POL} + C_{PERSDIR} + C_{PERSIND} + C_{CONMAT} + C_{SPARES} + C_{DEPOT} + C_{MISC} \quad (19.5)$$

19.5 Life Cycle Cost Estimation

The remaining cost unaddressed is the disposal cost. The disposal cost is estimated to be 1% of the life cycle cost. Therefore, the total life cycle cost can be calculated with equation 19.6.

$$LCC = \frac{(C_{RDTE} + C_{ACQ} + C_{OPS})}{0.99} \quad (19.6)$$

19.6 Cost Estimation Result

The code used in the calculation can be found in appendix N. The code is discontinuous because some costs are defined as a fraction of the total cost. An iterative process was used to calculate the actual cost. For example, the avionics cost for a military aircraft is defined as a percent of the unit price. First, a guess value was entered for the manufacturing cost. After the calculation, the calculated manufacturing cost was compared with the guessed manufacturing cost. The guess value was adjusted until the two values equaled each other.

For RDTE, ten prototype aircraft would be built, with two aircraft for static tests. Because of the small size of the aircraft and the moderate amount of new technology used on the aircraft, the test and simulation facilities cost was set to zero as existing facilities should be adequate for the program.

Table 19.1 - Life Cycle Cost Breakdown

	Cost Component	Symbol	Cost (USD)	
RDTE	Airframe Engineering and Design Cost	C_{aed_r}	368,700,000	
	Development and Testing Cost	C_{dst_r}	30,257,000	
	Flight Test Airplanes Cost	C_{fta_r}	844,800,000	
		Cost of Engine and Avionics	$C_{(e+a)_r}$	42,844,000
		Manufacturing Labor Cost	C_{man_r}	376,770,000
		Manufacturing Material Cost	C_{mat_r}	31,342,000
		Tooling Cost	C_{tool_r}	344,860,000
		Quality Control Cost	C_{qc_r}	48,980,000
	Flight Test Operations Cost	C_{fto_r}	10,924,000	
	Test and Simulation Facilities Cost	C_{tsfr}	0	
	RDTE Profit	C_{pro_r}	156,830,000	
	Cost to Finance RDTE	C_{fin_r}	156,830,000	
Total RDTE Cost	C_{RDTE}	1,568,300,000		
Manufacturing	Aircraft Engineering and Design Cost	C_{aed_m}	345,810,000	
	Aircraft Production Cost	C_{apc_m}	11,330,000,000	
		Cost of Engine and Avionics	$C_{(e+a)_m}$	5,355,500,000
		Cost of interior	C_{int_m}	0
		Manufacturing Labor Cost	C_{man_m}	3,853,300,000
		Manufacturing Material Cost	C_{mat_n}	376,770,000
		Tooling Cost	C_{tool_m}	439,310,000
		Quality Control Cost	C_{qc_m}	500,920,000
	Production Flight Test Operations Cost	C_{fto_m}	10,924,000	
	Cost to finance manufacturing	C_{fin_m}	1,476,700,000	
	Total Manufacturing Cost	C_{MAN}	14,767,000,000	
	Manufacturing Profit	C_{PRO}	1,476,700,000	
Acquisition Cost	C_{ACQ}	16,244,000,000		
Operation	Fuel, Oil and Lubricants Cost	C_{POL}	1,127,900,000	
	Direct Personnel Cost	$C_{PERSDIR}$	26,699,000,000	
	Indirect Personnel Cost	$C_{PERSIND}$	14,534,000,000	
	Consumable Material Cost	C_{CONMAT}	3,856,500,000	
	Spares Cost	C_{SPARES}	14,709,000,000	
	Depot Cost	C_{DEPOT}	15,059,000,000	
	Miscellaneous Cost	C_{MISC}	15,426,000,000	
	Total Operating Cost	C_{OPS}	87,555,000,000	
	Hourly Operating Cost	$C_{OPS/HR}$	20,187	
	Disposal Cost	C_{DISP}	1,064,300,000	
	Life Cycle Cost	LCC	106,430,000,000	
	Unit Price per Airplane	AEP	17,812,000	

For serial production, an estimated 1,000 aircraft would be built. This is due to the expandable nature of a UCAV and the fact that this aircraft was designed for operating in contested airspaces, which is relatively uncommon on the modern battlefield. Since each manned fighter would carry two drones on the wingtips, this would be equivalent to equipping 500 manned fighters.

After the cold war, affordability has become a big part of weapons procurement. The calculated unit price per airplane is 17.8 million dollars. This number seems high for a small drone. It is about a quarter of the unit price for an F-35A in 2022. Although smaller, this drone still has all the necessary parts of an aircraft. This number may not be out of the realm of possibility. The hourly operating cost was calculated to be 20,187 dollars.

19.6 Cost Estimation Discussion

It is difficult to say whether or not these are accurate estimates. It has been decades since the Airplane Design book was written. While Roskam tried to compensate for inflation and rising labor cost in the calculation, some predictions may not match reality. Even if those predictions hold, this aircraft differs significantly from the aircraft Roskam used to formulate his equations. For example, W_{ampr} is a recurring parameter used in the calculation of different costs. W_{ampr} stands for Aeronautical Manufacturers Planning Report weight of the airplane. One way to obtain this number is by looking up the corresponding weight for a given takeoff weight using a figure in the book. The first data point has a takeoff weight of about 10,000 pounds. The trend line has a suggested validity limit between 5,000 and 1,000,000 pounds. This aircraft design, with a target gross weight of 3,000 pounds, falls short of this scope.

Another way to validate the result is by comparing it with similar programs. However, there is no existing data for comparison. UCAV is a recent concept, and many developments are still ongoing. This UCAV is also different from other loyal wingman drones in development because it is much smaller and lighter than others.

20. Reference

- [1] Hallstead, William., “Parasite Aircraft.” *Aviation History*, Vol 12, No 2, 2001, pp. 38
- [2] Johnsen, Federick, A., “Mother Ships,” *Aviation History*, Vol 28, No 3, 2018, pp. 46-53
- [3] Polmar, Norman., “Historic Aircraft,” *Naval History*, Vol 21, No 5, 2007, pp. 12-13
- [4] “Project Tip-Tow,” *Aviation History*, Vol 22, No 3, 2012, pp. 14-45
- [5] Anderson, Clarence. E., “Dangerous Experiments,” *Flight Journal*, Vol 6, 2000, pp 64-72
- [6] “April 27, 1956: The FICON Project was Completed After Seven Flights of an RF-84K from a Modified B-36,” *Air Force Test Center*, 2021
- [7] Zhang, H., Huang, C., Zhang, Z., Wang, X., Han, B., Wei, Z., Li, Y., Wang, L., & Zhu, W., “The Trajectory Generation of UCAV Evading Missiles based on Neural Networks,” *Journal of physics. Conference series*, Vol 1486, No 2, 2020, pp.22-25
- [8] “XQ-58A Valkyrie,” Kratos, 2018. Retrieved from <https://www.kratosdefense.com/-/media/k/pdf/usd/xq-58a-valkyrie.pdf>
- [9] “Boeing Airpower Teaming System,” Boeing. Retrieved from <https://www.boeing.com/defense/airpower-teaming-system/>
- [10] Raymer, D. P., “Sizing From A Conceptual Sketch,” *Aircraft Design: A Conceptual Approach, 2nd ed.*, AIAA, Washington, DC, 1992, pp.11-32.
- [11] Roskam, J., “Estimating Take-off Gross Weight, W_{TO} , Empty Weight, W_E , And Mission Fuel Weight, W_F ,” *Airplane Design Part I: Preliminary Sizing of Airplanes*, DARcorporation, Lawrence, Kansas, 2018, pp. 5-85.
- [12] Roskam, J., “Estimating Wing Area, S , Take-off Thrust, T_{TO} , (Or Take-off Power, P_{TO}) and Maximum Lift, $C_{L_{max}}$: Clean, Take-off and Landing,” *Airplane Design Part I: Preliminary Sizing of Airplanes*, DARcorporation, Lawrence, Kansas, 2018, pp. 89-192.
- [13] Roskam, J., “Class I Method for Empennage Sizing and Disposition and for Control Surface Sizing and Disposition,” *Airplane Design Part II: Preliminary Configuration Design and Integration of the propulsion System*, DARcorporation, Lawrence, Kansas, 2018, pp.187-216.
- [14] Raymer, D. P., “Aerodynamics,” *Aircraft Design: A Conceptual Approach, 2nd ed.*, AIAA, Washington, DC, 1992, pp.257-312.
- [15] Raymer, D. P., “Landing Gear and Subsystems,” *Aircraft Design: A Conceptual Approach, 2nd ed.*, AIAA, Washington, DC, 1992, pp.229-256.
- [16] Roskam, J., “Class II Method for Estimating Structure Weight,” “Class II Method for Estimating Powerplant Weight,” “Class II Method for Estimating Fixed Equipment Weight,”

Airplane Design Part V: Component Weight Estimation, DARcorporation, Lawrence, Kansas, 2018, pp. 67-112.

[17] Roskam, J., “Drag Polar Prediction Methods,” *Airplane Design Part VI: Preliminary Calculation of Aerodynamic, Thrust and Power Characteristics*, DARcorporation, Lawrence, Kansas, 2018, pp. 21-113.

[18] Roskam, J., “Fuselage Layout Design,” *Airplane Design Part III: Layout Design of Cockpit, Fuselage, Wing and Empennage: Cutaways and Inboard Profiles*, DARcorporation, Lawrence, Kansas, 2018, pp. 35-153.

[19] Roskam, J., “Methods for Constructing V-n Diagrams,” *Airplane Design Part V: Component Weight Estimation*, DARcorporation, Lawrence, Kansas, 2018, pp. 31-45.

[20] Roskam, J., “Class I Method for Stability and Control Analysis,” *Airplane Design Part II: Preliminary Configuration Design and Integration of the propulsion System*, DARcorporation, Lawrence, Kansas, 2018, pp. 259-280.

[21] Gera, J., “Dynamics and Controls Flight Testing of the X-29A Airplane,” NASA TM-86803, January 1986.

[22] Roskam, J., “Airplane Pitching Moment: Flaps Up,” *Airplane Design Part VI: Preliminary Calculation of Aerodynamic, Thrust and Power Characteristics*, DARcorporation, Lawrence, Kansas, 2018, pp. 318-328.

[23] Roskam, J., “Installed Power and Thrust Prediction Methods,” *Airplane Design Part VI: Preliminary Calculation of Aerodynamic, Thrust and Power Characteristics*, DARcorporation, Lawrence, Kansas, 2018, pp. 139-202.

[24] Roskam, J., “Performance,” *Airplane Design Part VII: Determination of Stability, Control and Performance Characteristics: FAR and Military Requirements*, DARcorporation, Lawrence, Kansas, 2018, pp. 111-176.

[25] Roskam, J., *Airplane Design Part VIII: Airplane Cost Estimation: Design, Development, Manufacturing and Operating*, DARcorporation, Lawrence, Kansas, 2018.

Appendix A. RDS Weight Estimate 500 lb Payload

MISSION SIZING OR RANGE

Seg. 2 CRUISE : 980.7 km/h at 5000.0 m RANGE = 1500.0 km

TOTAL RANGE =	1500.0	TOTAL LOITER TIME =	0.00
FUEL WEIGHT =	453.6	EMPTY WEIGHT =	596.1
USEFUL LOAD (-Wf)=	227.3	AIRCRAFT GROSS WEIGHT =	1276.9

AIRCRAFT DATA FILE : Dragoon_Quick.RDSDAT

MISSION FILE : Dragoon.rdsdms

UNITS : MKS

Using ICAO Standard Atmosphere

Empty Weight Sizing Coefficient C = -.1

Service Ceiling defined by Rate Of Climb = 30.5 mpm

Number of Steps for Cruise, Loiter, and Climb = 1

Sizing Sensitivity = 0.0001

Max # Sizing Iterations = 200

Max Descent Angle = -30

Maximum Landing Approach Angle = -3

Optimal Climb Speed is used between input start & end speeds

Sizing Calculation with 'Rubber' Engine

Segment #1 COMBAT

Altitude = 5000. m

Cruise Vel = 980.73 km/h

Mach = 0.8505

THRUST SETTING USED: 100. %

Current Wt = 1363.6 W/S = 330. T/W = 1.

CL = 0.5915 CD0 = 0.0165 K = 0.143

L/D = 8.884 CLmax = 1. (usable)

C = 25.5

n = 5. (load factor)

TURN RATE = 10.097 deg/sec

TURN TIME = 213.92 sec

MISSION SEGMENT WEIGHT FRACTION = 0.9465

Segment #2 CRUISE

RANGE = 1500. CLIMB/DESCENT RANGE CREDIT = 0.0

Altitude = 5000. m

Cruise Vel = 980.73 km/h

Mach = 0.8505

Current Wt = 1290.7 W/S = 312.34

T/W = 0.4902 (available)

T/W = 0.1637 (required)

THRUST SETTING USED = 15.5 % of Dry (Continuous) Power

CL = 0.112 CD0 = 0.0165 K = 0.143

L/D = 6.107 CLmax = 1. (usable)

C = 38.25

SEGMENT CRUISE TIME = 91.702 min

SEGMENT CRUISE DISTANCE = 1500. km

SPECIFIC RANGE (km/kg) = 3.438

MISSION SEGMENT WEIGHT FRACTION = 0.7132

Segment #3 DESCENT

Current Wt = 920.46 W/S = 222.75

DISTANCE TRAVELED = 0.0

MISSION SEGMENT WEIGHT FRACTION = 0.9900

Segment #4 LANDING

Current Wt = 911.26 W/S = 220.52

MISSION SEGMENT WEIGHT FRACTION = 0.9950

RESERVE & TRAPPED FUEL ALLOWANCE= 1.06

Sizing Iterations		Useful Load (less Wf)=227.3		
Iteration #	W0guess	We	Wfuel	W0calculated
1	1363.6	632.3	484.4	1343.9
2	1348.9	626.1	479.1	1332.5
3	1276.9	596.0	453.6	1276.8

RDS SIZING RESULTS MKS

AIRCRAFT DATA FILE: Dragoon_Quick.RDSDAT

MISSION FILE: Dragoon.rdsdms

T/W = 1.000

Thrust = 12.5

W/S = 330.00

Wing Area = 3.9

Wo as-drawn = 1363.6 kg

Sizing Calculation with 'Rubber' Engine

MISSION SEGMENT BURN	MISSION SEGMENT AIRCRAFT WEIGHT	Wi/WO WEIGHT FRACTION OR DROPPED WEIGHT	-SEGMENT (kg)	FUEL BURN -TOTAL	FUEL (end of Seg)
				1276.8	

1 COMBAT SEGMENT	0.9465	0.9465	68.3	68.3	1208.5
2 CRUISE SEGMENT	0.7132	0.6750	346.6	415.0	861.9
3 DESCENT SEGMENT	0.9900	0.6683	8.6	423.6	853.3
4 LANDING SEGMENT	0.9950	0.6649	4.3	427.9	849.0

Reserve & trap = 25.7

Total fuel = 453.5

Seg. 2 CRUISE : 980.7 km/h at 5000.0 m RANGE = 1500.0 km

(Ranges are reduced during analysis for climb/descent range credit)

TOTAL RANGE = 1500.0 TOTAL LOITER TIME = 0.00

FUEL WEIGHT = 453.6 EMPTY WEIGHT = 596.1
USEFUL LOAD (-Wf)= 227.3 AIRCRAFT GROSS WEIGHT = 1276.9

----- RDS-Student Version win10.3 -----

Appendix B. RDS Weight Estimate 850 lb Payload 1000 km Range

MISSION SIZING OR RANGE

Seg. 2 CRUISE : 980.7 km/h at 5000.0 m RANGE = 1000.0 km

TOTAL RANGE =	1000.0	TOTAL LOITER TIME =	0.00
FUEL WEIGHT =	391.3	EMPTY WEIGHT =	665.4
USEFUL LOAD (-Wf)=	386.4	AIRCRAFT GROSS WEIGHT =	1443.1

AIRCRAFT DATA FILE : Dragoon_Quick.RDSDAT

MISSION FILE : Dragoon.rdsdms

UNITS : MKS

Using ICAO Standard Atmosphere

Empty Weight Sizing Coefficient C = -.1

Service Ceiling defined by Rate Of Climb = 30.5 mpm

Number of Steps for Cruise, Loiter, and Climb = 1

Sizing Sensitivity = 0.0001

Max # Sizing Iterations = 200

Max Descent Angle = -30

Maximum Landing Approach Angle = -3

Optimal Climb Speed is used between input start & end speeds

Sizing Calculation with 'Rubber' Engine

Segment #1 COMBAT

Altitude = 5000. m

Cruise Vel = 980.73 km/h

Mach = 0.8505

THRUST SETTING USED: 100. %

Current Wt = 1363.6 W/S = 330. T/W = 1.

CL = 0.5915 CD0 = 0.0165 K = 0.143

L/D = 8.884 CLmax = 1. (usable)

C = 25.5

n = 5. (load factor)

TURN RATE = 10.097 deg/sec

TURN TIME = 213.92 sec

MISSION SEGMENT WEIGHT FRACTION = 0.9465

Segment #2 CRUISE

RANGE = 1000. CLIMB/DESCENT RANGE CREDIT = 0.0

Altitude = 5000. m

Cruise Vel = 980.73 km/h

Mach = 0.8505

Current Wt = 1290.7 W/S = 312.34

T/W = 0.4902 (available)

T/W = 0.1637 (required)

THRUST SETTING USED = 15.5 % of Dry (Continuous) Power

CL = 0.112 CD0 = 0.0165 K = 0.143

L/D = 6.107 CLmax = 1. (usable)

C = 38.25

SEGMENT CRUISE TIME = 61.135 min

SEGMENT CRUISE DISTANCE = 1000. km

SPECIFIC RANGE (km/kg) = 3.438

MISSION SEGMENT WEIGHT FRACTION = 0.7982

Segment #3 DESCENT

Current Wt = 1030.2 W/S = 249.32

DISTANCE TRAVELED = 0.0

MISSION SEGMENT WEIGHT FRACTION = 0.9900

Segment #4 LANDING

Current Wt = 1019.9 W/S = 246.83

MISSION SEGMENT WEIGHT FRACTION = 0.9950

RESERVE & TRAPPED FUEL ALLOWANCE= 1.06

Sizing Iterations		Useful Load (less Wf)=386.4		
Iteration #	W0guess	We	Wfuel	W0calculated
1	1363.6	632.3	369.7	1388.4
2	1382.2	640.1	374.8	1401.2
3	1443.1	665.4	391.3	1443.1

RDS SIZING RESULTS MKS

AIRCRAFT DATA FILE: Dragoon_Quick.RDSDAT

MISSION FILE: Dragoon.rdsdms

T/W = 1.000

Thrust = 14.2

W/S = 330.00

Wing Area = 4.4

Wo as-drawn = 1363.6 kg

Sizing Calculation with 'Rubber' Engine

MISSION SEGMENT BURN	MISSION SEGMENT AIRCRAFT WEIGHT	Wi/WO	FUEL BURN	FUEL
	WEIGHT FRACTION OR DROPPED WEIGHT	-SEGMENT	-TOTAL	(end of Seg)
		(kg)	1443.1	

1 COMBAT SEGMENT	0.9465	0.9465	77.2	77.2	1365.9
2 CRUISE SEGMENT	0.7982	0.7555	275.6	352.8	1090.3
3 DESCENT SEGMENT	0.9900	0.7480	10.9	363.7	1079.4
4 LANDING SEGMENT	0.9950	0.7442	5.4	369.1	1074.0

Reserve & trap = 22.1

Total fuel = 391.3

Seg. 2 CRUISE : 980.7 km/h at 5000.0 m RANGE = 1000.0 km

(Ranges are reduced during analysis for climb/descent range credit)

TOTAL RANGE = 1000.0 TOTAL LOITER TIME = 0.00

FUEL WEIGHT = 391.3 EMPTY WEIGHT = 665.4
USEFUL LOAD (-Wf)= 386.4 AIRCRAFT GROSS WEIGHT = 1443.1

----- RDS-Student Version win10.3 -----

Appendix C. Matlab Matching Graph

Contents

- Stall
- Cruise
- Landing (Roaskom)
- Landing (Analytical)
- Climbing
- Maneuvering
- Plot

```
clc, clear all, close all

g = 9.81;
rho_sl = 1.225;
rho_cruise = 0.7364; % was using .6601 for some time. thats 6km not 5km

v_cruise = 0.85*320.5; % Mach to m/s
v_stall = 150*0.51444; % kt to m/s
v_stall2 = 200*0.51444; % kt to m/s
v_combat = 0.6*320.5; % Mach to m/s
v_LDG = 1.2 * v_stall; % Assuming approach speed, not sure what ldg is.

CL_max = .55;
Cd0 = 0.025;
e = 0.8;
AR = 3;
c = 4000/180; % Suppose if it ends mission at 1km and reclimb to 5km.
n_max = 5;
mu = 0.5;
d_l = 600;
```

Stall

```
w_s_stall_s = CL_max*1/2*rho_sl*v_stall^2/g;
w_s_stall = w_s_stall_s*ones(1,101);
t_w_blank = linspace(0,1000,101);

w_s_stall_s_FW = CL_max*1/2*rho_sl*v_stall^2/g;
w_s_stall_FW = w_s_stall_s_FW*ones(1,101);

w_s_stall_s_FW2 = CL_max*1/2*rho_sl*v_stall2^2/g;
w_s_stall_FW2 = w_s_stall_s_FW2*ones(1,101);
```

Cruise

```
q_cruise = 0.5*rho_cruise*v_cruise^2;
w_s_cruise = linspace(0,1000,101);
t_w_cruise = 1/0.9 * (rho_sl/rho_cruise)^0.75 * ((Cd0*q_cruise./(w_s_cruise*g)) ...
+ (w_s_cruise*g/pi/AR/e/q_cruise));
```

Landing (Roaskom)

```

v_a = 1.2*v_stall;
w_s_l_s = CL_max*1/2*rho_sl*v_a^2/g;
w_s_l = w_s_l_s*ones(1,101);
w_s_to = w_s_l_s/.9*ones(1,101);

```

Landing (Analytical)

```

w_s_l_a = linspace(10,1000,100);
KA = rho_sl / 2 ./ (w_s_l_a * g) * (mu * CL_max - Cd0);
t_w_l_a = KA*v_LDG^2 ./ (1-exp(d_l*2*g*KA)) + mu;

```

Climbing

```

CL_climb = sqrt(3*pi*e*AR*Cd0);
CD_climb = 4*Cd0;
w_s_climb = linspace(0,1000,101);
t_w_climb = (rho_sl/rho_cruise)^0.75 * (c./sqrt(w_s_climb*g^2/rho_sl/CL_climb) + CD_climb/CL_climb);

```

Maneuvering

```

q_combat = 0.5*rho_cruise*v_combat^2;
w_s_combat = linspace(0,1000,101);
t_w_combat = (rho_sl/rho_cruise)^0.75 * (Cd0*q_combat./(w_s_climb*g) + ...
    w_s_climb*g*n_max^2/pi/AR/e/q_combat);

```

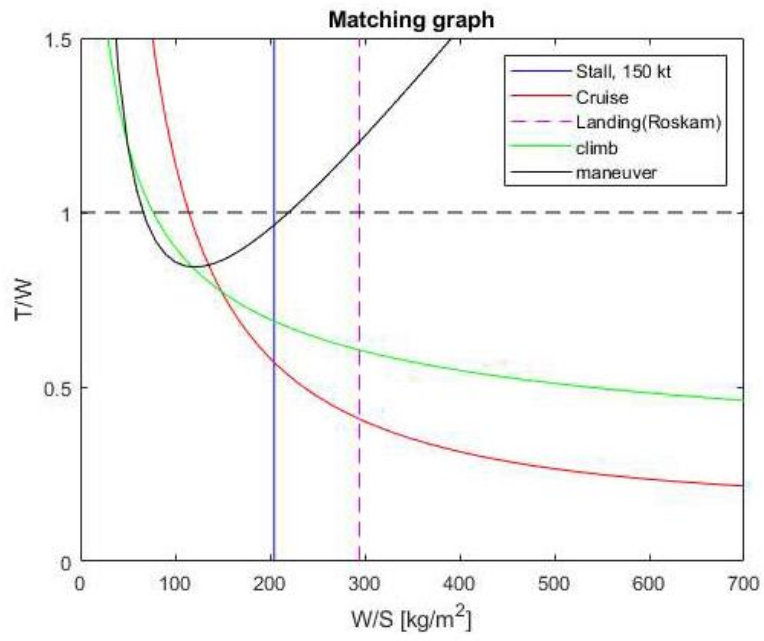
Plot

```

figure,
%plot(w_s_stall, t_w_blank)
%hold on
plot(w_s_stall_FW, t_w_blank, 'b')
hold on
%plot(w_s_stall_FW2, t_w_blank, 'c')
%hold on
plot(w_s_cruise, t_w_cruise, 'r')
hold on
plot(w_s_l, t_w_blank, 'm--')
hold on
%plot(w_s_to, t_w_blank, '--')
%hold on
%plot(w_s_l_a, t_w_l_a, 'm')
%hold on
plot(w_s_climb, t_w_climb, 'g')
hold on
plot(w_s_combat, t_w_combat, 'k')
hold on
plot(linspace(0,1000,101),ones(1,101),'k--')
title('Matching graph')
legend('Stall, 150 kt', 'Cruise', 'Landing(Roskam)', 'climb', 'maneuver')
%legend('Stall', 'Stall (Flying Wing)', 'Cruise', 'Landing(Roskam)', 'to', ...
% 'Landing (Analytical)', 'climb', 'maneuver')
xlabel('W/S [kg/m^2]')
ylabel('T/W')

```

```
xlim([0 700])  
ylim([0 1.5])
```



Published with MATLAB® R2020a

Appendix D. Matlab Excel Canard Area Measurement

	Gripen 0.019765		Typhoon 0.03		Rafale 0.020683		Dragoon
	Pixel	meter	Pixel	meter	Pixel	meter	
Wing root chord	253	5.000	236	7.080	262	5.419	
Wing tip chord	57	1.127	47	1.410	76	1.572	
Wing root location	59	1.166	39.5	1.185	94.5	1.955	
Wing tip location	212.5	4.200	182.5	5.475	263.5	5.450	
Wing location	386	7.629	211	6.330	396	8.191	
Wing tip offset	185	3.656	182	5.460	174	3.599	
Canard root chord	99	1.957	52	1.560	68	1.406	
Canard tip chord	25	0.494	19	0.570	29	0.600	
Canard root location	50.5	0.998	20	0.600	66	1.365	
Canard tip location	117.5	2.322	67	2.010	134	2.772	
Canard location	266	5.257	85	2.550	266	5.502	
Canard tip offset	104	2.056	47	1.410	60	1.241	

Wing mac	4.061	5.571	4.578	
Sw	30.249	53.202	45.622	6.7
Sc	7.15	4.88	6.66	1.52
Tail volumexflr5	0.18	0.08	0.12	0.16

	Viggen	0.022698		Vertical	Sw	6.7	
	Pixel	meter			bw	4	
wing span 1	36	0.817			Lvt	1.00625	
wing span 2	116	2.633			Sv	1.56	
wing span 3	178	4.040			cvt	0.058573 <	0.07
wing span 4	186	4.222					
wing span 5	234	5.311					
Wing chord 1	305	6.923	New	Vertical	Sw	4.15	
Wing chord 2	225	5.107			bw	3.2	
Wing chord 3	123	2.792			Lvt	0.98	807.96
Wing chord 4	122	2.769			Sv	0.88	
Wing chord 5	25	0.567			cvt	0.06494	
Wing offset 1	0	0.000					200
Wing offset 2	74	1.680	New	Vertical	Sw	4.15	
Wing offset 3	171	3.881			bw	3.2	874.8
Wing offset 4	171	3.881			Lvt	0.84684	
Wing offset 5	264	5.992			Sv	1	
Wing location	383	8.693			cvt	0.063768	
Canard span 1	50	1.135					
Canard span 2	122	2.769	New	Vertical	Sw	4.15	
Canard chord 1	152	3.450			bw	3.2	
Canard chord 2	29	0.658			Lvt	0.923	
Canard offset	117	2.656			Sv	1	
Canard location	232	5.266			cvt	0.069503	
		5.43	New	Canard			
		48.918				4.15	
						0.64	
		0.24				0.13	

Appendix E. Excel Class I Weight and Balance

	Aircraft			Using average	
	F-102A	F-106A	Average	Dragoon	RDS
Design Gross Weight (lb)	25,500	30,590		3000.000	2809.180
Group					
Wing	0.118	0.108	0.113	339.0	317.4
Empennage	0.021	0.023	0.022	66.0	61.8
Fuselage	0.134	0.144	0.139	417.0	390.5
Engine Section	0.002	0.001	0.0015	4.5	4.2
Landing Gear	0.041	0.04	0.0405	121.5	113.8
Structure (Total)	0.316	0.316	0.316	948.0	887.7
Structure (given)	0.315	0.316	0.3155	946.5	886.3
Engine	0.195804				
Air Induct System	0.027176				
Fuel System	0.015451				
Propulsion System	0.010902				
Power Plant (Total)	0.249333				
Power Plant (Given)	0.249	0.264	0.2565	769.5	720.6
Avionics + Intrum	0.005529				
Surface Control	0.016196				
Hydraulic	0.012471				
Peumatic					
Electrical	0.023294				
Electronics	0.078471				
Armament	0.023098				
Air conditioning	0.010157				
Anti icing					
Furnishings	0.008902				
Auxillary Gear	0.003059				
Fixed Equipment (Total)	0.181176				
Fixed Equipment (Given)	0.181	0.19	0.1855	556.5	521.1
Empty Weight (Total)	0.745	0.77	0.7575	2272.5	2128.0
Empty Weight (Given)	0.75	0.766	0.758	0.758	0.758

Using F-102A			Block A?		Block C	
Dragoon	RDS		F-102A	WIKI	F-16	WIKI
3000.0	2809.2	Empty weight	19017	19350	14725	18900
		Group				
354.0	331.5	Wing	3000	0.158	1699	0.090
63.0	59.0	Empennage	535	0.028	650	0.044
402.0	376.4	Fuselage	3409	0.179	3069	0.208
6.0	5.6	Engine Section	39	0.002	598	0.041
123.0	115.2	Landing Gear	1056	0.056	867	0.059
948.0	887.7	Structure (Total)	8039	0.423	6883	0.467
945.0	884.9	Structure (given)	8039	0.423	6883	0.467
587.4	550.0	Engine	4993	0.263	3019	0.205
81.5	76.3	Air Induct System	693	0.036		
46.4	43.4	Fuel System	394	0.021	349	0.024
32.7	30.6	Propulsion System	278	0.015	283	0.019
748.0	700.4	Power Plant (Total)	6358	0.334	3651	0.248
747.0	699.5	Power Plant (Given)	6358	0.334	3651	0.248
16.6	15.5	Avionics + Intrum	141	0.007	179	0.012
48.6	45.5	Surface Control	413	0.022	719	0.049
37.4	35.0	Hydraulic + Penumatic	318	0.017	361	0.025
		Electrical	594	0.031	380	0.026
69.9	65.4	Electronics	2001	0.105	994	0.068
235.4	220.4	Armament	589	0.031	566	0.038
69.3	64.9	Air cond + pressurization	259	0.014	233	0.016
30.5	28.5	Anti Ice				
		Furnishings	227	0.012	594	0.040
26.7	25.0	Auxillary Gear	78	0.004	165	0.011
9.2	8.6	Fixed Equipment (Total)	4620	0.243	4191	0.285
543.5	509.0	Fixed Equipment (Given)	4620	0.243	4191	0.285
543.0	508.5					
2235.0	2092.8					
2250.0	2106.9					

F-15C		F/A-18A		AV-8B	
27204		22957		12807	
3642	0.134	3798	0.165	1443	0.113
1104	0.041	945	0.041	372	0.029
6245	0.230	4685	0.204	2060	0.161
102	0.004	143	0.006	141	0.011
1393	0.051	1992	0.087	1011	0.079
12486	0.459	11563	0.504	5027	0.393
6091	0.224	4294	0.187	3815	0.298
1464	0.054	423	0.018	236	0.018
1128	0.041	1002	0.044	542	0.042
522	0.019	558	0.024	444	0.035
9205	0.338	6277	0.273	5037	0.393
151	0.006	94	0.004	80	0.006
810	0.030	1067	0.046	698	0.055
433	0.016	364	0.016	176	0.014
607	0.022	547	0.024	424	0.033
1787	0.066	1538	0.067	697	0.054
627	0.023	387	0.017	152	0.012
685	0.025	593	0.026	218	0.017
		21	0.001		
294	0.011	317	0.014	298	0.023
119	0.004	189	0.008		
5513	0.203	5117	0.223	2743	0.214

Instrument only F-15 to AV-8

RDS empty weight	F-102	Adjusted	Adjusted	Adjusted	Location	Moment	
	1311.42 weight						
Group	fraction	fraction	in kg	in lb	In m	in ft	
Wing	0.158	0.135	80.5	177	3.3	10.9	1927.98
Empennage	0.028	0.045	26.8	59	3.5	11.4	673.63
Fuselage	0.179	0.205	122.2	269	2.5	8.4	2245.44
Engine Section	0.002	0.010	6.0	13	3.2	10.6	138.49
Landing Gear	0.056	0.060	35.8	79	3.0	9.9	781.84
Structure (Total)	0.423				1.3	4.1	
Structure (given)	0.423				3.9	12.9	
Engine	0.263	0.300	178.6	393	3.6	11.7	4611.86
Air Induct System	0.036	0.036	21.5	47	2.1	6.9	327.17
Fuel System	0.021	0.040	23.8	52	2.7	8.7	458.73
Propulsion System	0.015	0.020	11.9	26	2.8	9.2	242.35
Power Plant (Total)	0.334						
Power Plant (Given)	0.334						
Avionics + Intrum	0.007	0.000	0.0	0			
Surface Control	0.022	0.025	14.9	33	3.3	10.7	351.62
Hydraulic + Penumatic	0.017	0.015	8.9	20	3.5	11.6	227.20
Electrical	0.031	0.025	14.9	33	4.0	13.2	432.77
Electronics	0.105	0.075	44.7	98	0.8	2.6	259.66
Armament	0.031	0.000	0.0	0			
Air cond + pressurization	0.014	0.005	3.0	7	1.5	5.0	32.46
Anti icing							
Furnishings	0.012	0.000	0.0	0			
Auxillary Gear	0.004	0.004	2.4	5	1.5	5.0	25.97
Fixed Equipment (Total)	0.243						
Fixed Equipment (Given)	0.243						
Total		1.000	595.9	1311	2.944	9.7	12737.17
Difference in percent		0.032484					
Payload			227.3	500	2.5	8.4	4199.25
Fuel			453.0	996.6	2.7	8.7	8715.27
Total (w/ fuel)			1048.9	2308	2.817	9.3	21452.44
total (gross)			1276.2	2808	2.769	9.1	25651.69
Fuel (end of combat)			384.7	846.34	2.7	8.7	7401.24
Fuel (end of cruise)			38.1	83.82	2.7	8.7	733.01
Total (end of combat)			1207.9	2657	2.775	9.2	24337.67
Total (end of cruise)			861.3	1895	2.826	9.3	17669.43
Total (landed)			823.2	1811	2.834	9.4	16936.42
Total (end of combat)	w/o payload		980.6	2157	2.829	9.3	20138.42
Total (end of cruise)	w/o payload		634.0	1395	2.926	9.7	13470.18

z location		Moment		
ln m	in ft			
0.2	0.6	1145.22	30.8	67.8 738.342
0.6	2.1	1422.70	0.0	0
0.1	0.2	518.70	119.9	263.7 2202.502
-0.1	-0.2	-31.99	0.0	0
-0.5	-1.7	-1290.04 depolyed	71.1	156.5 1555.031
1.3	4.1		8.9	19.5 80.4375
3.9	12.9		27.8	61.2 787.644
			0.0	0
-0.1	-0.2	-1065.34	178.6	393 4611.855
0.0	-0.1	-32.39	13.5	29.6 205.128
0.2	0.5	227.07	74.0	162.9 1424.561
-0.1	-0.3	-79.98	10.6	23.3 215.292
			0.0	0
			0.0	0
			0.0	0
			0.0	0
0.2	0.8	278.49	118.8	261.3 2802.443
0.1	0.2	52.48	0.0	0
0.1	0.2	99.97	85.3	187.7 2477.64
0.1	0.2	59.98	18.9	41.5 109.56
			0.0	
0.1	0.2	7.50	0.0	
			0.0	
			0.0	
0.1	0.2	6.00	0.0	
			0.0	
			0.0	
0.031	0.1	1318.38 625mm from ground	758.2	1668 17210.43
			0.0	
			0.0	
-0.2	-0.7	-2771.51	227.3	500 21409.68
0.2	0.5	4314.06	453.0	996.6
0.080	0.3	5632.44	1211.2	2664.6 25925.70
0.034	0.1	2860.93	1438.5	3164.6 30124.95
0.2	0.5	3663.62		
0.2	0.5	362.84		
0.028	0.1	2210.49		fuel cg 2.65
-0.019	-0.1	-1090.29		
-0.026	-0.1	-1453.13		
0.075	0.2	4981.99	CJ610-9	421 3100
0.038	0.1	1681.22	CJ610-4	393 2950

		lxx	lzz	lxz
2.9	9.57	1.777835961	10.19090349	4.2564956
1.3	4.29	9.936756712	7.110676849	8.4057757
3.9	12.87	0.182398733	20.85769078	-1.950491
2.5	8.25	0.061249158	0.39023474	-0.154601
3	9.9	10.09850784	0.159886145	-1.270674
2.1	6.93	0	0	0
2.5	8.25	0	0	0
3.6	11.88	0	0	0
3.2	10.56	1.835485141	66.88994959	-11.08041
3.3	10.89	0.080811149	15.29149586	1.1116309
3.3	10.89	0.335583461	2.062934959	-0.832038
4	13.2	0.205736942	0.24769348	0.2257426
2.5	8.25	0	0	0
2.5	8.25	0	0	0
2.8	9.24	0	0	0
		0	0	0
		0.648680818	1.39413935	0.950974
		0.013346249	2.76275361	0.1920219
		0.022243748	16.61392685	0.6079112
		0.066731244	205.5353005	-3.703461
		0	0	0
		0.00444875	6.21594787	-0.166293
		0	0	0
		0	0	0
		0.003559	4.972758296	-0.133034
		0	0	0
		0	0	0
10.31801	3.126668	0	0	0
		0	0	0
		0	0	0
		0	0	0
9.875315	2.99252	12.16591608	36.20733307	20.987982
		6.3755791	39.19264957	-15.80746
9.729678	2.948387	43.81487009	436.0962751	1.6400692
9.519355	2.884653			

Appendix F. Matlab Class II Weight and Balance

Contents

- Wing
- Empennage weight
- Fuselage weight
- Landing gear weight
- Air induction sys weight
- Fuel sys weight
- Propulsion sys weight
- Flight control sys
- Instrumentation, avionics and electronics
- Electrical sys
- Sum

```
clc, clear all, close all
```

Wing

```
K_w = 1.0; % fixed wing

n_ult = 7.33; %?8.67 for fighter, 7.33 for attacker, USAF, 7.33 for USN all

t_c_max = .1008;

W_TO = 3000;

LE_swept = 55.22;

lambda = 0.1; % Taper ratio

AR = 2.47;

S = 4.15*3.3^2;

W_w = 3.08*(((K_w*n_ult*W_TO)/t_c_max)*((tand(LE_swept) - 2*(1-lambda)/...
AR/(1+lambda))^2 + 1.0)*1e-6)^0.593*(AR*(1+lambda))^0.89*S^0.741
```

```
W_w =

    67.7530
```

Empennage weight

```
% Vertical
z_h = 0;
b_v = 2*3.3;
S_v = 0.88*3.3^2;
M_H = 0.85;
l_v = 1.00625*3.3;
```

```

S_r = .2 * S_v;
AR_v = 2.29;
lambda_v = 0.167;
quarter_sweep_v = 48.43;

W_v = 0.19*((1 + z_h/b_v)^0.5 * (W_TO*n_ult)^0.363 * S_v^1.089 * M_H^0.601 ...
    * l_v^(-0.726) * (1 + S_r/S_v)^0.217 * AR_v^0.337 * (1+lambda_v)^0.363 ...
    * (cosd(quarter_sweep_v)^(-0.484)))^1.014

% Canard
% Using sizing for wing

t_c_max = .086;

LE_swept = 55.28;

lambda = .067; % Taper ratio

AR = 2.66;

S = 0.64*3.3^2;

W_c = 3.08*(((K_w*n_ult*W_TO)/t_c_max)*((tand(LE_swept) - 2*(1-lambda)/...
    AR/(1+lambda))^2 + 1.0)*1e-6)^0.593*(AR*(1+lambda))^0.89*S^0.741

W_emp = W_v + W_c

```

```

W_v =
    61.1870

```

```

W_c =
    19.4610

```

```

W_emp =
    80.6480

```

Fuselage weight

```

K_in1 = 1.25;
q_D = .5*(0.7364*23.77e-4/1.225)*(320*.9*3.3)^2;
l_f = 4.5*3.3;
h_f = 0.68*3.3;
W_f = 10.43*K_in1^1.42*(q_D/100)^0.283*(W_TO/1000)^0.95*(l_f/h_f)^0.71

```

```

W_f =
    263.6524

```

Landing gear weight

$$W_g = 62.21 * (W_{T0}/1000)^{0.84}$$

$$W_g =$$

156.5460

Air induction sys weight

$$\begin{aligned} N_{in1} &= 2; \\ L_d &= 2*3.3; \\ A_{in1} &= (.45/2)^2 * \pi / 2 * 3.3^2; \\ P_2 &= 30; \\ W_{ai} &= 0.32 * N_{in1} * L_d * A_{in1}^{0.65} * P_2^{0.6} \end{aligned}$$

$$W_{ai} =$$

29.6060

Fuel sys weight

$$\begin{aligned} N_e &= 1; \\ N_t &= 1; \\ W_F &= 453*2.2; \\ K_{fsp} &= 5.87; \\ W_{fs} &= 80 * (N_e + N_t - 1) + 15 * N_t^{0.5} * (W_F / K_{fsp})^{0.333} \end{aligned}$$

$$W_{fs} =$$

162.9167

Propulsion sys weight

$$\begin{aligned} K_{ec} &= 0.686; \\ W_{ec} &= K_{ec} * (1_f * N_e)^{0.792} \\ W_e &= 417; \\ W_{ess} &= 38.93 * (W_e / 1000)^{0.918} \\ W_p &= W_{ec} + W_{ess} \end{aligned}$$

$$W_{ec} =$$

5.8121

W_ess =

17.4409

W_p =

23.2530

Flight control sys

```
K_fcf = 138; % Assuming canard qualifies as horizontal tail  
W_fc = K_fcf*(W_TO/1000)^0.581
```

W_fc =

261.2682

Instrumentation, avionics and electronics

```
N_pil = 0;  
W_iae = N_pil*(15+0.032*(W_TO/1000)) + N_e*(5+0.006*(W_TO/1000)) + ...  
0.15*(W_TO/1000)+0.012*W_TO
```

W_iae =

41.4680

Electrical sys

```
W_els = 426*((W_fs + W_iae)/1000)^0.51
```

W_els =

189.5563

Sum

```
W = W_w + W_emp + W_f + W_g + W_ai + W_fs + W_p + W_fc + W_iae + W_els  
W_wF = W + W_F  
W_L = 500  
W_Mat = [W_w W_c W_v W_f W_g W_ai W_fs W_e W_p W_fc W_iae W_els W_F W_L]
```

```

x_Mat = [2 1 3 0 3 2.5 3 3.5 3.2 3 2.5 4 3 2.5]
%W_Mat = [W_w W_c W_v W_f W_g W_ai W_fs W_e W_p W_fc W_iae W_els ]
%x_Mat = [2 1 3 0 3 2.5 3 3.5 3.2 3 2.5 4 ]

temp = 0;
for i = 1:length(W_Mat)
    temp = temp + W_Mat(i)*x_Mat(i);
end

cg = temp / sum(W_Mat)
sum(W_Mat)

```

W =

1.2767e+03

W_WF =

2.2733e+03

W_L =

500

W_Mat =

Columns 1 through 7

67.7530 19.4610 61.1870 263.6524 156.5460 29.6060 162.9167

Columns 8 through 14

417.0000 23.2530 261.2682 41.4680 189.5563 996.6000 500.0000

x_Mat =

Columns 1 through 7

2.0000 1.0000 3.0000 0 3.0000 2.5000 3.0000

Columns 8 through 14

3.5000 3.2000 3.0000 2.5000 4.0000 3.0000 2.5000

cg =

2.7554

ans =

3.1903e+03

Appendix G. RDS Weight and Balance – Fighters

RDS WEIGHTS

GROUP WEIGHT STATEMENT : Using Fighter/Attack Equations

File Name:Dragoon_Quick.rdsdwt 05-10-2022 23:04:01 MKS

STRUCTURES GROUP	326.4	EQUIPMENT GROUP	393.8
Wing	56.9	Flight Controls	140.1
Horiz. Tail	5.8	Instruments	0.0
Vert. Tail	67.7	Hydraulics	49.2
Fuselage	69.6	Electrical	187.3
Main Lndg Gear	41.5	Avionics	0.0
Nose Lndg Gear	18.9	Furnishings & Misc	0.0
Engine Mounts	6.9	Air Conditioning	16.8
Firewall	0.0	Handling Gear	0.4
Engine Section	3.8	APU installed	0.0
Air Induction	55.4		
		Misc Empty Weight	0.0
PROPULSION GROUP	270.0	TOTAL WEIGHT EMPTY	990.2
Engine(s)	189.0		
Tailpipe	3.8	USEFUL LOAD GROUP	373.4
Engine Cooling	0.0	Fuel	146.1
Oil Cooling	17.2	Oil	0.0
Engine Controls	0.0	Payload	227.3
Starter	5.2	TAKEOFF GROSS WEIGHT	1363.6
Fuel System	54.9		

We/Wo 72.6 %

Wf/Wo 10.7 %

Empty CG = 3.0

Loaded-NoFuel CG = 2.9

Gross Weight CG = 2.9

Below are the weights and locations as used for CG calculations

These can be copied into RDS Resource spreadsheet

'RDS-win_Weight-Balance.xlsx' for CG analysis and trade studies

	Weight	X-Location
STRUCTURES GROUP		
Wing	56.9	2.000
Horiz. Tail	5.8	1.000
Vert. Tail	67.7	3.000
Fuselage	69.6	0.000
Main Lndg Gear	41.5	4.250
Nose Lndg Gear	18.9	0.000
Engine Mounts	6.9	3.200
Firewall	0.0	3.200
Engine Section	3.8	3.200
Air Induction	55.4	1.000
PROPULSION GROUP		
Engine(s)	189.0	3.200
Tailpipe	3.8	4.500

Engine Cooling	0.0	4.500
Oil Cooling	17.2	4.500
Engine Controls	0.0	4.500
Starter	5.2	4.500
Fuel System	54.9	3.000

EQUIPMENT GROUP

Flight Controls	140.1	4.000
Instruments	0.0	0.000
Hydraulics	49.2	4.000
Electrical	187.3	4.000
Avionics	0.0	0.000
Furnishings & Misc	0.0	0.000
Air Conditioning	16.8	0.000
Handling Gear	0.4	0.000
APU installed	0.0	0.000
Misc Empty Weight	0.0	0.000

USEFUL LOAD GROUP

Fuel	146.1	3.000
Oil	0.0	4.500
Payload	227.3	2.500

TAKEOFF GROSS WEIGHT 1363.6 2.9

----- RDS-Student Version win10.3 -----

Appendix H. RDS Weight and Balance – General Aviation

RDS WEIGHTS

GROUP WEIGHT STATEMENT : Using General Aviation Equations

File Name:Dragoon_GA.rdsdwt 05-10-2022 22:57:32 MKS

STRUCTURES GROUP	383.2	EQUIPMENT GROUP	207.0
Wing	54.7	Flight Controls	10.2
Horiz. Tail	22.7	Hydraulics	146.1
Vert. Tail	25.7	Electrical	50.7
Fuselage	208.0		
Main Lndg Gear	58.7	Misc Empty Weight	0.0
Nose Lndg Gear	13.4	TOTAL WEIGHT EMPTY	927.0

PROPULSION GROUP	336.9	USEFUL LOAD GROUP	
	436.6		
Engine(s)	189.0	Fuel	209.3
Eng Installation	115.0	Oil	0.0
Fuel System	32.9	Payload	227.3
		TAKEOFF GROSS WEIGHT	1363.6

We/Wo 68.0 %

Wf/Wo 15.4 %

Empty CG = 2.5
Loaded-NoFuel CG = 2.5
Gross Weight CG = 2.6

Below are the weights and locations as used for CG calculations

These can be copied into RDS Resource spreadsheet

'RDS-win_Weight-Balance.xlsx' for CG analysis and trade studies

	Weight	X-Location
STRUCTURES GROUP		
Wing	54.7	2.000
Horiz. Tail	22.7	1.000
Vert. Tail	25.7	3.000
Fuselage	208.0	0.000
Main Lndg Gear	58.7	4.250
Nose Lndg Gear	13.4	1.000
PROPULSION GROUP		
Engine(s)	189.0	3.200
Eng Installation	115.0	3.200
Fuel System	32.9	3.000
EQUIPMENT GROUP		
Flight Controls	10.2	3.000

Hydraulics	146.1	4.000
Electrical	50.7	4.000
Misc Empty Weight	0.0	0.000

USEFUL LOAD GROUP

Fuel	209.3	3.000
Oil	0.0	3.000
Payload	227.3	2.500

TAKEOFF GROSS WEIGHT 1363.6 2.6

----- RDS-Student Version win10.3 -----

Appendix I. Matlab Drag Polar

Contents

- Common
- Parameter
- CL alpha
- Wing drag
- Fuselage Drag
- Payload Drag
- Empennage - canard
- Empennage - vertical
- Sum

```
clc, clear all, close all
```

Common

```
rho = [1.225 0.7364];  
n = ((0.85 - 0.25) / 0.05) + 2;  
M = linspace(0.25, 0.85, n);  
U1 = M * 320.5;  
mu = [1.789e-5 1.628e-5];  
GW = 2800;
```

Parameter

```
S_c = 0.64;  
S = 4.15;
```

CL alpha

```
CL_alpha_w = .0759;  
CL_alpha_c = .0768;  
CL_alpha_v = .0937;  
b = 3.2;  
d_f = .8397;  
K_wf = 1 + 0.025*(d_f/b) - 0.25*(d_f/b)^2;  
eta_c = 1;  
d_epsilon_d_alpha = 0.2;  
CL_alpha_wf = K_wf * CL_alpha_w;  
CL_alpha = CL_alpha_wf + CL_alpha_c * eta_c * S_c / S * ...  
    (1 + d_epsilon_d_alpha);  
  
alpha_0l_ratio = 1;  
alpha_0l = -.75;  
alpha_0Lw = alpha_0l * alpha_0l_ratio;  
CL_0wf = (0 - alpha_0Lw) * CL_alpha_wf;  
alpha_0Lc = alpha_0Lw;  
  
CL_0 = CL_0wf + CL_alpha_c * eta_c * S_c / S * (-alpha_0Lc);
```

Wing drag

CD_wing was .0086 CL_wing over CD_wing was 8.4561, now 11.6179

```
l_f = 5;
cbar_w = 1.566; % was 1.93

for i = 1:2
    RN_fus(i,:) = rho(i) * U1 * l_f ./ mu(i);
    RN_w(i,:) = rho(i) * U1 * cbar_w ./ mu(i);
end

R_wf = [1.06 1.045 1.025 1.015 1.0125 1.01 1.015 1.02 1.02 1.02 1.02 ...
        1.02 1.02; 1.07 1.0625 1.06 1.055 1.045 1.035 1.0325 1.03 1.03 1.03 ...
        1.03 1.03 1.03];
R_LS = [.96 .965 .9725 .98 .95 1.01 1.025 1.04 1.04 1.04 1.04 1.04]; ...
% 45.23, was 41.64 deg and 40.21 deg
Cf_w = 1e-2* [.305 .295 .285 .277 .275 .265 .2625 .26 .26 .26 .26 .26; ...
            0.325 .315 .31 .3 .295 .2925 .285 .28 .28 .28 .28 .28];
Lprime = 2; % before .3c
tc_w = .1008;
Swet_w = 5.692751;

for i = 1:2
    for j = 1:13
        CD_0w(i,j) = R_wf(i,j) * R_LS(i) * Cf_w(i,j) * (1 + Lprime * ...
            tc_w + 100 * tc_w^4) * Swet_w / S;
    end
end

A = 2.467;
for i = 1:2
    CL(i,:) = GW/2.2*9.81/.5/rho(i)./U1.^2/S;
end
CL_w = 1.05* CL;
l_LE = 23.21/2/2*1.566/1000;

for i = 1:2
    R_l_LE(i,:) = rho(i) .* U1 * l_LE ./ mu(i);
    for j = 1:13
        R2 (i,j) = R_l_LE(i,j)*cotd(55.22)*sqrt(1-M(j)^2*cosd(55.22)^2);
    end
end

R = [.76 .79 .805 .82 .83 .84 .845 .85;
     .7 .73 .75 .77 .785 .80 .81 .82];

% From fig 4.13, originally 0.7, .65 with 6.7 m2 wing

for i = 1:2
    e(i,:) = 1.1*(CL_alpha_w * 180 / pi / A) ./ (R(i,:) * ...
        (CL_alpha_w * 180/pi / A)+(1-R(i,:))*pi);
    for j = 1:8
        CD_Lw(i,j) = CL_w(i,j)^2/pi/A/e(i,j);
        CD_w(i,j) = CD_0w(i,j) + CD_Lw(i,j);
        CL_CD_w(i,j) = CL_w(i,j) / CD_w(i,j);
    end
end

% Transonic
```

```

2.04 * 0.1008 ^ .33333;
sqrt(abs(.75^2 - 1))/(0.1008^.3333);
M_test = linspace(0.75,1.2,10);
CD_wv_curve = [2/57 .125 0.25 0.7 1.5 2.3 2.6 2.7 2.75 2.8] .* ...
0.1008 ^ (5/3);
M_DD_swept = .8 / sqrt(cosd(47.2));
CD_wave_peak_swept = max(CD_wv_curve) * cosd(47.2)^2.5;
M_CD_wave_peak_swept = 1.2 / sqrt(cosd(47.2));

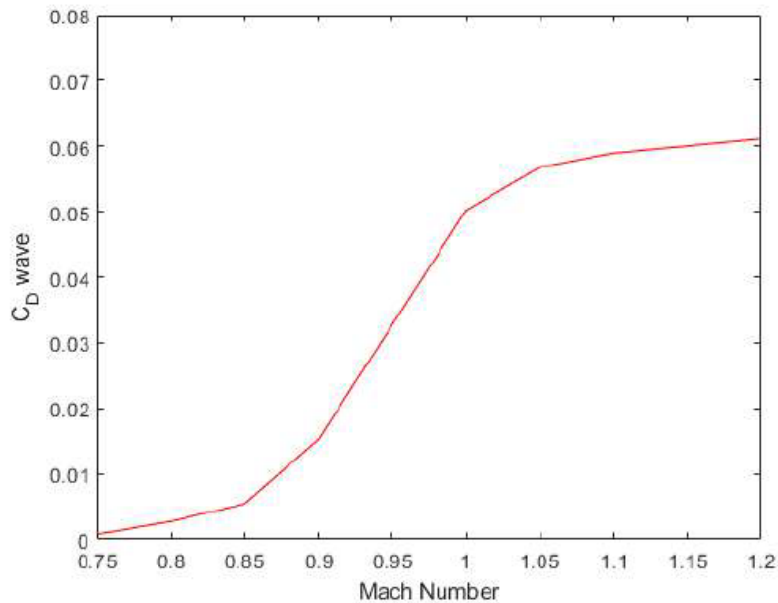
figure,
plot(M_test,CD_wv_curve,'r')
xlabel("Mach Number")
ylabel("C_D wave")
ylim([0 0.08])

% Critical mach number is > M 0.9, beyond cruise speed.
% Wave drag is negligible.

fig_5_13_1 = (M.^2 - 1) / (.101 ^ (2/3));
fig_5_13_2 = A * .101 ^ (1/3);
fig_5_13_3 = A * tand(55.22);
fig_5_13_4 = [.83+.73 .82+.72 .81+.71 .8+.7 .79+.68]/2 ;
CD_L_CL_sq = fig_5_13_4 .* .101^(1/3);

for i = 1:2
    for j=9:13
        CD_Lw(i,j) = CD_L_CL_sq(j-8)*CL_w(i,j)^2;
        CD_w(i,j) = CD_0w(i,j) + CD_Lw(i,j);
        CL_CD_w(i,j) = CL_w(i,j) / CD_w(i,j);
    end
end
end

```



Fuselage Drag

```
Cf_fus = 1e-2* [.258 .249 .243 .236 .232 .228 .225 .22 .22 .22 .22 .22];
           .278 .267 .259 .253 .248 .243 .239 .235 .235 .235 .235 .235];

S_wet_fus = 12.035;
S_fus = .5538;
S_b_fus = .20;
d_f = sqrt(4/pi*S_fus);
d_b = sqrt(4/pi*S_b_fus);
eta = .62;
cd_c = 0;
S_plf_fus = 3.908;

for i = 1:2
    for j = 1:8
        CD_0fus_base(i,j) = R_wf(i,j) * Cf_fus(i,j) * (1 + 60/(l_f/d_f)^3);
        CD_b_fus(i,j) = (0.029 * (d_b/d_f)^3 / (CD_0fus_base(i,j) * ...
            (S/S_fus))^.5) * (S_fus/S);
        CD_0fus(i,j) = R_wf(i,j) * Cf_fus(i,j) * (1 + 60/(l_f/d_f)^3 + ...
            0.0025 * (l_f/d_f)) * S_wet_fus / S + CD_b_fus(i,j);
        alpha_deg(i,j) = ((GW/2.2*9.81/(.5*rho(i)*U1(j)^2)/S) - CL_0) / ...
            CL_alpha;
        M_c(i,j) = M(j) * sind(alpha_deg(i,j));
        alpha_rad(i,j) = alpha_deg(i,j) * pi/180;
        CD_Lfus(i,j) = 2 * alpha_rad(i,j) ^2 * S_b_fus / S + ...
            eta * cd_c * abs(alpha_rad(i,j))^3 * S_plf_fus / S;
    end
end

CD_wave_fus = [0 0 0 0 0 0 0 .01 .02 .03 .04 .05];

for i = 1:2
    for j = 9:13
        CD_f_fus = Cf_fus * S_wet_fus / S;
        CD_p_fus(i,j) = Cf_fus(i,j) * (60/(l_f/d_f)^3 + ...
            0.0025 * (l_f/d_f)) * S_wet_fus / S;
        CD_0fus_base(i,j) = R_wf(i,j) * Cf_fus(i,j) * (1 + 60/(l_f/d_f)^3);
        CD_b_fus(i,j) = (0.029 * (d_b/d_f)^3 / (CD_0fus_base(i,j) * ...
            (S/S_fus))^.5) * (S_fus/S);
        CD_0fus(i,j) = R_wf(i,j) * (CD_f_fus(i,j) + CD_p_fus(i,j)) + ...
            CD_b_fus(i,j) + CD_wave_fus(j) * S_fus / S;
        alpha_deg(i,j) = ((GW/2.2*9.81/(.5*rho(i)*U1(j)^2)/S) - CL_0) / ...
            CL_alpha;
        alpha_rad(i,j) = alpha_deg(i,j) * pi/180;
        CD_Lfus(i,j) = (alpha_rad(i,j))^2 * S_b_fus / S;
    end
end

CD_fus = CD_0fus + CD_Lfus;
```

Payload Drag

R_wf and Cf values to be replaced

```

l_AIM9 = 3.02;
for i = 1:2
    RN_AIM9(i,:) = rho(i) * U1 * l_AIM9 ./ mu(i);
end

Cf_AIM9 = 1e-2*[.258 .249 .243 .236 .232 .228 .225 .22 .22 .22 .22 .22];
             [.278 .267 .259 .253 .248 .243 .239 .235 .235 .235 .235 .235];

S_wet_AIM9 = 2.021;
S_AIM9 = 0.0013;
S_b_AIM9 = S_AIM9;
d_AIM9 = sqrt(4/pi*S_AIM9);
d_b_AIM9 = d_AIM9;
eta_AIM9 = .80; % too high fitness ratio, assuming eta continues appr .8
cd_c = 0;
S_plf_fus = 3.908;

for i = 1:2
    for j = 1:8
        CD_0AIM9_base(i,j) = R_wf(i,j) * Cf_fus(i,j) * ...
            (1 + 60/(l_AIM9/d_AIM9)^3);
        CD_b_AIM9(i,j) = (0.029 * (d_b_AIM9/d_AIM9)^3 / ...
            (CD_0AIM9_base(i,j) * (S/S_AIM9)^.5) * (S_AIM9/S);
        CD_0AIM9(i,j) = R_wf(i,j) * Cf_AIM9(i,j) * (1 + 60/(l_AIM9/d_AIM9)...
            ^3 + 0.0025 * (l_AIM9/d_AIM9)) * S_wet_AIM9 / S + CD_b_AIM9(i,j);
        CD_LAIM9(i,j) = 2 * alpha_rad(i,j) ^2 * S_b_fus / S + ...
            eta * cd_c * abs(alpha_rad(i,j))^3 * S_plf_fus / S;

    end
end

CD_wave_fus = [0 0 0 0 0 0 0 .01 .02 .03 .04 .05];

for i = 1:2
    for j = 9:13
        CD_f_AIM9 = Cf_AIM9 * S_wet_AIM9 / S;
        CD_p_AIM9(i,j) = Cf_AIM9(i,j) * (60/(l_AIM9/d_AIM9)^3 + ...
            0.0025 * (l_AIM9/d_AIM9)) * S_wet_fus / S;
        CD_0AIM9_base(i,j) = R_wf(i,j) * Cf_AIM9(i,j) * ...
            (1 + 60/(l_AIM9/d_AIM9)^3);
        CD_b_AIM9(i,j) = (0.029 * (d_b_AIM9/d_AIM9)^3 / ...
            (CD_0AIM9_base(i,j) * (S/S_AIM9)^.5) * (S_AIM9/S);
        CD_0AIM9(i,j) = R_wf(i,j) * (CD_f_AIM9(i,j) + CD_p_AIM9(i,j)) + ...
            CD_b_AIM9(i,j) + CD_wave_fus(j) * S_AIM9 / S;
        CD_LAIM9(i,j) = alpha_rad(i,j)^2 * S_b_AIM9 / S;

    end
end

CD_AIM9 = CD_0AIM9 + CD_LAIM9;

```

Empennage - canard

```

l_f = 4.5;
cbar_c = 0.60;

for i = 1:2
    RN_c(i,:) = rho(i) * U1 * cbar_c / mu(i);

```

```

end

R_wf_c = 1;
R_LS = [.96 .965 .9725 .98 .95 1.01 1.025 1.04 1.04 1.04 1.04 1.04]; ...
    % 45.23, was 41.64 deg and 40.21 deg
Cf_c = 1e-5*[358 347 338 329 320 312 306 302 302 302 302 302]; ...
    385 372 360 350 344 339 334 328 328 328 328 328];
Lprime = 2; % before .3c
tc_c = .086;
S_c = .64;
Swet_c = .796956;

for i = 1:2
    for j = 1:13
        CD_0c(i,j) = R_wf_c * R_LS(i) * Cf_c(i,j) * (1 + Lprime * ...
            tc_c + 100 * tc_c^4) * Swet_c / S;
    end
end

A_c = 2.66;
l_LE_c = 6.13/2/.75*.60/1000;
delta_c_quarter = 47.27;
delta_c_LE = 55.28;

for i = 1:2
    R_l_LE_c(i,:) = rho(i) .* U1 * l_LE_c ./ mu(i);
    for j = 1:13
        R2_c(i,j) = R_l_LE_c(i,j)*cotd(delta_c_quarter)*sqrt(1-M(j)^2*...
            cosd(delta_c_quarter)^2);
    end
end

R3_c = A_c / 15 * cosd(delta_c_quarter);
R_c = [.75 .77 .785 .8 .81 .82 .825 .83;
    .68 .71 .73 .75 .765 .78 .79 .795];

cg_GW = 2.7;
CL_c = CL_w * (2.8225 - cg_GW) / (cg_GW - 1.3);

for i = 1:2
    e_c(i,:) = 1.1*(CL_alpha_c * 180 / pi / A_c) ./ (R_c(i,:) * ...
        (CL_alpha_c * 180 / pi / A_c) + (1-R_c(i,:))*pi);
    % Same method as wing instead of fixed 0.5
    e_c = 0.5 * ones(size(e_c));
    for j = 1:8
        CD_Lc(i,j) = CL_c(i,j)^2/pi/A_c/e_c(i,j);
        CD_c(i,j) = CD_0c(i,j) + CD_Lc(i,j);
        CL_CD_c(i,j) = CL_c(i,j) / CD_c(i,j);
    end
end

% Transonic

% Critical mach number is > M 0.9, beyond cruise speed.
% Wave drag is negligible.

fig_4_13_1_c = (M.^2 -1) / (tc_c ^ (2/3));
fig_4_13_2_c = A_c * tc_c ^ (1/3);
fig_4_13_3_c = A_c* tand(delta_c_LE);
fig_4_13_4_c = [.6 .6 .6 .6 .6];

```

```

CD_L_CL_sq_c = fig_4_13_4_c .* tc_c^(1/3);

for i = 1:2
    for j=9:13
        CD_Lc(i,j) = CD_L_CL_sq_c(j-8)*CL_c(i,j)^2;
        CD_c(i,j) = CD_0c(i,j) + CD_Lc(i,j);
        CL_CD_c(i,j) = CL_c(i,j) / CD_c(i,j);
    end
end
end

```

Empennage - vertical

```

cbar_v = 1.02;

for i = 1:2
    RN_v(i,:) = rho(i) * U1 * cbar_v ./ mu(i);
end

R_vf = 1.0;
R_LS_v = [.98 1.0 1.025 1.075 1.015 1.025 1.04 1.06 1.06 1.06 1.06 ...
    1.06]; % 43.2
Cf_v = 1e-5*[329 317 308 300 293 287 282 278 278 278 278 278; ...
    349 339 330 322 314 308 302 298 298 298 298 298];

Lprime_v = 1.2; % at or after .3c
tc_v = .1000;
Swet_v = 1.809519;

for i = 1:2
    for j = 1:13
        CD_0v(i,j) = R_vf * R_LS_v(i) * Cf_v(i,j) * (1 + Lprime_v * ...
            tc_v + 100 * tc_v^4) * Swet_v / S;
    end
end

CD_v = CD_0v;

```

Sum

```

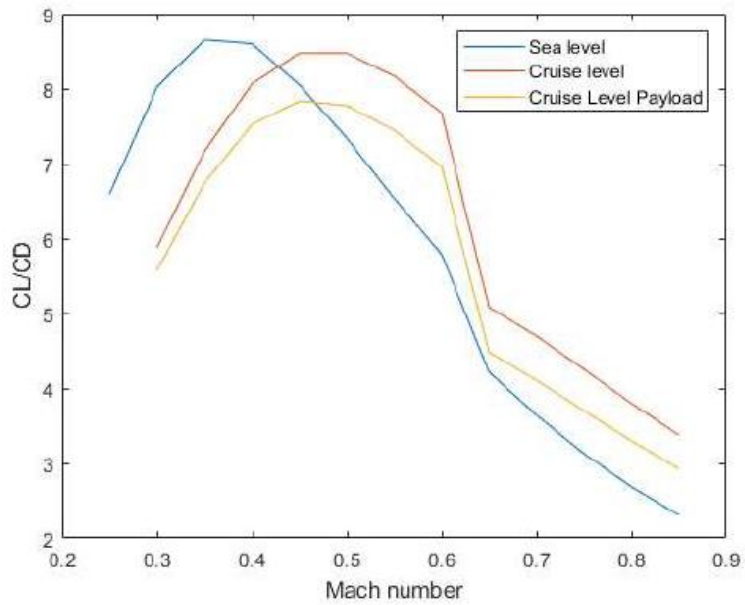
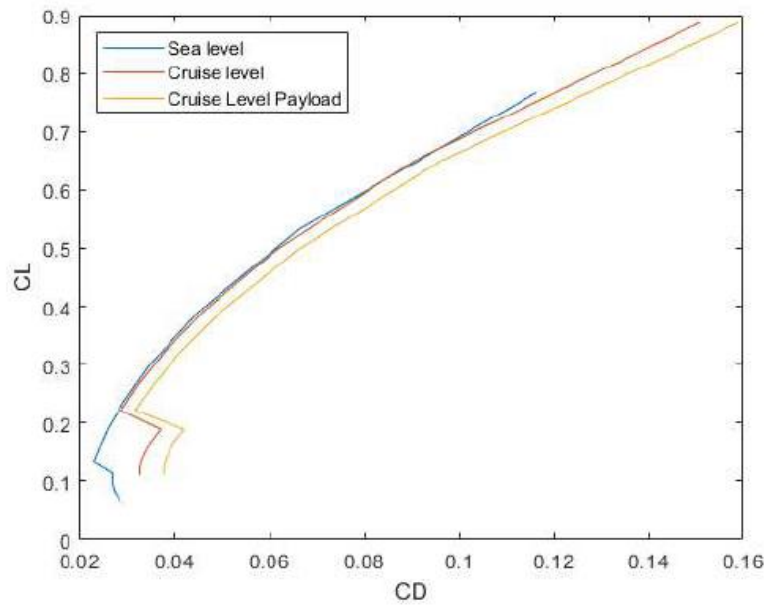
CD0 = CD_0w + CD_0c + CD_0v + CD_0fus + 2*CD_0AIM9;
CD_sl = CD_w(1,:) + CD_c(1,:) + CD_v(1,:) + CD_fus(1,:);
CD_cruise = CD_w(2,:) + CD_c(2,:) + CD_v(2,:) + CD_fus(2,:);
CD_cruise_payload = CD_w(2,:) + CD_c(2,:) + CD_v(2,:) + CD_fus(2,:) + ...
    2*CD_AIM9(2,:);
CL_sl = CL(1,:);
CL_cruise = CL(2,:);
CL_cruise(1) = [];
CD_cruise(1) = [];
CD_cruise_payload(1) = [];
M_cruise = M(2:13);

figure,
plot(CD_sl,CL_sl)
hold on
plot(CD_cruise,CL_cruise)
hold on
plot(CD_cruise_payload,CL_cruise)
legend('Sea level', 'Cruise level', 'Cruise Level Payload', 'location', ...

```

```
    'northwest')
xlabel('CD')
ylabel('CL')

figure,
plot(M, CL_sl./CD_sl)
hold on
plot(M_cruise, CL_cruise./CD_cruise)
hold on
plot(M_cruise, CL_cruise./CD_cruise_payload)
legend('Sea level', 'Cruise level', 'Cruise Level Payload')
xlabel('Mach number')
ylabel('CL/CD')
```



Appendix J. Matlab V-n Diagram

Contents

- Common
- vS
- vA
- -vS
- vA
- vH
- gust E
- plot

```
clc, clear all, close all
```

Common

```
rho = 0.0014254; % in slugs/ft3, = .7346 kg/m3  
rho_sl = 0.0023769; % in slugs/ft3, = 1.225 kg/m3  
GW = 2808;  
S = 4.15*3.3^2;  
T = 3100*.9;  
CD = 0.035;  
c = 1.68781; % knot ft/s conversion  
c_bar = 1.57;  
g = 9.81*3.3;
```

vS

```
CLmax = 1;  
CNmax = 1.1*CLmax;  
vS = (2 * GW/S / rho_sl / CNmax)^.5;
```

vA

```
nlim_pos = 7.33;  
nlim_neg = 3.00;  
vA = vS * nlim_pos ^ .5;
```

-vS

```
CLmax = .85;  
CNmax = 1.1*CLmax;  
vS_neg = (2 * GW/S / rho_sl / CNmax)^.5;
```

vA

```
vA_neg = vS * nlim_neg ^ .5;
```

vH

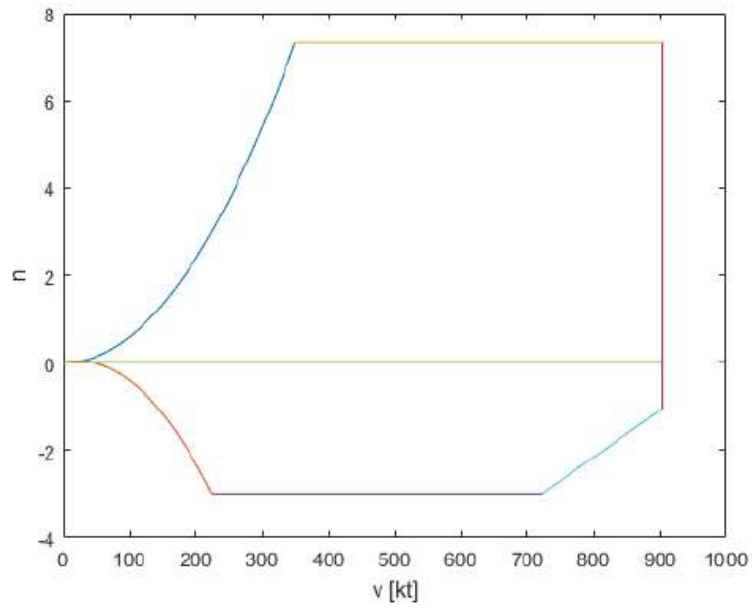
```
vH = sqrt(2*T/CD/S/rho_sl);  
vL = 1.25 * vH;
```

gust E

```
Ude = 25;  
CL_alpha = (0.25-.03)/4;  
mu_g = 2 * GW/S/rho_sl/c_bar/g/CL_alpha;  
Kg = 0.88 * mu_g / (5.3 + mu_g);  
nlimE = 1 + (Kg*Ude*vL*CL_alpha)/498/(GW/S);
```

plot

```
pos_stall_x = linspace(0,vA/1.68781,101);  
pos_stall_y = 5.99376e-5 * pos_stall_x.^2 - 5.26176e-11 * pos_stall_x + ...  
7.10543e-15;  
  
neg_stall_x = linspace(0,vA_neg/1.68781,101);  
neg_stall_y = - 7.50005e-5 * neg_stall_x.^2 + 3.36991e-3 * neg_stall_x + ...  
4.44089e-15;  
  
figure,  
%plot([0 vS vA]/c, [0 1 nlim_pos], '--')  
%hold on  
plot(pos_stall_x, pos_stall_y)  
hold on  
%plot([0 vS_neg vA_neg]/c, -[0 1 nlim_neg], '--')  
%hold on  
plot(neg_stall_x, neg_stall_y)  
hold on  
plot([vA vL]/c, nlim_pos*[1 1])  
hold on  
plot([vA_neg vH]/c, -nlim_neg*[1 1])  
hold on  
plot([0 vL/c],[0 0])  
hold on  
plot([vH vL]/c, -[3 nlimE])  
hold on  
plot([vL vL]/c, [-nlimE nlim_pos])  
xlabel("v [kt]")  
ylabel("n")
```



Published with MATLAB® R2020a

Appendix K. Matlab Stability X-Plot

Contents

- Longitudinal
- Directional Stability
- Wing lift slope
- de facto directional stability
- Trim diagram

```
clc, clear all, close all
```

Longitudinal

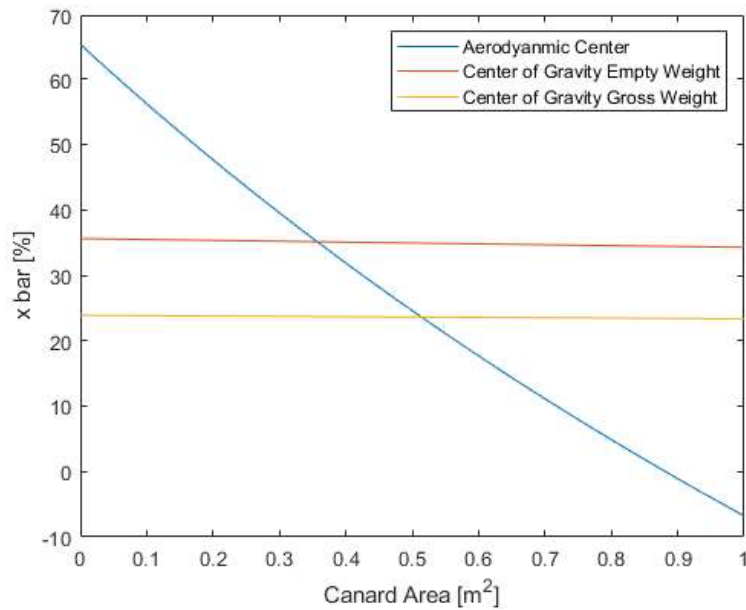
```
S_c = linspace(0,1,101);
A_w = 2.467;
d_epsilon_d_alpha = 0.2; % .65 forward, really rough estimate
S = 4.15;
b = 3.2;
S_fus = .5538;

CL_alpha_w = .0759;
d_f = sqrt(4/pi*S_fus);
K_wf = 1 + .0025 * d_f/b - 0.25 * (d_f/b)^2;
CL_alpha_wf = K_wf*CL_alpha_w;
A_c = 2.66;
CL_alpha_c = 0.0768;
x_ac_wf = 3.4225;
x_ac_c = 1.5;
x_w_LE = 2.4;
cbar_w = 1.566;
F = 1 + CL_alpha_c * (1 + d_epsilon_d_alpha) * S_c / S / CL_alpha_wf ;
xbar_ac_A = (x_ac_wf/cbar_w - CL_alpha_c * (1 + d_epsilon_d_alpha) * ...
    x_ac_c/cbar_w * S_c / S / CL_alpha_wf) ./ F;

S_c0 = 0.64;
x_c = 1.55;
w0 = 595.9;
w0_gross = 1276.2;
w_c_prime = 26.8 * .02 / .094 / S_c0;
x_cg = (12737/2.2/3.3 + w_c_prime * x_c * (S_c - S_c0)) ./ ...
    (w0 + w_c_prime * (S_c - S_c0));
x_cg_gross = (25652/2.2/3.3 + w_c_prime * x_c * (S_c - S_c0)) ./ ...
    (w0_gross + w_c_prime * (S_c - S_c0));

figure,
plot(S_c, (xbar_ac_A-x_w_LE/cbar_w)*100)
hold on
plot(S_c, (x_cg-x_w_LE)/cbar_w*100)
hold on
plot(S_c, (x_cg_gross-x_w_LE)/cbar_w*100)
legend('Aerodynamic Center', 'Center of Gravity Empty Weight', ...
    'Center of Gravity Gross Weight')
ylabel('x bar [%]')
xlabel('Canard Area [m^2]')

% static margin: 8.52% gross, 19.73% empty
```



Directional Stability

```

S_v = linspace(0,2,201);
b = 3.2;
x_v = 38.946-2.917; % 2.917 empty

Cn_beta_w = 0; % Roskam

h = .758;
w_f = 1.068;
l_f = 5;
x_m = 2.917;
S_B_S = 3.37;
x_m_l_f = x_m / l_f;
l_sq_S_B_S = l_f^2 / S_B_S;
sqrt_h1_h2 = 1;
h_w_f = h/w_f;

K_N = .0016;

% RN_fus = 27.4M at sl stall. 61.6M at cruise
K_R1 = 1.84; % 1.67 / 1.84
Cn_beta_f = -57.3 * K_N * K_R1 * (S_B_S*l_f/S/b);

Cn_beta_wf = Cn_beta_w + Cn_beta_f;

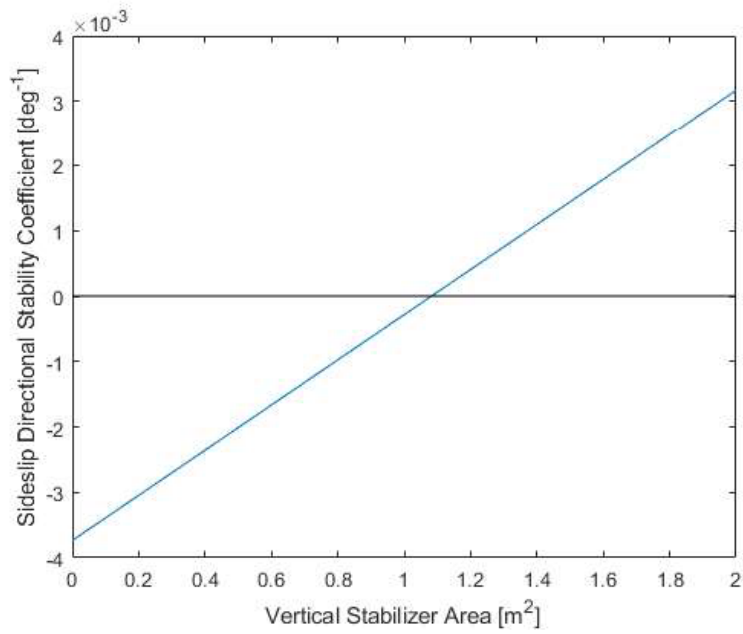
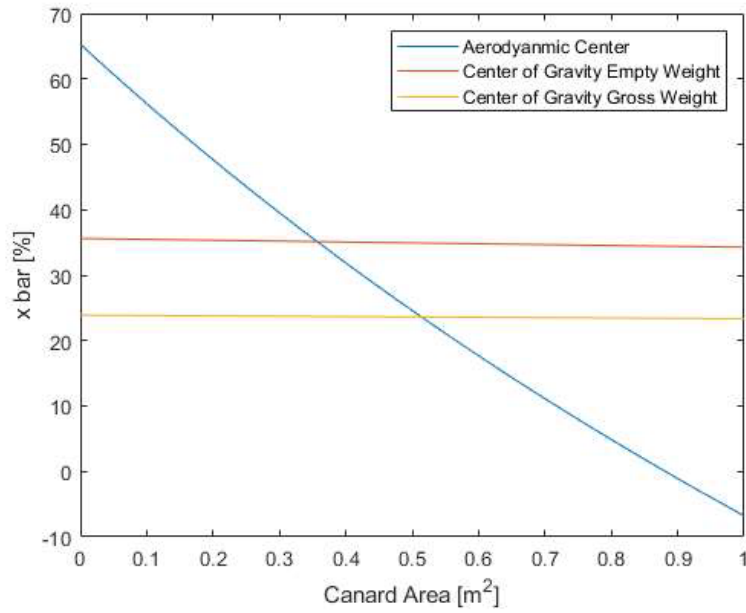
Cl_alpha_v = 0.0937;

Cn_beta = Cn_beta_wf + Cl_alpha_v * S_v / S * x_v / b;

figure,
plot(S_v, Cn_beta*pi/180)
hold on

```

```
plot(S_v, zeros(length(S_v)), 'k')
ylabel('Sideslip Directional Stability Coefficient [deg-1']')
xlabel('Vertical Stabilizer Area [m2']')
```



Wing lift slope

```
M = 0.85;
A_v = 2;
delta_w_semi_c = 54.25;
delta_c_semi_c = 54.18;
delta_v_semi_c = 46.77;
beta = sqrt(1-M^2);
cl_alpha_w_M_dot_21 = (.316 - .083) / 2;
cl_alpha_c_M_dot_21 = (.795 - .090) / 6;
cl_alpha_v_M_dot_21 = .693 / 6;
cl_alpha_w_M = cl_alpha_w_M_dot_21 * sqrt(1-.21^2) / beta;
cl_alpha_c_M = cl_alpha_c_M_dot_21 * sqrt(1-.21^2) / beta;
cl_alpha_v_M = cl_alpha_v_M_dot_21 * sqrt(1-.21^2) / beta;
k_w = cl_alpha_w_M / (2*pi/beta);
k_c = cl_alpha_c_M / (2*pi/beta);
k_v = cl_alpha_v_M / (2*pi/beta);
CL_alpha_w = 2*pi * A_w / (2 + sqrt((A_w^2 * beta^2/k_w^2)*...
    (1+tand(delta_w_semi_c)^2/beta^2)+4));
CL_alpha_c = 2*pi * A_c / (2 + sqrt((A_c^2 * beta^2/k_c^2)*...
    (1+tand(delta_c_semi_c)^2/beta^2)+4));
CL_alpha_v = 2*pi * A_v / (2 + sqrt((A_v^2 * beta^2/k_v^2)*...
    (1+tand(delta_v_semi_c)^2/beta^2)+4));
```

de facto directional stability

```
S_v_actual = 1; %1,1.2
Cn_beta_actual = -.000284; %-.000284, .0001301
delta_C_n_beta = 0.001 - Cn_beta_actual;

b_v = 1;
two_r1 = .75;
b_v_2r1 = b_v / two_r1;
A_vf_A_v = 1.55;
z_H = 0.2;
z_H_b_v = -z_H / b_v;
A_vhf_A_vf = 1.1;
%A_v_eff = A_vf_A_v * A_v * (1 + K_vh * (A_vhf_A_vf - 1))
% for horizontal stab not canard;

k_prime = .85; % c_f/c = .25, 20 DEG
K_b = .97-.14;
alpha_delta_CL_c1 = 1.14;
cl_delta_cl_delta_theory = .97;
cl_delta_theory = 4.1*pi/180;
eta_v = 1;
Cy_delta_r = CL_alpha_v / cl_alpha_v_M * k_prime * K_b * ...
    alpha_delta_CL_c1 * cl_delta_cl_delta_theory * cl_delta_theory * ...
    S_v_actual / S * eta_v;

l_v = 3.946 - 2.944;
z_v = .88 - .031;
alpha = 0;
Cn_delta_r = -Cy_delta_r * (l_v * cosd(alpha) + z_v*sind(alpha)) / b;

k_b = delta_C_n_beta / abs(Cn_delta_r);
```

Trim diagram

```

w = 1276.2; % 595.9, 1276.2 gross
S_c_actual = 0.64;
x_ref = 2.759 - 2.405; % negative if in front of LE, using aft CG
x_cg = 2.759 - 2.405; % 2.917 aft, 2.7 forward
alpha = [0 5 10];
i_c = [-5 0 5 10 15];

delta_c_quarter_w = 47.27;
cm0_r = -.0025;
cm0_t = -.0025;
deltaCm0_epsilon_t = -.002;
epsilon_t = 0;
Cm0_w = A_w * cosd(delta_c_quarter_w)^2 / ...
(A_w + 2*cosd(delta_c_quarter_w)) * (cm0_r + cm0_t)/2 + ...
deltaCm0_epsilon_t * epsilon_t; % for low sweep angle

dk = .8;
alpha_0_l = -.8;
alpha0_ratio = 1;
alpha0_L_w = alpha_0_l * alpha0_ratio;
dx_i = [.25 .25 .25 .25 3.4 .6];
i_cl_f = [-11.49 -2.83 -1.9 -.87 0 0] ;
w_f_i = [.191 .310 .364 .395 1.060 .490];
temp = w_f_i.^2 .* (alpha0_L_w + i_cl_f) .* dx_i;
Cm0_f = dk / 36.5 / S / cbar_w * sum(temp);
Cm0_wf = (Cm0_w + Cm0_f); %* Cm0_Mach_ratio

x_ac_c = .9;
xbar_ref = x_ref/cbar_w;
xbar_ac_c = x_ac_c/cbar_w;
CL0_c = .0089;
Cm0_c = (xbar_ref + xbar_ac_c) * CL0_c;

Cm0 = Cm0_wf + Cm0_c;

eta_c = 1;
CL_alpha = CL_alpha_wf + CL_alpha_c * eta_c * S_c_actual / S * ...
(1 + d_epsilon_d_alpha);
xbar_ac_w = .8225/cbar_w;
xbar_ac_wf = xbar_ac_w; % ac shift due to fuselage omitted
xbar_ac_A = (xbar_ac_wf * CL_alpha_wf - eta_c * CL_alpha_c * ...
(1 + d_epsilon_d_alpha) * S_c_actual / S * xbar_ac_c) / CL_alpha;

dCm_dCL = xbar_ref - xbar_ac_A;

xbar_cg = x_cg/cbar_w;
vbar_c = (xbar_ac_c + xbar_cg) * S_c_actual / S;
Cm_i_c = CL_alpha_c * eta_c * vbar_c;

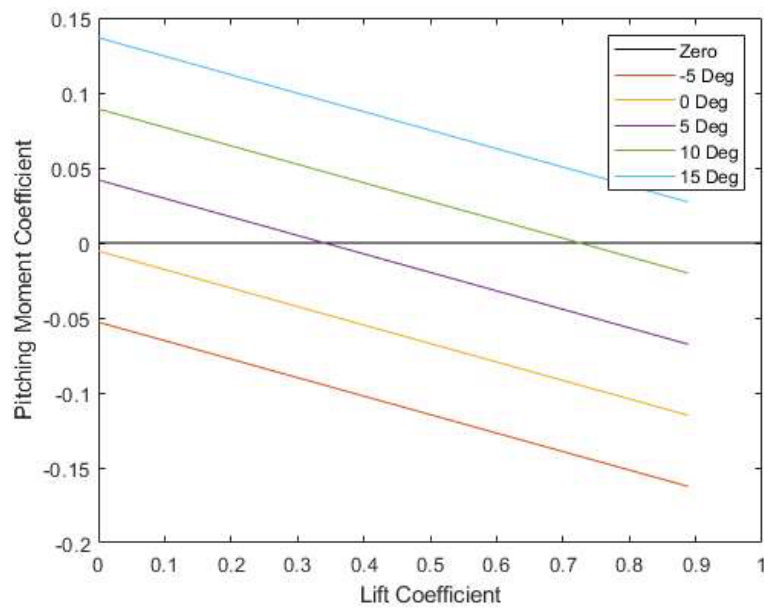
CL = CL_alpha * alpha;

for i = 1:length(i_c)
    Cm(i,:) = Cm0 + dCm_dCL * CL + Cm_i_c * i_c(i);
end

figure,
plot([0 1], [0 0], 'k', 'DisplayName', 'Zero')
hold on
plot(CL, Cm(1,:), 'DisplayName', sprintf('%d Deg', i_c(1)))
hold on

```

```
plot(CL, Cm(2,:), 'DisplayName', sprintf('%d Deg', i_c(2)))
hold on
plot(CL, Cm(3,:), 'DisplayName', sprintf('%d Deg', i_c(3)))
hold on
plot(CL, Cm(4,:), 'DisplayName', sprintf('%d Deg', i_c(4)))
hold on
plot(CL, Cm(5,:), 'DisplayName', sprintf('%d Deg', i_c(5)))
legend
xlabel('Lift Coefficient')
ylabel('Pitching Moment Coefficient')
```



Published with MATLAB® R2020a

Appendix L. Matlab Installed Thrust and Inlet

Contents

- [Common](#)
- [Inlet sizing](#)
- [Inlet pressure loss estimation \(imperial\)](#)
- [Air data \(metric\)](#)

```
clc, clear all, close all
```

Common

```
rho = 14.2536e-4;  
rho_m = 0.7346;  
M1 = 0.85;  
U1 = M1*320.5*3.3;  
gamma = 1.4;  
mu_m = 1.628e-5;
```

Inlet sizing

```
k_gas = 0.0003;  
T_TO = 2850;  
  
mdot_gas = k_gas * T_TO;  
  
mdot_cool = 0.06*mdot_gas;  
  
mdot_a = mdot_gas + mdot_cool;  
  
Ac = mdot_a / rho / U1;
```

Inlet pressure loss estimation (imperial)

```
M0 = .85;  
M_fan = .5;  
Ainf = Ac * M_fan / M0 * ((1+(gamma-1)/2*M0^2)/(1+(gamma-1)/2*M_fan^2)) ^ ...  
    ((gamma+1) / 2 / (gamma -1));  
mu_inl = Ac / Ainf;  
  
delta_l = 2.26; % m  
RN_d = rho_m * M_fan*343 * delta_l / mu_m;  
Cf_d = .00265;  
  
per_c = .869*2*3.3;  
per_f = 1.41*3.3;  
A_f = .16*3.3^2;  
A_c2 = .07186*3.3^2;  
l_f = 3.25*3.3;  
l_c = 1*3.3;  
  
theta_D = 2*atand(2*(per_c*A_f - per_f*A_c2)/per_c/per_f/(l_f-l_c));  
f = 2.5;  
CFd = f*Cf_d;
```

```

I = (A_c2/A_f)^2 * (per_f/A_f) * (l_f-l_c);
delta_p_tot_q = I * Cf_d / mu_inl^2;

```

Air data (metric)

```

alt_max = 10000;
h = linspace(0,alt_max,alt_max/10+1);
T_TO = 12700; %CJ610-4

T = 15.04 - 0.00649*h;
p = 101290 * ((T + 273.15) / 288.08).^5; % Pa
rho_mat = p /1000 ./ (.2869 * (T + 273.15)); % p needs to be in kPa

```

```

q = .5*rho_mat*(U1/3.3)^2; % SI
p_tot = p + q; % SI

% eta_inl_inc = 1 - delta_p_tot_q; % old
eta_inl_inc = 1 - delta_p_tot_q*p_tot; % SI Cancels out

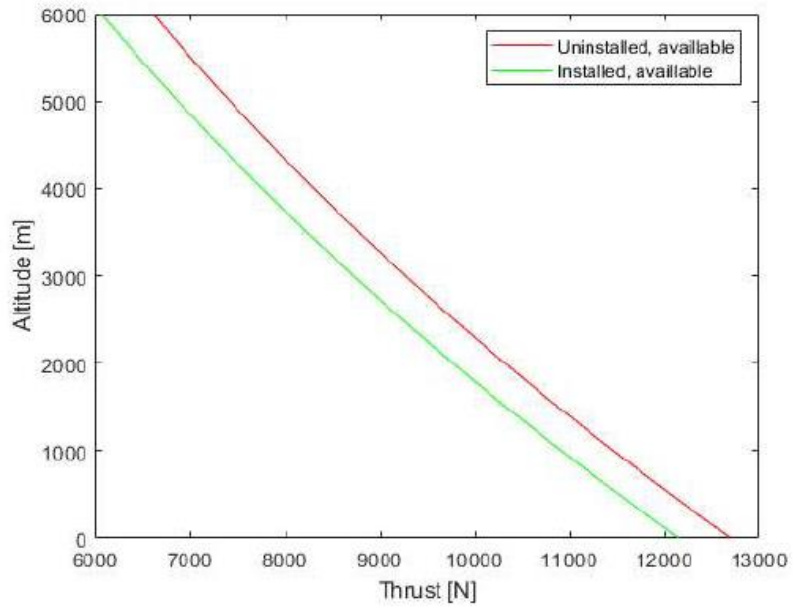
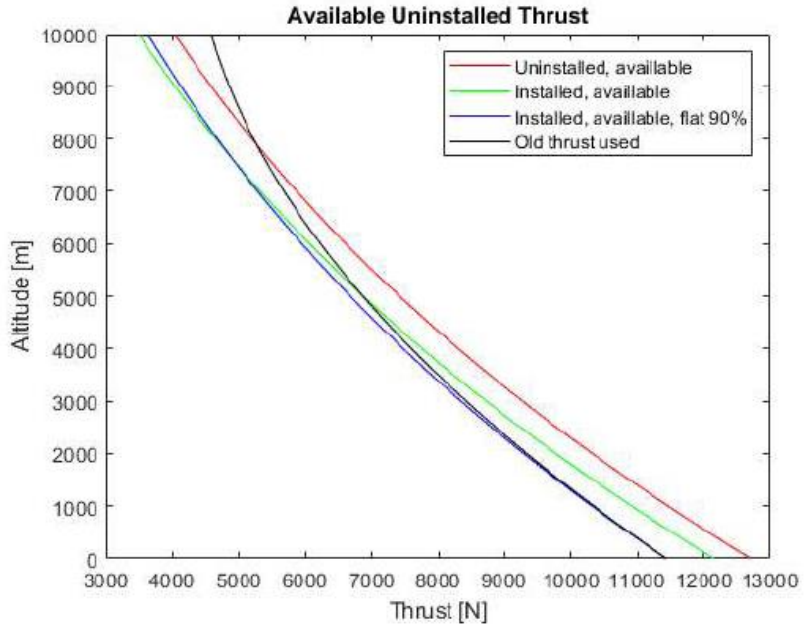
T_tst_av = T_TO .* p/p(1) .* sqrt((T(1)+273.15)./(T+273.15));
T_old = T_TO * .9 * (4e-9*h.^2-1e-4.*h + 1.0008); % old

K_t = 0.475;
P_el = 100;
P_mech = 100;
p_pneum = 0.03*mdot_a;
P_extr = P_el + P_mech + p_pneum;
T_av = (T_tst_av*.224809*(1-0.35*K_t*M1*(1-eta_inl_inc)) - ...
        550*(P_extr/U1))/ .224809;

figure,
plot(T_tst_av,h,'r')
hold on
plot(T_av,h,'g')
hold on
plot(.9*T_tst_av,h,'b')
hold on
plot(T_old,h,'k')
xlabel('Thrust [N]')
ylabel('Altitude [m]')
title('Available Uninstalled Thrust')
legend('Uninstalled, available', 'Installed, available', ...
        'Installed, available, flat 90%', 'Old thrust used')

figure,
plot(T_tst_av,h,'r')
hold on
plot(T_av,h,'g')
xlabel('Thrust [N]')
ylabel('Altitude [m]')
ylim([0 6000])
legend('Uninstalled, available', 'Installed, available')

```



Appendix M. Matlab Critical Performance

Contents

- Common
- Weight in N
- Air data (metric)
- Thrust
- Stall
- Cruise, Range
- Climb
- Maneuver
- Landing

```
clc, clear all, close all
```

Common

```
S = 4.15;  
g = 9.81;  
GW = 2808;  
w0_payload = GW/ 2.2*g;  
w0 = (GW - 500)/2.2*g;  
we = 1311/2.2*g;  
CL_max = .925;  
M1 = 0.85;  
U1 = M1*320.5;
```

Weight in N

```
w1_payload = (GW/2.2-68.3)*g;  
w1 = ((GW-500)/2.2-68.3)*g;  
w2_payload = w1_payload - 346.6*g;  
w2 = w1 - 346.6*g;
```

Air data (metric)

```
alt_max = 10000;  
h = linspace(0,alt_max,alt_max/10+1);  
T_T0 = 12700; %CJ610-4  
  
T = 15.04 - 0.00649*h;  
p = 101290 * ((T + 273.15) / 288.08).^5;  
rho_mat = p/1000 ./ (.2869 * (T + 273.15)); % p needs to be in kPa
```

Thrust

```
q = .5*rho_mat*(U1)^2; % SI  
p_tot = p + q; % SI  
  
% eta_inl_inc = 1 - delta_p_tot_q; % old  
eta_inl_inc = 0.9980; % SI Cancels out
```

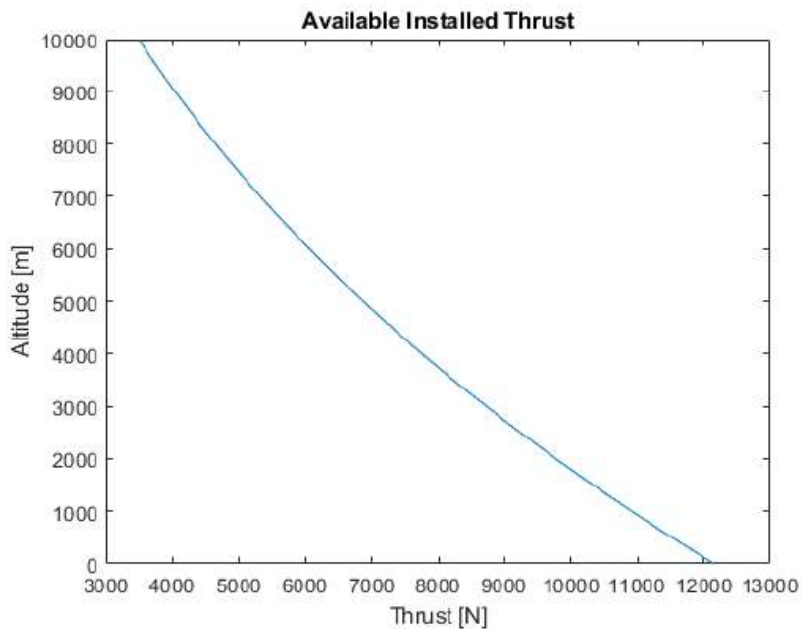
```

T_tst_av = T_T0 .* p/p(1) .* sqrt((T(1)+273.15)./(T+273.15));

K_t = 0.475;
P_extr = 200.027;
T_av = (T_tst_av*.224809*(1-0.35*K_t*M1*(1-eta_inl_inc)) - ...
        550*(P_extr/U1/3.3))/0.224809;

figure,
plot(T_av,h)
xlabel('Thrust [N]')
ylabel('Altitude [m]')
title('Available Installed Thrust')

```



Stall

```

a = sqrt(1.4*287*(T+273.15));

vs_gross = sqrt(2*w0_payload./rho_mat./CL_max/S);
vs_wo_p = sqrt(2*w0./rho_mat./CL_max/S);
vs_empty = sqrt(2*we./rho_mat./CL_max/S);

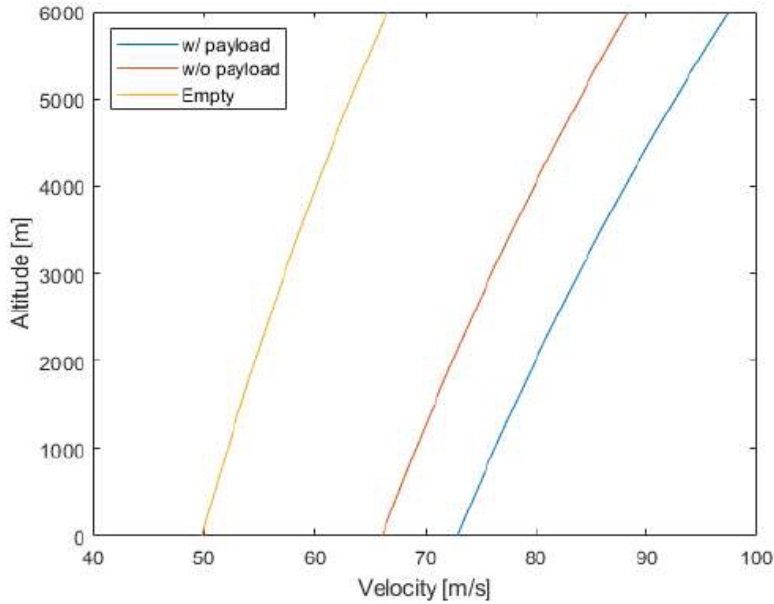
figure,
plot(vs_gross,h)
hold on
plot(vs_wo_p,h)
hold on
plot(vs_empty,h)
xlabel('Velocity [m/s]')
ylabel('Altitude [m]')
ylim([0 6000])

```

```

legend('w/ payload', 'w/o payload', 'Empty', 'location', 'northwest')
%title('Stall locus')

```



Cruise, Range

```

rho_cruise_m = 0.7364;
M1_mat = linspace(0.30,0.85,12);
U1_mat = 320.5*M1_mat;
CL_cruise_payload = (GW/2.2-68.3)*9.81/.5/rho_cruise_m./U1_mat.^2/S; % metric
CL_cruise = ((GW-500)/2.2-68.3)*9.81/.5/rho_cruise_m./U1_mat.^2/S; % metric

rho_cruise_i = 0.0014254; %imperial
fmj = 1.677;
cj = 0.98;
CD_cruise_paylaod = [0.1590 0.0966 0.0663 0.0503 0.0410 0.0354 0.0318 ...
0.0460 0.0436 0.0422 0.0417 0.0417];
CD_cruise = [0.1507 0.0909 0.0618 0.0465 0.0377 0.0323 0.0289 0.0411 ...
0.0386 0.0373 0.0367 0.0366];

% Constant altitude
R_payload_nm_CA = fmj / cj * (rho_cruise_i*S*3.3^2) ^ -.5 .* ...
CL_cruise_payload.^5 ./CD_cruise_paylaod * ((w1_payload/g*2.2)^.5 - ...
(w2_payload/g*2.2)^.5);
R_nm_CA = fmj / cj * (rho_cruise_i*S*3.3^2) ^ -.5 .* CL_cruise.^5 ./...
CD_cruise * ((w1/g*2.2)^.5 - ...
(w2/g*2.2)^.5);

R_payload_km_CA = R_payload_nm_CA * 1.852;
R_km_CA = R_nm_CA * 1.852;

% Constant Speed
R_payload_nm_CS = U1_mat.*1.944 / cj .* CL_cruise_payload ./ CD_cruise_paylaod ...

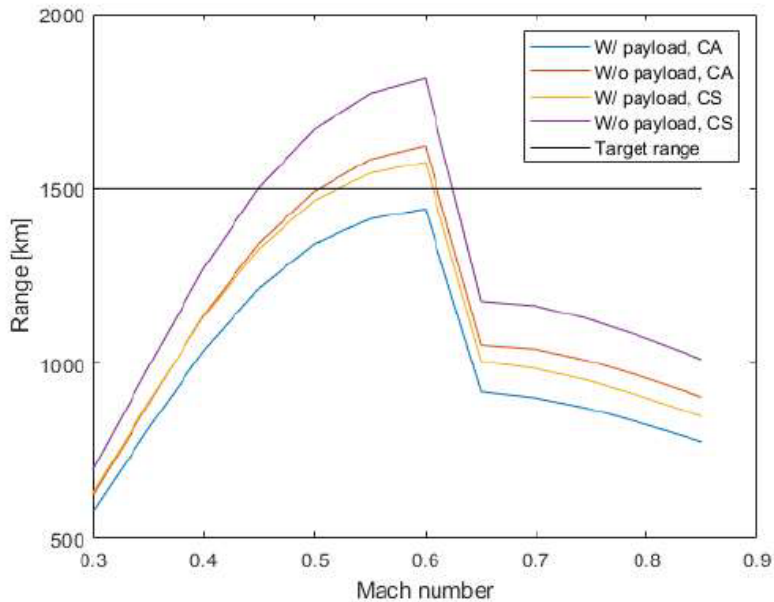
```

```

    * log(w1_payload / w2_payload);
R_nm_CS = U1_mat.*1.944 / cj .* CL_cruise ./ CD_cruise * log(w1 / w2);
R_payload_km_CS = R_payload_nm_CS *1.852;
R_km_CS = R_nm_CS *1.852;

figure,
plot(M1_mat,R_payload_km_CA)
hold on
plot(M1_mat,R_km_CA)
plot(M1_mat,R_payload_km_CS)
plot(M1_mat,R_km_CS)
plot(M1_mat,1500*ones(1,length(M1_mat)),'k')
legend('W/ payload, CA','W/o payload, CA','W/ payload, CS',...
       'W/o payload, CS', 'Target range')
xlabel('Mach number')
ylabel('Range [km]')

```



Climb

```

CD0 = 0.0180;
CD0_payload = 0.0234;
A = 2.47;
e = 0.8;

CL_RC_max = sqrt(3*CD0*pi*A*e);
CL_RC_max_payload = sqrt(3*CD0_payload*pi*A*e);
CD_RC_max = 4*CD0;
CD_RC_max_payload = 4*CD0_payload;

v_RC_max = sqrt(2*w1_payload ./ rho_mat / S / CL_RC_max);
v_RC_max_payload = sqrt(2*w1 ./ rho_mat / S / CL_RC_max_payload);

```

```

% For military aircraft, RC at altitude is just RC max
RC = 60 * v_RC_max * 3.3 .* (T_av./w1 - (CL_RC_max / CD_RC_max) ^ -1);
RC_payload = 60 * v_RC_max * 3.3 .* (T_av./w1_payload - (CL_RC_max_payload / ...
    CD_RC_max_payload) ^ -1);

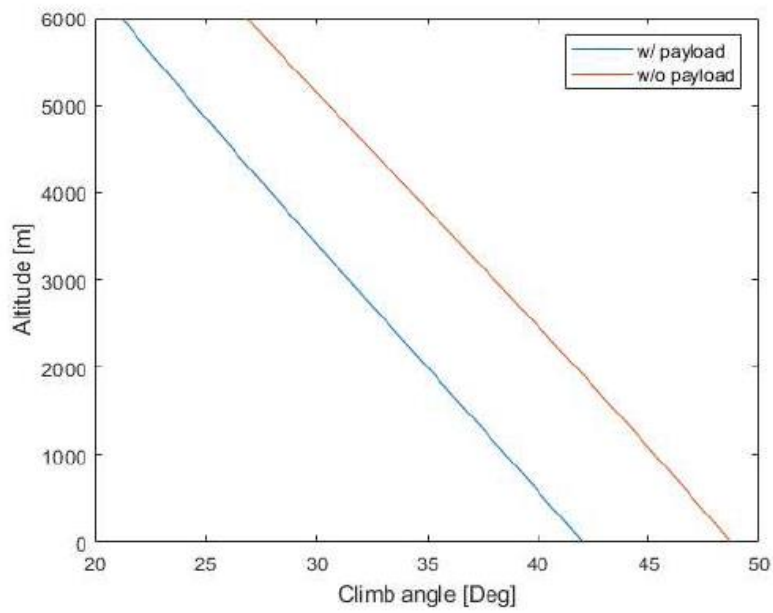
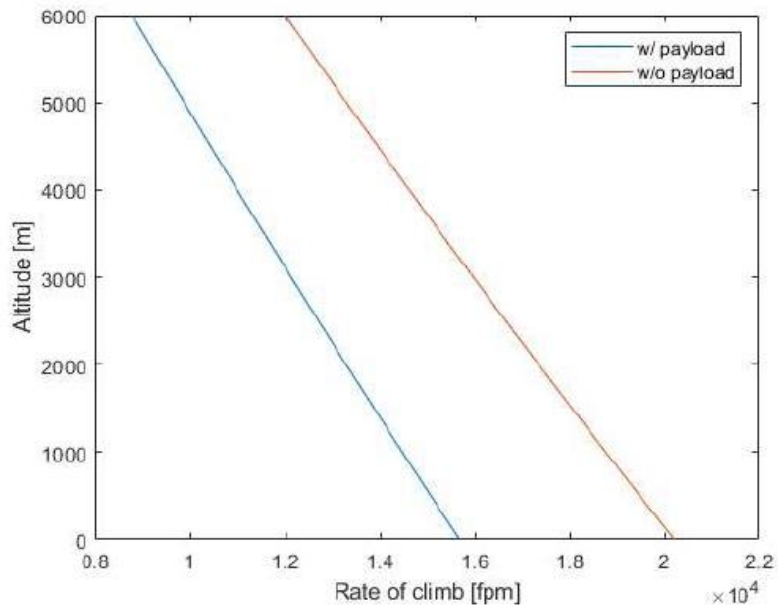
figure,
plot(RC_payload, h)
hold on
plot(RC, h)
legend('w/ payload', 'w/o payload')
xlabel('Rate of climb [fpm]')
ylabel('Altitude [m]')
ylim([0 6000])
%title('Rate of climb, service ceiling at 100, combat ceiling at 500, ...
%   cruising ceiling at 300')

CGR = (T_av./w1 - (CL_RC_max / CD_RC_max) ^ -1 );
CGR_payload = (T_av./w1_payload - (CL_RC_max / CD_RC_max) ^ -1 );

figure,
plot(atan(CGR_payload), h)
hold on
plot(atan(CGR), h)
xlabel('Climb angle [Deg]')
ylabel('Altitude [m]')
legend('w/ payload', 'w/o payload')
ylim([0 6000])

%title('Climb angle')

```



Maneuver

```
n_man = 5;
M_man = linspace(.5,.85,8);
M_man = linspace(.25,.85,13);
```

```

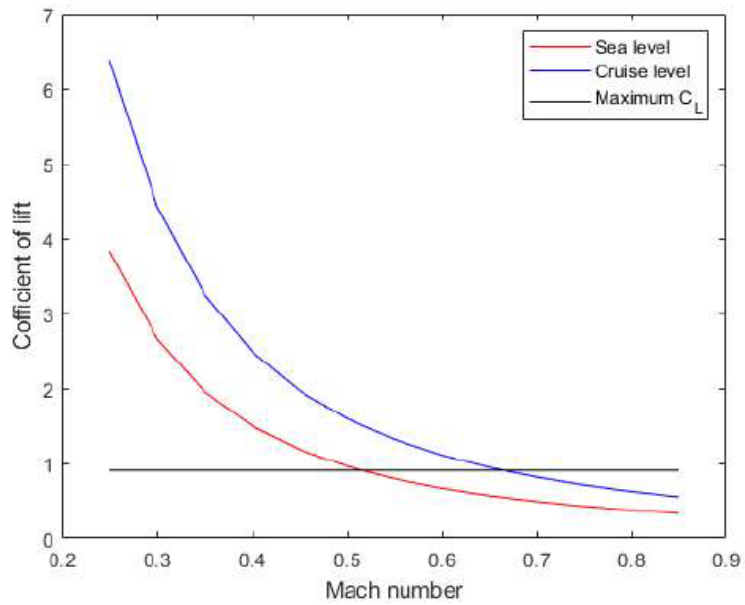
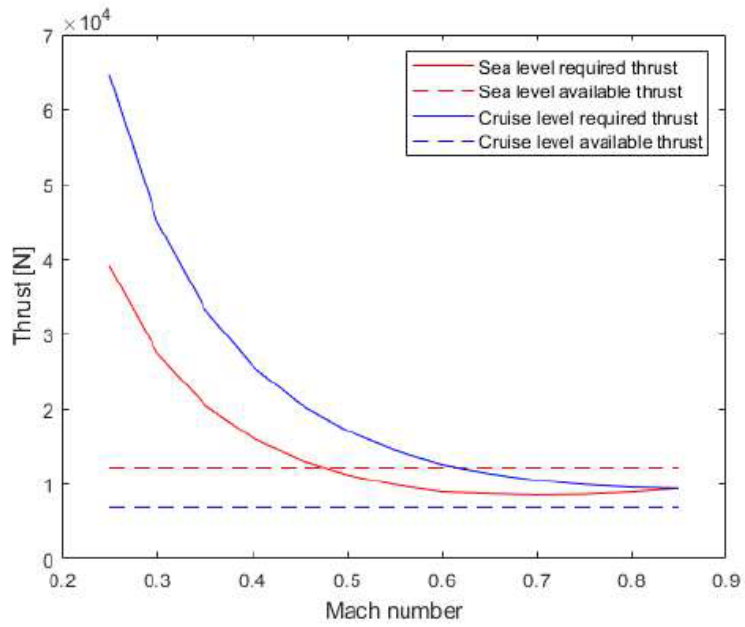
CD0_man = [.0233 .0232 .0230 .0264 .0277 .0290 .0304 .0317;
           .0249 .0245 .0242 .0277 .0291 .0304 .0318 .0331];
CD0_man = [.0262 .0253 .0246 .0240 .0237 .0233 .0232 .0230 .0264 .0277 ...
           .0290 .0304 .0317; .0278 .0269 .0264 .0258 .0253 .0249 .0245 .0242 ...
           .0277 .0291 .0304 .0318 .0331];
rho_man = [1.225 0.7364];
v_man = 320.5*M_man;

for i = 1:2
    q_man(i,:) = .5*rho_man(i).*v_man.^2;
    CL_1(i,:) = w0_payload ./ q_man(i,:) ./ S;
    CL_man(i,:) = n_man * CL_1(i,:);
    T_reqd(i,:) = (CD0_man(i,:) + CL_man(i,:).^2 / pi / A / e) .* ...
                 q_man(i,:) .* S;
end

figure,
pt1 = plot(M_man, T_reqd(1,:), 'r');
hold on
pt2 = plot(M_man, 12150*ones(1,13), 'r--');
pt3 = plot(M_man, T_reqd(2,:), 'b');
pt4 = plot(M_man, 6873*ones(1,13), 'b--');
hold off
xlabel('Mach number')
ylabel('Thrust [N]')
legend('Sea level required thrust', 'Sea level available thrust', ...
       'Cruise level required thrust', 'Cruise level available thrust')
%title('Required and available thrust in a 5-G sustained turn')

figure,
plot(M_man, CL_man(1,:), 'r')
hold on
plot(M_man, CL_man(2,:), 'b')
hold on
plot(M_man, .904*ones(1,13), 'k')
xlabel('Mach number')
ylabel('Coefficient of lift')
legend('Sea level', 'Cruise level', 'Maximum C_L')
%title('Coefficient of lift in a 5-G sustained turn')
% Available thrust 9320 N @ 2420 m

```



Landing

```

v_SL = [vs_gross(1) vs_wo_p(1) vs_empty(1)] * 3.3;
v_A = 1.2 .* v_SL;
a_bar = 0.4 * 9.81 * 3.3;

```

```
gamma_bar = 0.10;
delta_n = 0.10;
hL = 50;

v_TD = v_A .* sqrt(1 - gamma_bar^2 / delta_n );
s_air = 1 / gamma_bar * ((v_A.^2 - v_TD.^2) ./ 2 / g / 3.3 + hL);
s_air_m = s_air / 3.3;
s_LG = v_TD .^ 2 / 2 / a_bar ;
s_LG_m = s_LG/3.3;
s_L = s_air + s_LG;
s_L_m = s_L ./ 3.3;
```

Published with MATLAB® R2020a

Appendix N. Matlab Cost Analysis

Contents

- [Jump Start](#)
- [Research, development, test and evaluation cost](#)
- [Manufacturing and acquisition cost](#)
- [Operation cost military](#)

```
clc, clear all, close all
```

Jump Start

```
C_MAN = 1.4767e10;  
F_pro_m = 0.1;  
C_PRO = F_pro_m * C_MAN;  
N_m = 1000;
```

Research, development, test and evaluation cost

```
C_RDTE = 1.5683e9;% guess, 1.5683e9  
  
w_TO = 2808;  
  
W_ampr = exp(0.1936 + 0.8645 * log(w_TO)); % Out of range (5e3,1e6)  
  
V_max = 1218.3/1.6878; % = v_H, keas  
N_rdte = 10; % 6 - 20  
F_diff = 2.0; % difficulty, 1.0 - 2.0  
F_cad = 0.8;  
CEF = 6.31752+0.104415*(2022-2017); % 2022  
R_e_r = 76*CEF; % medium security  
  
MHR_aed_r = 0.0396 * W_ampr^0.791 * V_max^1.526 * N_rdte^0.183 * F_diff * ...  
    F_cad;  
C_aed_r = MHR_aed_r * R_e_r;  
  
% Development support and testing cost  
  
C_dst_r = 0.008325 * W_ampr^0.873 * V_max^1.890 * N_rdte^0.346 * CEF * ...  
    F_diff;  
  
% Flight test airplanes cost  
  
T_TO_e = 2950;  
C_e_r = exp(2.3044 + 0.8858*log(T_TO_e)); % using pre 1989 engine  
N_e = 1;  
AEP = (C_MAN + C_PRO + C_RDTE)/N_m; % ch 4  
C_avionics_r = 0.30*AEP;  
  
N_st = 2; % Static test  
MHR_man_r = 28.984 * W_ampr^0.740 * V_max^0.543 * N_rdte^0.524 * F_diff;  
R_m_r = 43*CEF;  
C_man_r = MHR_man_r*R_m_r;  
  
F_mat = 2.5; % 1.0-3.0, AL, SS, composite, C composite
```

```

C_mat_r = 37.632 * F_mat * W_ampr^0.689 * V_max^0.624 * N_rdte^0.792 * ...
    CEF;

N_r_r = 0.33;
MHR_tool_r = 4.0127 * W_ampr^0.764 * V_max^0.899 * N_rdte^0.178 * ...
    N_r_r^0.066 * F_diff;
R_t_r = 55*CEF;
C_tool_r = MHR_tool_r*R_t_r;

C_qc_r = 0.13*C_man_r;

C_e_plus_a_r = (C_e_r*N_e + C_avionics_r) * (N_rdte - N_st);
C_fta_r = C_e_plus_a_r + C_man_r + C_mat_r + C_tool_r + C_qc_r;

% Flight test operations cost

F_obs = 1.5; % 1.0 - 3.0
C_fto_r = 0.001244 * W_ampr^1.160 * V_max^1.371 * (N_rdte-N_st)^1.281 * ...
    CEF*F_diff*F_obs;

% Test and simulation facilities cost

C_tsf_r = 0;

% RDTE profit

F_pro_r = 0.10;
C_pro_r = F_pro_r*C_RDTE;

% Cost to finance

F_fin_r = 0.1; % 0.1 - 0.2
C_fin_r = F_fin_r*C_RDTE;

C_RDTE = C_aed_r + C_dst_r + C_fta_r + C_fto_r + C_tsf_r + C_tsf_r + ...
    C_pro_r + C_fin_r;

```

Manufacturing and acquisition cost

```

C_MAN = 1.4767e10; % guess, 1,4767e10

N_m = 1000;
N_p = N_m + N_rdte;

% Airframe engineering and design cost

MHR_aed_p = 0.0396 * W_ampr^0.791 * V_max^1.526 * N_p^0.183 * F_diff*F_cad;
R_e_m = R_e_r;
C_aed_m = MHR_aed_p*R_e_m - MHR_aed_r*R_e_r;

% Airplane program production cost

C_e_m = C_e_r;
C_avionics_m = C_avionics_r;
C_e_plus_a_m = (C_e_m*N_e + C_avionics_m) * N_m;

C_int_m = 0; % No interior

MHR_man_p = 28.984 * W_ampr^0.740 * V_max^0.543 * N_p^0.524 * F_diff;

```

```

R_m_m = R_m_r;
C_man_m = MHR_man_p*R_m_m - MHR_man_r*R_m_r;

C_mat_p = 37.632 * F_mat * W_ampr^0.689 * V_max^0.624 * N_p^0.792 * CEF;
C_mat_m = C_mat_p - C_mat_r;

N_r_m = N_r_r;
MHR_tool_p = 4.0127 * W_ampr^0.764 * V_max^0.899 * N_p^0.178 * ...
    N_r_m^0.066 * F_diff;
R_t_m = R_t_r;
C_tool_m = MHR_tool_p*R_t_m - MHR_tool_r*R_t_r;

C_qc_m = 0.13*C_man_m;

C_apc_m = C_e_plus_a_m + C_int_m + C_man_m + C_mat_m + C_tool_m + C_qc_m;

% production flight test operations cost

```

Operation cost military

```

% Program cost of fuel, oil and lubricant

F_OL = 1.005;
W_F_used = 996.6;
FP = 3.5; % JP-8 instead of JP-4, jet_a1_fuel.com
FD = (6.47 + 7.01) / 2;
U_ann_flt = 250;
N_mission = U_ann_flt / 2; % Low flight hour estimate , 2 hours per mission,
% 1.5 hours of cruise max, 0.5 hours loiter

% Rerun if n_program changes
N_serv = 868; % guess
N_acq = N_m;
N_res = 0.10*N_acq;
L_R = 1.5e-5; % 1.9 avg
N_yr = 20;
N_loss = L_R * N_serv * U_ann_flt * N_yr;
N_serv = N_acq - N_res - 0.5*N_loss;
C_POL = F_OL * W_F_used * FP/FD * N_mission * N_serv * N_yr;

% Program cost of direct personnel

MHR_flthr = 20; % Small size, low number of devices, function, instrument
R_m_ml = 45*CEF;
C_mpersdir = N_serv * N_yr * U_ann_flt * MHR_flthr * R_m_ml;
C_PERSDIR = C_mpersdir; % UAV, 0 crew

% Program cost of indirect personnel

f_persind = (0.16 + 0.13 + 0.14 + 0.20 + 0.20)/5;

% Program cost of consumable materials

R_conmat = 6.50 * CEF;
C_CONMAT = N_serv * N_yr * U_ann_flt * MHR_flthr * R_conmat;

% Program cost of spares

f_spares = (0.13 + 0.16 + 0.27 + 0.12 + 0.16)/5;

```

```

% Program cost of depot
f_depot = (0.20 + 0.15 + 0.22 + 0.13 + 0.16)/5;

% Program cost of msic items
C_MISC = 4 * C_CONMAT;

C_OPS = (C_POL + C_PERSDIR + C_MISC) / (1 - f_persind - f_spares - f_depot);
C_OPS_HR = C_OPS / N_serv / N_yr / U_ann_flt;

C_PERSIND = f_persind * C_OPS;
C_SPARES = f_spares * C_OPS;
C_DEPOT = f_depot * C_OPS;

% Manufacturing and acquisition cost continued

t_pft = 20;
F_ftoh = 4.0;
C_fto_m = N_m * C_OPS_HR * t_pft * F_ftoh;

% Cost to finance manufacturing

F_fin_m = 0.1;
C_fin_m = F_fin_m * C_MAN;

% Profit

F_pro_m = 0.1;
C_PRO = F_pro_m * C_MAN;

C_MAN = C_aed_m + C_apc_m + C_fto_m + C_fin_m;
C_ACQ = C_MAN + C_PRO;
AEP = (C_MAN + C_PRO + C_RDTE)/N_m;

LCC = (C_RDTE + C_ACQ + C_OPS)/.99;
C_DISP = 0.01 * LCC;

```

```

fprintf("The total R&D, test and evaluation cost is %.2f. \n", C_RDTE)
fprintf("The program acquisition cost is %.2f. \n", C_ACQ)
fprintf("The unit cost is %.2f. \n", C_ACQ/N_m)
fprintf("The program operation cost is %.2f. \n", C_OPS)
fprintf("The hourly operation cost is %.2f. \n", C_OPS_HR)
fprintf("The program disposal cost is %.2f. \n", C_DISP)
fprintf("The life cycle cost is %.2f. \n", LCC)

```

```

The total R&D, test and evaluation cost is 1568331690.75.
The program acquisition cost is 16243893844.08.
The unit cost is 16243893.84.
The program operation cost is 87555203859.71.
The hourly operation cost is 20186.80.
The program disposal cost is 1064317468.63.
The life cycle cost is 106431746863.17.

```